# ABSTRACT

Kristjan Louise Thompson. THE ROLE OF AXL AND AXL-LIKE PROTEINS IN MURINE SPERMATOGENESIS. (Under the direction of Dr. Ann O. Sperry), Department of Anatomy & Cell Biology, August 2009.

Mice lacking the *Axl* receptor tyrosine kinase (RTK) and its family members exhibit detrimental effects on their reproductive ability. AXL is localized to Sertoli cells, which are the major nurturing cells in the seminiferous epithelium. A sequence homology search identified an uncharacterized protein, AXL-LIKE, which we hypothesize is an endogenous dominant-negative of AXL. The structure of AXL-LIKE is essentially identical to AXL in the extracellular domain, but the intracellular portion of AXL-LIKE lacks the tyrosine kinase domain. The purpose of this study was to determine the expression of *Axl-like* within early developing testes, as well as its interaction with AXL and the role of AXL-LIKE in AXL function.

Relative *Axl* and *Axl-like* mRNA transcript levels were highest in early postnatal testes, specifically at 7 days post partum (dpp), compared to 14dpp and 21dpp. *Axl* transcript levels on embryonic day 15 (e15) were significantly less than on 7dpp for *Axl*, but not *Axl-like*. Overexpression of AXL in COS-7 cells increased filopodial number, which was suppressed by co-expressing AXL-LIKE. Cells co-expressing AXL and AXL-LIKE were smaller and rounded compared to control or AXL only overexpressing cells. There was a redistribution of AXL localization, from cell membrane to vesicular bodies, when AXL-LIKE and AXL were co-expressed. Immunoprecipitation studies determined AXL and AXL-LIKE were not associated with one another; however

introduction of AXL-LIKE reduced the amount of AXL present within cells as determined by western blot analysis. Overexpression of AXL increased cellular protein phosphorylation and this effect was eliminated when AXL-LIKE was co-expressed.

The mRNA transcript levels detected in the testes and embryonic tissue using real time-PCR appear to be correlated with the number of Sertoli cells. This suggests a role for AXL-LIKE within this cell type. This study is the first to show that expression of AXL-LIKE, an endogenous truncated isoform of *Axl*, inhibits the function of AXL *in vitro*. Though no direct interaction was observed between the two proteins, AXL-LIKE may affect a downstream signaling pathway of AXL or cause alterations in the recycling of AXL.

# THE ROLE OF AXL AND AXL-LIKE PROTEINS IN MURINE SPERMATOGENESIS

A Dissertation
Presented to
The Academic Faculty of the Department of
Anatomy & Cell Biology

by

Kristjan Louise Thompson

In Partial Fulfillment
of the Requirements for the Degree
Doctor of Philosophy in Anatomy & Cell Biology

East Carolina University
August 2009

# THE ROLE OF AXL AND AXL-LIKE PROTEINS IN MURINE SPERMATOGENESIS

by
Kristjan Louise Thompson, B.S.

APPROVED BY:

DIRECTOR OF DISSERTATION: ____Ann O. Sperry_____
Ann O. Sperry, Ph.D.

COMMITTEE MEMBER: ____Randall H. Renegar_____
Randall H. Renegar, Ph.D.

COMMITTEE MEMBER: ____Yan-Hua Chen_____
Yan-Hua Chen, Ph.D.

COMMITTEE MEMBER: ____Joseph M. Chalovich_____
Joseph M. Chalovich, Ph.D.

CHAIR OF THE DEPARTMENT OF ANATOMY & CELL BIOLOGY:

_____Cheryl B. Knudson_____
Cheryl B. Knudson, Ph.D.

DEAN OF THE GRADUATE SCHOOL:

_____Paul J. Gemperline_____
Paul J. Gemperline, Ph.D.

# ACKNOWLEDGEMENTS

I wish to thank Dr. Ann O. Sperry for allowing me to perform my dissertation work in her lab. It has been a great experience being subjected to such a variety of scientific methodology that I feel I would not have gotten in another lab. She has been a good mentor as well as a good friend. Thank you for your leadership!

To Dr. Randall Renegar and Dr. Yan-Hua Chen, for sticking with me for my entire time here in the Anatomy and Cell Biology Department. I have enjoyed working with you in the lab as well as being part of my pre-candidacy and dissertation committees. Thank you for all of your guidance and support through this entire process. I also appreciate the advice and direction Dr. Joseph Chalovich has provided as a member on my dissertation committee.

To the other members of the Anatomy and Cell Biology Department, Dr. Donald Fletcher, Dr. Hubert Burden, Dr. John Smith, Dr. David Terrian, and Dr. Edward Apetz, thank you for your candor and "open door." I value all of your advice, in scientific as well as non-scientific avenues, and will miss you all. To Drs. Warren and Cheryl Knudson, thank you for you scientific expertise and advice in the lab, as well as for help with my dissertation.

To Rong Wang, for being an amazing teacher and friend. I will truly miss you and will never forget your kindness and understanding. You are like a mother to me and I wish you and your family the best.

I would finally like to thank my fellow peers. To Christina Fitch, Kristen Boyle, and Matthew Paine. You have no idea how great of friends I consider you. From listening to me complain and talking me off the ledge (on more than one occasion), I KNOW that I would not be here today without you guys. Thank you so much for your friendship, love, and support. To former graduate students, Sarah James and Sonja Bareiss, those trenches sure were steep, but we all finally made it out. Thanks for all the memories! I would like to thank the fellow graduate students in the department, Liliana Mellor, Amy Friesland, Na Luo, June Nopparat, and Zhe Lu, for being a listening ear and to have good luck with the rest of your time here. Now you've seen me get through it, you guys will do great.

# TABLE OF CONTENTS

**PAGE**

# LIST OF FIGURES

# LIST OF TABLES

# LIST OF ABBREVIATIONS

ABP……Androgen-Binding Protein

AXL-DN……..…....AXL- Dominant Negative

BSA……...……..Bovine Serum Albumin

CML…….…….Chronic Myelogenous Leukemia

DAPI……..…4, 6-Di-Amidino-2-Phenyl-Indole dihydrochloride

DMEM……Dulbecco's Modified Eagle Medium

DPC……..……..……Days Post Coitum

DPP……...……Days Post Partum

DTT……..Dithiothreitol

EGFR…….Epidermal Growth Factor Receptor

ERK……..……Extracellular Signal-Regulated Kinase

EST……Expressed Sequence Tag

FBS……Fetal Bovine Serum

FITC……Fluorescein isothiocyanate

GAS6……...……..Growth Arrest Specific 6

GFP…….…….Green Fluorescent Protein

HRP……..……Horseradish Peroxidase

HSP…….……Heat Shock Protein

IL……..……Interleukin

LH……..….Luteinizing Hormone

LMP……...……..Low Melting Point

MAPK……..……Mitogen-activated Protein Kinase

MAPKAPK2……. Mitogen-Activated Protein Kinase-Activated Protein Kinase 2

MIF……...…….Müllerian Inhibitory Factor

N-CAM…….……..Neural Cell Adhesion Molecule

PBS…….….Phosphate Buffered Saline

PCR……Polymerase Chain Reaction

PFA……..…….Paraformaldehyde

PI3K……Phosphoinositide 3-Kinase

PMSF……..……..Phenylmethanesulphonylfluoride

PVDF……..…….Polyvinylidene fluoride

RT-PCR……..…….Reverse Transcriptase- Polymerase Chain Reaction

RTK…….……..…..Receptor Tyrosine Kinase

SDS……Sodium Dodecyl Sulfate

TAM……Tyro3, Axl, Mer

TBS……...….Tris Buffered Saline

TBST (Immunofluorescence)……....Tris-Buffered Saline- Triton X-100

TBST (Western blot)...……...……Tris-Buffered Saline- Tween

# CHAPTER I: INTRODUCTION

Spermatogenesis consists of a series of highly regulated cellular processes that transforms spermatogonia into mature sperm. These processes guarantee males the ability to reproduce. Sertoli cells help ensure spermatogenesis is sustained by properly regulating the environment of the seminiferous epithelium. Important to spermatogenesis and proper function of Sertoli cells are the members of the TAM family of receptor tyrosine kinases: *Tyro3*, *Axl*, and *Mer*. Sequence analysis of available databases revealed a putative splicing variant of the *Axl* receptor tyrosine kinase (termed *Axl-like*) that lacks the tyrosine kinases domain and is expressed in the testes. No information is available concerning the expression or function of this new isoform. The current study aimed to examine the expression of *Axl-like* in the developing testes and to determine whether its expression affects the function of *Axl in vitro*. In this section, I will describe the structure of the testis, the cell types present there, and the involvement of receptor tyrosine kinases in regulation of spermatogenesis.

## A. Testis development and histology

Mouse testis development

In the mouse, the primordial germ cells are first located in the epiblast of the embryo at approximately 5.25-5.5 days post coitum (dpc) (Lawson et al., 1999). The first visible identification of embryonic reproductive function is the appearance of the primordial germ cells at 7.25 dpc in the extraembryonic mesoderm that will later become the allantois (Ebner, 1871; Tam and Snow, 1981; Lawson et al., 1999). These primordial

germ cells originate in the wall of the yolk sac but then migrate into the gonadal region between 10.5 to 12.5 dpc (Itman et al., 2006). The gonad can then either differentiate into a testis or an ovary. The ability of the germ cell to transform into male or female is determined by signals from supporting cells in the undifferentiated gonad (Ford et al., 1975; Palmer and Burgoyne, 1991). At around embryonic day 10.5, there is a burst of *Sry* expression in the supporting cells of the male gonad, which will ultimately cause supporting cells to differentiate into those necessary for male reproductive maintenance. The *Sry* gene is conserved throughout evolution and is only found on the Y chromosome, specifically in the sex-determining locus, so individuals containing that chromosome will express *Sry*. *Sry* is important in this thesis because we use this gene in order to determine the sex of embryos utilized in real-time PCR experiments. SRY contains a high-mobility group (HMG) domain that causes bending of adjacent DNA (Ner, 1992). The HMG domain is located in many DNA-binding proteins and acts as a transcription factor by activating downstream sex-determining genes, such as *Sox9* (Van Der Wetering & Clevers, 1992). SOX9 is necessary to direct the supporting cells in the gonad to become male Sertoli cells rather than the granulosa cells in the female (Sekido et al., 2004). Although male germ cells are committed to differentiation along the male pathway at 12.5 dpc, there is no visible indication of male gonads (Adams and McLaren, 2002). Male primordial germ cells in the gonad at 13.5- 14.5 dpc are termed gonocytes (a term which includes spermatogonia). These gonocytes begin mitosis, but are then arrested in mitosis until after birth (Itman et al., 2006). Specifically, they are arrested in the G0/G1 phase of mitosis as prospermatogonia.

In order to understand the purpose of mitotic and meiotic divisions, it is necessary to understand genetic makeup and chromosome numbering. In mice, there are 20 chromosome pairs. When fertilization occurs, each parent yields half of their chromosomes, 20 from the mother's egg and 20 from the father's sperm. Primordial germ cells are termed "40, 2N," where 40 indicates the number of chromosomes, while 2N indicates the number of chromatids in the cell as a multiple of the haploid number of chromosomes (number of paired chromosomes) for the organism (N=20, while 2N=40).

At approximately day 5 postpartum (dpp), these prospermatogonia differentiate into type A spermatogonia or type B spermatogonia and by 7dpp the spermatogonia account for approximately 23% of cells within the testes, while Sertoli cells make up the other 77% (Regaud, 1901; Allen, 1918; Bellve et al., 1977; Itman et al., 2006). The cellular makeup of the testes from the late embryonic stage to adulthood is summarized in Table 1.1. As development continues, type A spermatogonia undergo mitosis to maintain a constant supply of germ cells throughout the reproductive life of the mouse. Some of the Type A spermatogonia differentiate into Type B spermatogonia, which then enter the meiotic phase of spermatogenesis (divisions are summarized in Figure 1.1). Type B spermatogonia enter meiosis I at 15 dpp and undergo DNA replication to form primary spermatocytes (40, 4N) (Itman et al., 2006). Primary spermatocytes complete meiosis I to form two secondary spermatocytes (20, 2N). The two secondary spermatocytes complete meiosis II to form four spermatids (20, 1N). At 20 dpp, these spermatids begin the final stage of spermatogenesis, called spermiogenesis, to complete the transition into mature sperm (20, 1N). At this time in the testes, the population is 28% Sertoli cells, 4%

**Table 1.1** Cell populations in the seminiferous tubules at different milestones in testes development. This table indicates the percentage of cell types present in the seminiferous epithelium at specific days of development. e = embryonic day, dpp = days postpartum, √ = present in the seminiferous epithelium but at an unknown percentage

| Cell Type | e15 | 7dpp | 14dpp | 21dpp | Adult |
|---|---|---|---|---|---|
| Germ cells arrested in mitosis | √ | | | | |
| Primitive Type A spermatogonia | | 5% | √ | √ | √ |
| Type A spermatogonia | | 9% | 6% | 4% | 1% |
| Type B spermatogonia | | 9% | 6% | 6% | 3% |
| Primary Spermatocytes | | | 51% | 57% | 21% |
| Secondary spermatocytes | | | | 1% | 1% |
| Round spermatids | | | | 4% | 31% |
| Mature sperm | | | | | 40% |
| Sertoli cells | √ | 77% | 37% | 28% | 3% |

Adapted from Bellve et al. 1977. Spermatogenic cells of the prepuberal mouse: isolation and morphological characterization. *J Cell Biol* 74, 68-85.

**Figure 1.1** Mitotic and meiotic divisions of spermatogonia to sperm. This cartoon depicts the division of a spermatogonial cell (2N) undergoing mitosis to either maintain the population of spermatogonia (curved arrow) or to differentiate into primary spermatocytes (4N). Primary spermatocytes undergo meiosis I for form two secondary spermatocytes (2N). The two secondary spermatocytes undergo meiosis II to yield four spermatids (1N). Spermatids transition to sperm (1N) by completing spermiogenesis where morphological changes shape them into elongated sperm.

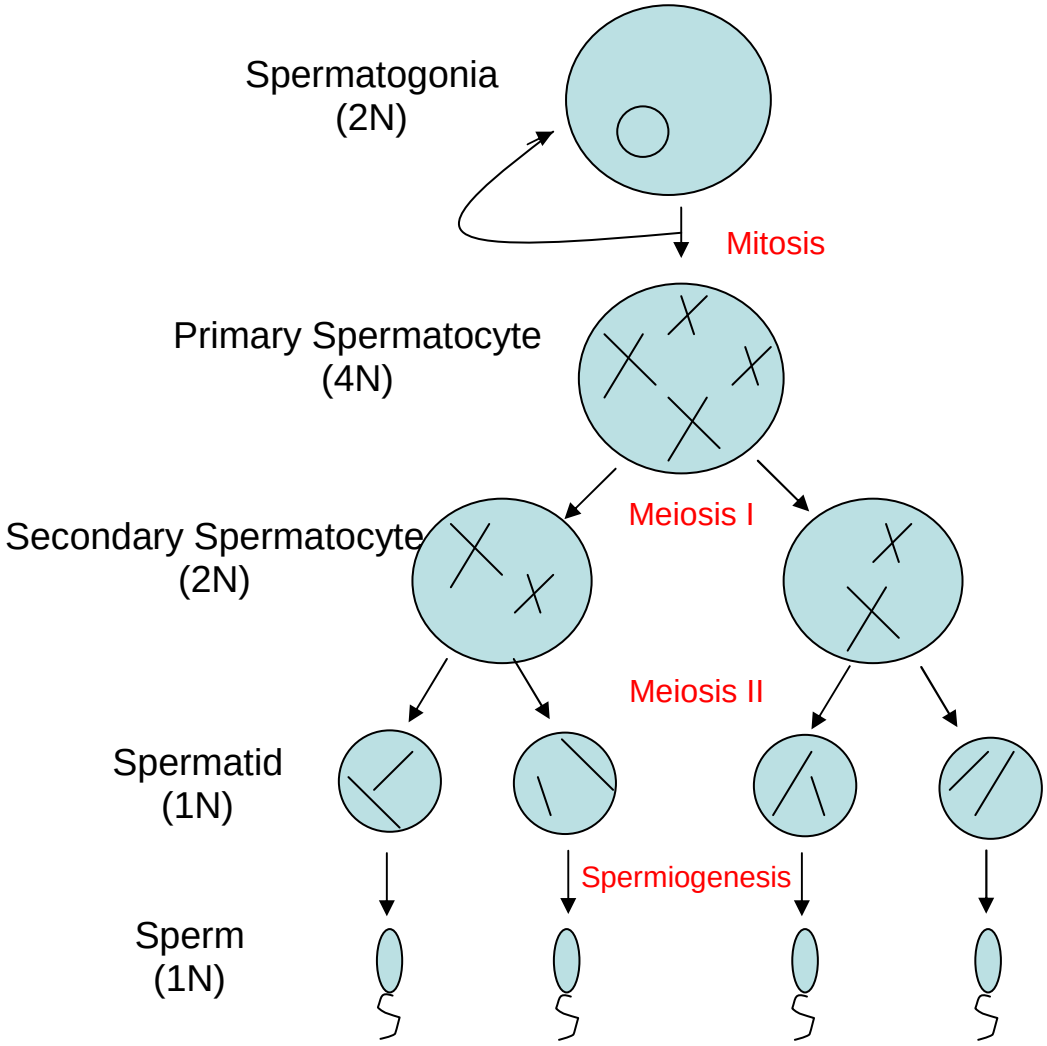
Spermatogonia
(2N)
Mitosis
Primary Spermatocyte
(4N)
Meiosis I
Secondary Spermatocyte
(2N)
Meiosis II
Spermatid
(1N)
Spermiogenesis
Sperm
(1N)

round spermatids, 1% secondary spermatocytes, 57% primary spermatocytes in various stages, and 10% spermatogonia (Bellve et al., 1977). During spermiogenesis, discussed in more detail later, round spermatids undergo morphological changes to become elongated sperm. There are four phases that spermiogenesis entails: Golgi, cap, acrosome, and maturation phase. Mature sperm are present at 35 dpp (Itman et al., 2006).

Testis histology

The testes are ovoid structures located within the scrotum of the male. They are incompletely surrounded by the tunica vaginalis on the lateral, medial, and anterior side of the testes. Deep to the tunica vaginalis, the testes are surrounded by a fibromuscular connective tissue called the tunica albuginea, which has an inner vascular layer called the tunica vasculosa. Septa emanate from the tunica albugenia toward the center of the testis to divide it into approximately 250 lobules. These lobules contain one to four seminiferous tubules that are embedded in the connective tissue stroma. The seminiferous tubules contain a fibromuscular tunica propria, which is separated from the seminiferous epithelium by a basal membrane. The seminiferous epithelium is composed of Sertoli cells and spermatogenic cells, both of which will be discussed in more detail later. Surrounding the seminiferous tubules is a loose connective tissue framework that contains clusters of interstitial Leydig cells (discussed in more detail later). Near the terminal end of each seminiferous tubule there is a tapering of the tubules to move into the straight tubules, also known as tubuli recti. These straight tubules enter into a complex labyrinth of channels within the mediastinum testis called the rete testes.

Cell types within the testes

There are several cell types within the testes, but only three will be discussed here: spermatogenic cells, Leydig cells, and Sertoli cells. In the mouse, spermatogenic cells originate from primordial germ cells starting at approximately 5 dpc and maintain the germ cell population throughout the lifetime of the male (Ginsberg et al., 1990). Spermatogenic cells are found in the seminiferous tubules along with Sertoli cells and are capable of either dividing to maintain the spermatogenic germ cell population or undergoing spermatogenesis to differentiate into mature sperm (Ginsberg et al., 1990). As spermatogenic cells undergo spermatogenesis they migrate from the basal to the luminal layer of the germinal epithelium (Ginsberg et al., 1990). Spermatogenic cells go through the following stages to ultimately become mature sperm: type A spermatogonia, type B spermatogonia, primary spermatocytes, secondary spermatocytes, spermatids, and spermatozoa.

Leydig cells are found in the interstitial tissue between seminiferous tubules beginning at around 12.5 dpc in the mouse. Leydig cells are responsible for testosterone secretion; there are two populations of Leydig cells in the mouse, fetal and adult (Baker and O'Shaughnessy, 2001). Unlike adult Leydig cells, fetal Leydig cells are an important component of male sex differentiation since they do not require LH to stimulate production of androgens, which occurs around 13 dpc (O'Shaughnessy et al., 2005). In addition to ensuring masculinization, Leydig cells also play a role in the descent of the testes into the scrotum through secretion of insulin-like 3 (INSL3) and androgens. The

adult population of Leydig cells requires interaction with LH in order to function (Baker and O'Shaughnessy, 2001; Zhang et al., 2001).

Sertoli cells are found within the seminiferous tubules and their apical and lateral cell membranes surround developing spermatogenic cells. Sertoli cells form tight junctions with adjacent Sertoli cells resulting in division of the germinal epithelium into two compartments: the adluminal section (between the tight junctions and the lumen of the seminiferous tubule) and the basal compartment (between the basal lamina and the tight junctions) (Dym and Fawcett, 1970). These tight junctions help form the blood-testis barrier that separates the environment of the lumenal and basal compartments. In newborn mice, the predominant junction between adjacent Sertoli cells is that of the gap junction (Nagano and Suzuki, 1976). As mice increase in age, the gap junctions decrease in size and occluding junctions become prevalent along the Sertoli cell surface, ultimately becoming circumferentially distributed around the entire cell surface (Nagano and Suzuki, 1976). Sertoli cells function through their interaction with Follicle Stimulating Hormone (FSH), however, during early fetal life Sertoli cell function is independent of its interaction with FSH (Tougard et al., 1977). FSH stimulation causes Sertoli cells to synthesize androgen-binding protein (ABP) which binds testosterone to maintain high levels within the seminiferous tubules to ensure spermatogenesis occurs. Sertoli cells also secrete inhibin, which acts as an inhibitor of FSH secretion from the adenohypophysis, and Müllerian Inhibitory Factor (MIF), that inhibits the development of the paramesonephric duct, the primordium of the female reproductive tract.

Another important function of Sertoli cells is to phagocytose apoptotic spermatogenic cells and residual bodies (Xiong et al., 2008). More than half of spermatogenic cells die by apoptosis during their differentiation to mature sperm (Roosen-Runge, 1955; Oakberg, 1956). Residual bodies are small membrane bound cytoplasmic masses that dissociate from developing spermatids around step 9 of spermiogenesis (discussed at a later time) (Kerr and de Kretser, 1974). They contain lipid vesicles, mitochondria, Golgi apparatus, and ribosomal material (Nyquist et al., 1973). Residual bodies are ultimately degraded by lysosomes (Niemi and Kormano, 1965) and their contents transported to the lumen of the seminiferous tubule. Without proper removal of apoptotic germ cells and residual bodies, healthy spermatogenic cells cannot proceed through spermatogenesis, possibly because of tissue injury caused by an increase in the acidity in the environment following lysis of apoptotic cells (reviewed in Ren and Savill, 1998).

Divisions of spermatogenesis

Primordial germ cells give rise to spermatogenic cells capable of maintaining the stem cell population or undergoing spermatogenesis to create mature sperm. Spermatogenesis takes approximately 35 days within the mouse testis (Brinster, 2007). Spermatogenesis consists of three separate phases: production of primary spermatocytes, meiosis, and spermiogenesis (Oakberg, 1956b).

The production of primary spermatocytes is the initial phase of spermatogenesis and occurs in the basal compartment of the seminiferous epithelium. This sequence of events was discussed earlier, but will be briefly reiterated here. Dettin et al. (2003) used

the following terminology to describe the spermatogonia in 6dpp mouse testis. It should be noted that the nomenclature used to describe spermatogonia in adult and immature rodents is different, with pale and dark not being employed to describe spermatogonia in adult mice. The mitotic proliferation of primitive germ cells gives rise to pale or dark type A (Ap or Ad) spermatogonia (Dettin et al., 2003). The Type Ap spermatogonia can then differentiate into Type Ap or Type B spermatogonia. Type B spermatogonia are the gonocytes that will become spermatocytes and ultimately mature spermatids. In contrast, type Ad spermatogonia rarely divide by mitosis and are considered quiescent surplus stem cells (Dettin et al., 2003). By five days of age, 50% of the gonocytes within each seminiferous tubule were undergoing active mitosis to yield primary spermatocytes (Nebel et al., 1961).

In the meiotic phase, primary spermatocytes proceed through two successive nuclear divisions: meiosis I and meiosis II. There is no DNA synthesis (S phase) in this process so that each successive division reduces the chromosome number by half. Ultimately the meiotic division of one spermatocyte will produce four haploid spermatids with half the number of chromosomes, a reduction from 2N to N, where N equals the copy number of chromosomes. Meiosis has been observed as early as 8 days in the prepuberal mouse (Nebel et al., 1961). Meiosis I occurs when a primary spermatocyte divides to become two secondary spermatocytes. Meiosis I also contains an extended prophase that allows for alignment and recombination of homologous chromosomes (Cobb and Handel, 1998). Prophase I consists of 6 transitional stages that are named because of the changes observed in the chromatin of the nucleus (Tobias, 1956; Ohno et

al., 1957): preleptotene, leptotene, zygotene, pachytene, diplotene, and diakinesis. Specifically in the preleptotene stage, the chromatin granules resemble delicately beaded filaments, until they become clearly filamentous at the leptotene stage. Following leptotene, the zygotene stage is marked by the pairing of the homologous chromosomes that appear as bunches of long loops attached to the nuclear envelope. The chromosomes become shorter and thicker during pachytene, and then become partially separated during the diplotene stage. Meiosis II is the division of the two secondary spermatocytes to form four spermatids. The chromosome behavior in meiosis II is similar to that occurring in mitosis of somatic cells; the chromosome number is not reduced.

Spermiogenesis is the transformation of round spermatids into elongated, free-swimming spermatozoa capable of fertilization. There are 16 steps of spermiogenesis dealing with changes in the acrosome and nucleus, as described by Oakberg (1956a). Step 1, the Golgi phase, begins as a result of the second meiotic division with the formation of a new population of spermatids. It is called the Golgi phase because it is the first sign of spermatids developing polarity, as defined by the location of the Golgi apparatus within the cell. The Golgi apparatus identifies the future head region of the sperm and contains proacrosomal granules that will ultimately become the acrosome of the sperm. In step 2, proacrosomal granules, usually two, appear in the idiosome, also known as the centrosome. The fusion of the two proacrosomal granules into one large granule marks step 3. Step 4 defines the beginning of the cap phase of spermiogenesis. Enlargement of the granule and the process of it flattening and extending laterally over the nucleus characterize this stage. Step 5 is distinguished by the presence of two

projections appearing from the acrosomal granule as it continues extension of the cap. Continued development of the cap on the outer surface, so that it can be observed in the side view, is a hallmark of step 6. In step 7, the cap progresses to cover one-third to one-half of the nucleus. Step 8, the acrosome phase, marks not only the beginning of young spermatids orienting themselves toward the basement membrane, but also the initiation of spermatid nuclear elongation. In step 9, there is a definite change in the shape of the nuclei. The nucleus begins flattening, and the head cap begins to move caudally, where the nuclei appears more narrow and angular, over the dorsal side of the nucleus. Step 10 marks the continuation of the flattening and elongation of the nucleus, as well as the completion of the head cap's movement toward the dorsal, caudal portion of the nucleus. Transformation of the spermatid's caudal angles from rounded to sharp and acute angles is a characteristic of step 11. There is also the continuation of flattening and elongation of the nucleus and the movement of acrosomal material to the caudal portion of the nucleus. In step 12 the spermatid reaches its greatest total length. The acrosome has changed shape so that the anterior end appears square and is wedge-shaped as it lies over the nucleus. There is an abrupt shortening of the spermatid length in step 13. Also, the spermatid's caudal angles assume the shape that is present in mature sperm. In step 14, the acrosome appears as a crescent shape with the anterior tip ending in a slender, sharp point. At this point, the spermatids have assumed the general shape they will have as mature sperm. In step 15 the nucleus begins to narrow and the development of the tip of the maturing sperm continues. Finally, in step 16, the sperm is in its mature form as it

would be in its release from the seminiferous tubule. The acrosomic material and nucleus extend to the extreme anterior tip of the spermatid.

Stages of seminiferous epithelium

Not only are there steps of spermiogenesis, but there are also stages of the seminiferous epithelium. It is important to discern the difference between steps of spermiogenesis and stages of seminiferous epithelium, because many authors utilize the two terms almost interchangeably thereby creating confusion. Steps of spermiogenesis describe the morphological changes an individual spermatid undergoes to become a mature sperm, while the stages of seminiferous epithelium describe the collection of cell types that are located within a cross-section of the seminiferous tubule. Specific gene expression is associated with defined stages of the seminiferous epithelium. For example, the FSH receptor is expressed only in stage XII-IV of the twelve (XII) stages of seminiferous epithelium (Griswold et al., 1995). The following description of each stage of the seminiferous epithelium was described by Oakberg (1956a) and is summarized in Table 1.2. These stages are characterized by the presence of specific spermatogenic cell types and the degree of spermatid development in the seminiferous tubules. It should be noted that Type A spermatogonia are present at all stages of the seminiferous epithelia cycle. The differences in the other stages are summarized below. The duration of each stage is different and was determined by radiation exposure and subsequent visualization of spermatozoal disappearance. These intervals were reported by Oakberg (1956b) as well.

**Table 1.2** Stages of the seminiferous epithelium in murine testes. This table indicates the stages of the seminiferous epithelium listed as roman numerals at the top, while the cell types present in each stage are listed below. First (newly formed) and second (older) layer spermatocytes refer to their location in the seminiferous tubule. The first layer is closest to the basement membrane, while the second layer is farther from the basement membrane. This regional association is also the same for first and second layer spermatids because spermiogenesis requires longer than one 12-stage cycle for completion.

| Stage of Cycle | | I | II | III | IV | V | VI | VII | VIII | IX | X | XI | XII |
|---|---|---|---|---|---|---|---|---|---|---|---|---|---|
| Spermatogonia<br>A= Type A<br>B= Type B<br>In= Intermediate Type | | A | A<br>In | A<br>In | A<br>In<br>B | A<br>B | A<br>B | A | A | A | A | A | A |
| Spermatocytes I<br>R= Resting<br>L= Leptotene<br>Z= Zygotene<br>P= Pachytene<br>DI= Diplotene<br>M= Metaphase | First layer | | | | | | R | R | R<br>L | L | L<br>Z | Z | Z<br>P |
| | Second layer | P | P | P | P | P | P | P | P | P | P | DI | M-<br>I |
| Spermatids (first layer) | Phase | Golgi phase | | | Cap phase | | | | Acrosome phase | | | | |
| | Step | 1 | 2 | 3 | 4 | 5 | 6 | 7 | 8 | 9 | 10 | 11 | 12 |
| Spermatids (second layer) | Phase | Acrosome phase | | | Maturation phase | | | | | | | | |
| | Step | 13 | 14 | 14 | 15 | 15 | 15 | 16 | | | | | |

Adapted from Oakberg 1956a. A description of spermiogenesis in the mouse and its use in analysis of the cycle of the seminiferous epithelium and germ cell renewal. *Am J Anat*, 99 (3), 391-413.

In stage I of the cycle, Type A spermatogonia are present, as mentioned above. This stage is also characterized by the visualization of an older group of spermatocytes in the pachytene stage. Sertoli cells are generally located against the basement membrane in close association with the Type A spermatogonia. There are two generations of spermatids, one of newly formed ones (step 1), and one of older ones (step 13) seen on the lumenal side of the epithelium. The duration of this stage is 22.2 hours (Oakberg, 1956b).

Stage II of the cycle (18.1 hours) contains Type A spermatogonia that are in the process of differentiating into Type B spermatogonia (also termed intermediate type). Again, pachytene spermatocytes are present at this stage. Spermatids are at step 2 of spermiogenesis and are separated from the immature spermatozoa at step 14 of spermiogenesis. The step 14 spermatozoa are grouped in bundles and are moving toward the basal Sertoli cell nuclei.

Stage III contains a few Type A and many intermediate spermatogonia. Pachytene spermatocytes are observed at stage III. Younger (step 3) and older (step 14) spermatids are seen together, while the older spermatids are arranged in bundles. These bundles are situated in close proximity of the Sertoli nucleus. This stage is very brief at 8.7 hours.

In Stage IV of the cycle (18.6 hours in length), intermediate spermatogonia undergo mitosis and become Type B spermatogonia. Little change is seen in the spermatocytes, again remaining in the pachytene stage. The spermatids are characterized by steps 4 and 15.

At stage V, a few Type A and many Type B spermatogonia are present. No change is seen in the spermatocytes, while younger spermatids (step 5) are separated from the immature spermatozoa (step 15). Stage V takes approximately 11.3 hours to complete.

Stage VI of the seminiferous cycle again contains a few Type A and an abundant amount of Type B spermatogonia. The Type B spermatogonia begin mitotic division to produce young spermatocytes (labeled as resting spermatocytes in Table 1.1). Pachytene spermatocytes are again observed. Young spermatids (step 6) are present, as well as immature spermatozoa (step 15). This stage is 18.1 hours in length.

In Stage VII, the only spermatogonia present are that of Type A. The new generation of spermatocytes (R) are present, while the older pachytene stage spermatocytes are observed as well. Spermatids are observed in steps 7 and 16 of spermiogenesis. 20.6 hours are needed to complete this stage.

Stage VIII (20.8 hours) contains only Type A spermatogonia. Spermatocytes are in the resting stage early, but by the end of stage VIII they have entered the leptotene form. Pachytene spermatocytes are also observed. This stage marks the beginning of the acrosome phase of spermiogenesis, therefore step 8 spermatids are present. The older spermatids are again at step 16, and are released into the tubules.

Stage IX is similar to Stage VIII, in that they contain the same type of spermatogonia, Type A; and, there are leptotene and pachytene spermatocytes present. The spermatid population in this stage is that of spermiogenic step 9. Stage IX's duration is 15.2 hours.

In Stage X, Type A spermatogonia are present. The spermatocytes begin this stage in the leptotene form, but then differentiate into the zygotene form. Older spermatocytes are present in the pachytene form. Step 10 spermatids are present. This stage is also brief at 11.3 hours in length.

Stage XI (21.4 hours) is again characterized by Type A spermatogonia. Zygotene spermatocytes are present and the older spermatocytes have entered the diplotene form. Spermatids are present in spermiogenic step 11.

The final seminiferous epithelial stage, XII, is again characterized by Type A spermatogonia. The younger spermatocytes transition from the zygotene to the pachytene phase. The older spermatocytes undergo diakinesis, the final stage of prophase in meiosis I where the nuclear membrane dissolves and chromosome pairs shorten and thicken, followed by metaphase I. The secondary spermatocytes are only present for a short time within stage XII, and therefore immediately divide to form a new group of spermatids. There are also spermatids present in step 12 of spermiogenesis. The length of this stage is 20.8 hours.

Although the gross anatomical structure and cellular composition of the testes and seminiferous epithelium is well known, it is important to have a detailed understanding of the histology of the testes. This foundation is necessary to enable proper design and interpretation of experiments to examine gene expression in the developing testes. The relationship between testis histology and gene expression is vital to the current study because *Axl* and *Axl-like* are thought to be cell-type specific transcripts.

**B. Receptor Tyrosine Kinases and the testes**

Receptor Tyrosine Kinases

An appreciation of the function and distribution of Receptor Tyrosine Kinases (RTKs) in the testes is important to the current study because the proteins under investigation are members of this family of signaling molecules. Of the two RTKs in this current study, *Axl* is located in the testes and is necessary, along with its family members *Tyro3* and *Mer*, to ensure proper maintenance of spermatogenesis. *Axl-like* is a splicing variant of the *Axl* transcript and was first isolated in embryonic testes cDNA.

RTKs are membrane bound cell surface receptors that have an affinity for binding specific ligands such as hormones, growth factors, and cytokines (Wang et al., 2006; Kabbani, 2008). The presence of RTKs on the cellular surface allows cells to communicate with their environment and then interact with their intracellular machinery. RTKs modulate many different functions in the cell including induction of cellular proliferation, survival, differentiation, motility, and adhesion. In addition, RTKs are associated with the progression of many types of cancer as reviewed in Li and Hristova (2006). Functional RTKs possess an intracellular domain that contains a region of kinase activity that is activated in response to ligand binding and receptor dimerization. Phosphorylation of the tyrosine residues in this region allows for activation of downstream signaling pathways. Distinct domain sequence patterns in the extracellular domain of RTKs are the basis for their subclassification (Yarden and Ullrich, 1988). Although most RTKs are activated through ligand binding, RTKs are not solely activated in this manner. Cell Adhesion Molecules (CAMs), such as cadherins, syndecans, CD44,

and neutropilins can also interact with RTKs to cause activation of downstream signaling pathways (Steinfeld et al, 1996; Orian-Rousseau et al, 2002; Qian et al, 2004).

Upon activation, RTKs may then enter the endocytic system by several mechanisms including clathrin-mediated endocytosis and clathrin-independent endocytosis. Once RTKs are localized to early endocytic vesicles, they move into either the degradative pathway or the recycling pathway. The degradative pathway moves the receptors from early to late endosomes, and then finally to lysosomes for destruction. In the recycling pathway, the receptors can be returned to the plasma membrane through recycling endosomes (Herbst et al., 1994). Some RTKs are known to signal from endosomes. Examples are the insulin receptor and TRKA (Kelly and Ruderman, 1993; Ceresa et al., 1998). Zhang et al. (2000) reported that while cell surface TRK receptors promote NGF-induced survival, internalized receptors are active in promoting differentiation. TRK activation and subsequent internalization into the cytoplasm terminate AKT signaling, but cause a brief, robust increase in ERK activation.

RTKs and adhesion

E-cadherin has long been considered to be a structural protein because of its indirect connection to the cytoskeleton through ß-catenin and α-catenin. E-cadherin is associated with the WNT signaling pathway through its association with ß-catenin (Sharpe et al., 2001) and co-localizes with RTKs such as Epidermal Growth Factor Receptor (EGFR) (Hoschuetzky et al., 1994). E-cadherin appears to have an inhibitory effect on RTKs through alteration of ligand binding affinity (Qian et al., 2004). When E-cadherin was overexpressed in high-density plated Madin-Darby canine kidney (MDCK)

cells there was a loss of high affinity binding sites. In low-density plated MDCK cells, there was reduced expression of E-cadherin, resulting in a higher response of cells to ligand (EGF) stimulation. Fluorescence Recovery after Photobleaching (FRAP) experiments demonstrated that low-density plated human embryonic kidney 293 (HEK293) cells (with less E-cadherin present) were able to recover more efficiently after FRAP than high-density plated HEK293 cells (with more E-cadherin present). This experiment evaluated receptor mobility as a predictor of potential for receptor dimerization and subsequent activation of downstream signaling pathways. Results indicate that low-density plated cells had receptors that maintain their mobility more readily than high-density plated cells. Based on these findings, E-cadherin may be regulating RTK function. RTKs are over-activated and E-cadherin is lost in many cancer tissues (Behrens et al., 1984; Vleminckx et al., 1991). Qian et al. (2004) reported that E-cadherin negatively regulates the availability of the ligand binding site on RTKs and inhibits the mobility of MDCK and HEK293 cells. Loss of E-cadherin upregulates RTK signaling and decreases the adhesive properties of cells, ultimately increasing cancer metastasis.

RTKs within the testes

This study examines expression and function of two RTKs found in the testes, *Axl* and *Axl-like*. *Axl* is important in the maintenance of a suitable microenvironment for the development of male germ cells in the seminiferous epithelium (Lu et al., 1999; Xiong et al., 2008). However, the function of *Axl-like*, an alternatively spliced isoform of *Axl*, is not known. In addition to *Axl* and *Axl-like* and their related family members, *Tyro3* and

*Mer*, several other RTK protein families are expressed in the testes (Dolci et al., 2001; Kierszenbaum, 2006; Lawson et al., 2008). The SRC family of kinases contains eight members that have varying expression patterns within the testes and regulate a number of different cellular processes during spermatogenesis, including the capacitation-mediated increase in sperm protein phosphotyrosine (Kierszenbaum, 2006; Lawson et al., 2008). Capacitation of sperm is necessary for fertilization of the egg within the female fallopian tubes, and protein tyrosine phosphorylation is an important posttranslational modification that regulates sperm capacitation (Visconti et al., 1995a and b).

Members of the non-receptor tyrosine kinase subfamily Fps/Fes are also found in testicular cells, and these RTKs have been shown to be involved with regulation of cell-cell interactions in the rat testis (Chen et al, 2003). Fes-related protein (FER), a member of the Fps/Fes subfamily of protein tyrosine kinases, is expressed in two forms in the testes, a full-length FER and a soluble truncated form of FER (FERT) that contains only the intracellular portion and is testis specific (Kierszenbaum, 2006). Full-length FER and FERT link elongating spermatids to adjacent Sertoli cells and are found in the acroplaxome, which is a cytoskeletal plate consisting of an F-actin-keratin 5 complex that attaches the acrosome to the nucleus of spermatids in mice and rats during spermiogenesis (Kierszenbaum et al., 2003).

The RTK c-kit is also found within the testis in male germ cells, and its expression is necessary for maturation of several cell types. Binding of stem cell factor (SCF) to c-kit results in its dimerization followed by receptor autophosphorylation and

stimulation of several downstream signaling pathways. Mice deficient in c-kit display several different phenotypes including sterility (Dolci et al, 2001).

**C. The TAM family of RTKs**

TAM Receptor Tyrosine Kinases

The studies in this dissertation will focus on *Axl* RTK, a member of the TAM family of RTKs found in the testes, and *Axl-like*, a splicing isoform of *Axl*. The TAM family of RTKs is comprised of three members: *Tyro3*, *Mer*, and *Axl*. All three members share similar structural characteristics. Their extracellular N-terminal domain contains two immunoglobulin-related domains, followed by two fibronectin type III repeats. A single-pass transmembrane domain precedes an intracellular catalytically active protein tyrosine kinase domain (Lemke and Rothlin, 2008) (Figure 1.2). There are two known ligands for this family of RTKs, Growth Arrest Specific 6 (GAS6) and Protein S. GAS6 is a powerful agonist for all three family members, stimulating AXL most potently followed by TYRO3 and finally MER, while Protein S is a known ligand of TYRO3 and MER only (Lemke and Rothlin, 2008). GAS6 is 40% identical to Protein S and was originally cloned from serum-starved NIH3T3 cells (Manfioletti et al., 1993; Sasaki et al., 2006). The TAM receptors are expressed in many tissues and are implicated in many disease processes including cancer (reviewed in Linger et al., 2008).

Developmental expression of TAM family members within the testis

TYRO3, AXL, and MER are expressed in different testicular cells types at various stages of development. These differences reflect the distinct functions of each

**Figure 1.2** Structure of the TAM family of RTKs. The extracellular domain of the TAM family contains two immunoglobulin-like domains (semicircles), followed by two fibronectin type III repeats (green box). Next there is a single pass transmembrane domain, and finally a catalytically active tyrosine kinase (TK) domain (red box).

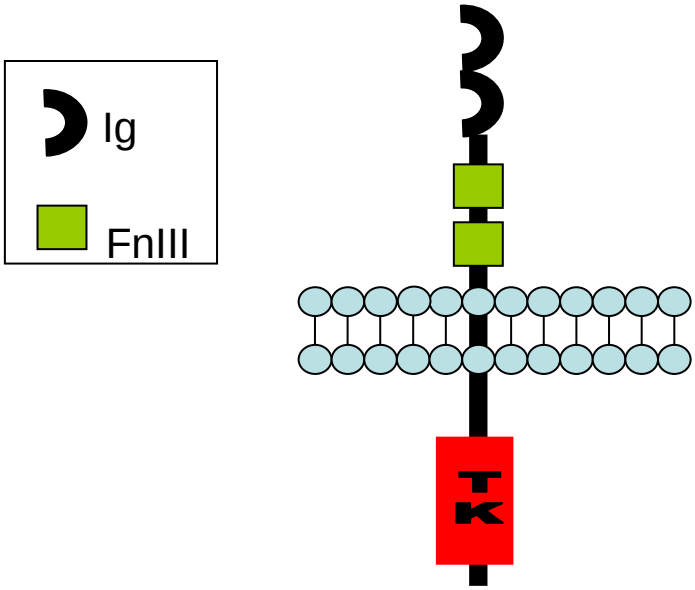


TYRO3/AXL/MER

family member in the testes. In early developing testes, TYRO3 and AXL are expressed only in Sertoli cells, while MER is found predominantly in the cytoplasm of primitive spermatogonia and Leydig cells, with low levels of expression in Sertoli cells (Wang et al., 2005). By postnatal day 14, MER expression in spermatogonia was absent, while cytoplasmic staining in Leydig cells is maintained. In mature testis, TYRO3 and AXL are localized to Sertoli cells in a stage-dependent manner. Stage-dependent staining suggests a role for Sertoli cells in regulating the function of other cell types that are present at that particular stage. TYRO3 is expressed in spermatocytes and round spermatids at stages I-VI (Wang et al., 2005). At stages VI-VIII, these authors reported strong staining around the heads of elongating spermatids, and that staining intensity decreased at stages IX-XII because of the disappearance of round spermatids and localization of staining around elongating spermatids (Wang et al., 2005). These same authors reported expression of AXL in Sertoli cells and Leydig cells at stages I-VI. MER staining in the adult maintained expression in Leydig cells (Wang et al., 2005).

Phenotypic characteristics of TAM Knockouts

Null alleles of TAM family members have been generated in mice. No single knockout receptor results in a phenotype, however, when multiple family members are eliminated specific phenotypes occur. Triple mutants of TAM receptors decrease testis function and sperm production. No individual TAM receptor is essential for embryonic development and subsequent reproductive function (Lu et al., 1999). In contrast, triple null allele females have irregular ovarian histology, although reproductive ability is not always affected. Wu et al. (2008) reported a high incidence of distal vaginal atresia in

female triple mutant mice, but *Mer* seems to play the most critical role in this finding. In male mice deletion of all three TAM RTKs completely abolished their ability to reproduce (Lu et al., 1999). Testes of triple mutant males were 1/3 the size of their wildtype counterparts, the epididymi were completely lacking in mature sperm, spermatogenesis was perturbed and seminiferous tubule cellular organization was disrupted (Lu et al., 1999). With regard to the seminiferous tubules, the number of round spermatids was reduced in tubule stages VII and VIII, significantly fewer spermatocytes were present at the pachytene stage of meiosis, and very few cells had the morphological characteristics of mature sperm (Lu et al., 1999). In older males (approximately 6 months of age), tubules were almost entirely depleted of germ cells. These data indicate that the TAM family of RTKs and their ligands were necessary for Sertoli cell function to be properly regulated. Sertoli cells are known to supply the essential physical and nutritive support for developing spermatogenic cells including spermatogonia, spermatocytes, and spermatids. This support depends upon the signaling interactions among cells found within the testes as well as from cells found in the pituitary. The TAM RTKs combined activation may be necessary for Sertoli cells to produce germ-cell trophins that are essential for proper environmental conditions.

*Axl* RTK

Each TAM family member is important for proper spermatogenesis to occur, but *Axl* is the specific member that will be further evaluated in this study. *Axl*, also known as UFO and Ark, is a receptor tyrosine kinase that was originally isolated in 1991 from patients with chronic myelogenous leukemia (CML) which is one of several chronic

myeloproliferative disorders (Liu et al., 1988; Janssen et al., 1991; O'Bryan et al., 1991; Rescigno et al., 1991; Hafizi and Dahlback, 2006). *Axl* is expressed in many tissues and has a variety of different functions in cells. *Axl* has been mapped to chromosome 19q13.1-2 in humans (Janssen et al., 1991; Rescigno et al., 1991) and a high frequency of abnormalities in this locus is found in malignant gliomas (Jenkins et al., 1989). The region of the murine genome corresponding to the human locus is on chromosome 7 near the quivering locus, which when mutated in mice is responsible for neurological disorders (D'Eustachio et al., 1988). The extracellular domain of AXL, namely the two immunoglobulin domains, resembles that of Neural Cell Adhesion Molecule (N-CAM) and exhibits an adhesive phenotype that is independent of its intracellular tyrosine kinase domain (Bellosta et al., 1995; McCloskey et al., 1997; Hafizi and Dahlback, 2006). AXL is overexpressed in several types of cancer including breast, colon, lung, esophageal, and thyroid cancers (reviewed in Linger et al., 2008). The oncogenic potential of AXL is found within its intracellular tyrosine kinase domain, which can be constitutively activated without the binding of its ligand to the extracellular domain (Hafizi and Dahlback, 2006). The binding partners of AXL are well known through yeast two-hybrid assays using a variety of cDNA libraries. AXL has been shown to function in the RAS/ERK pathway by interaction with SRC, GRB2, and RanBPM (RanBP9) and in the AKT signaling pathway via interaction with C1-TEN and PI3K (Hafizi et al., 2002; Hafizi et al., 2005a; Hafizi et al., 2005b). The interaction with PI3K implicates the role of AXL in cell survival, proliferation, and migration.

The function of *Axl* in aggregation

The extracellular domain of AXL is closely related to other cellular adhesion molecules such as N-CAM and L1. The two immunoglobulin domains on the extracellular portion of AXL allow this protein to be classified as part of the immunoglobulin superfamily of integral membrane proteins that mediate cell-cell interactions (Bellosta et al., 1995). However, the effect of AXL on cell-cell interaction has not been precisely characterized. Bellosta et al. (1995) demonstrated that when the extracellular domain of AXL is overexpressed in *Drosophila* S2 and NIH3T3 cells aggregation is enhanced. Confirmatory experiments with anti-AXL extracellular domain antibody fragments inhibited this aggregation of cells. CHO cells overexpressing full-length AXL had increased aggregation ability as compared to controls that overexpressed a chimeric protein containing the extracellular portion of FGFR-2 (BEK) with the intracellular part of AXL (Bellosta et al., 1995). Although Bellosta et al. (1995) found that the intracellular tyrosine kinase domain of AXL was not necessary to cause an induction of aggregation, Vajkoczy et al. (2006) reported that when the intracellular RTK domain of AXL is deleted (AXL-Dominant Negative) and the mutant gene introduced into gliomal cell lines, those cells appear to round up and lose their filopodia and cell-cell interaction abilities. These findings suggest that either the extracellular domain of AXL-DN or the lack of the intracellular domain acts to inhibit the function of full-length AXL in cell-cell adhesion and aggregation possibly by preventing endogenous AXL from being phosphorylated. This effect is likely to be mediated either by the absence of a

tyrosine kinase domain on AXL-DN or by AXL-DN induced sequestration of the native AXL within the cell leading to inhibition of natural signaling pathways.

Neither of the studies cited above (Bellosta et al., 1995; Vajkoczy et al., 2006) addressed the ability of AXL to aggregate when bound to its ligand GAS6. McCloskey et al. (1997) reported that in the murine myeloid cell line, 32D, overexpression of AXL has no effect on aggregation of the cells. However, when GAS6 is added to cells expressing full-length AXL, aggregation occurred. Introduction of a truncated form of AXL, expressing only the extracellular and transmembrane domains (AXL-ECD), caused an inhibition in the aggregation of this cell line in a dose dependent manner (varying amounts of AXL-ECD) when stimulated with GAS6. The varying ability of AXL and its mutated forms to induce, inhibit, or block aggregation seems to suggest that its function is dependent on the cell line in which it is expressed.

Axl-like

The TAM family of RTKs is well studied, not only in the testes, but also in a variety of tissues. Our laboratory wanted to determine if there are any other proteins in the testes related to AXL or other members of the TAM family. A sequence homology search of the National Center for Biotechnology Information's (NCBI) database for expressed sequence tags (ESTs) identified two uncharacterized ESTs related to AXL. The first was derived from a type of mammary tumor, and the second was expressed in the testes. The second transcript (accession number AK033237) was originally isolated from murine embryonic day 15 male testis cDNA (NCBI website), and encoded a truncated version of *Axl*. Our laboratory has termed this transcript *Axl-like*, based on its

structural characteristics and similarity to *Axl* (Figure 1.3). *Axl* and *Axl-like* contain identical sequences in the extracellular and transmembrane domain but diverge at the end of exon 15 of *Axl*. *Axl-like* does not contain the intracellular tyrosine kinase domain. Essentially, *Axl-like* appears to be a naturally occurring kinase-inactive version of *Axl*. The difference in *Axl-like* and the man-made AXL-DN lies in two main locations. First, the AXL-DN constructs do not contain the read-through into the intronically expressed portion of exon 15 (Figure 1.3 B). Secondly, the AXL-DN constructs only have a deletion of the tyrosine kinase domain, while *Axl-like* does not contain several exons prior to the tyrosine kinase domain.

It was previously discussed that the natural function of RTKs is to respond to ligand stimulation by dimerization, followed by autophosphorylation, and interaction with other proteins to activate downstream signaling pathways. With a dominant-negative protein lacking the RTK domain, this cascade of events is blocked. In this situation, the kinase-inactive RTK interacts with its wild-type counterpart but is unable to phosphorylate its wild-type partner and therefore normal signaling pathways cannot be activated. The proposed action of AXL-LIKE upon AXL is similar to that just described (Figure 1.4). While normal dimerization and phosphorylation of AXL causes cellular migration, adhesion, survival, and proliferation, the dimerization of AXL and AXL-LIKE may result in inhibition of these cellular actions.

**Figure 1.3** Comparison of the structural arrangement of *Axl* and *Axl-like*. (A) Depiction of the exon-intron arrangement of the gene encoding *Axl* and *Axl-like*. *Axl-like* is an alternatively spliced transcript from the *Axl* gene. The red exon indicates differences in sequences between the two isoforms. Exon 15 in *Axl-like* is a large exon that represents a read-through the intervening intron of *Axl-like*. The red asterisk (*) indicates the primary phosphorylation site, while the green asterisks indicate a possible secondary phosphorylation site. Blue diamonds indicates the position of stop codons. (B) A closer examination of the amino acid sequence of exon 15 of *Axl-like* compared to 15 and 16 of *Axl*. The additional amino acid sequence encoded by the intron are indicated by red lettering. The sequence of *Axl* does not contain the intronic portion. The green asterisk indicates a possible secondary phosphorylation site.

A.


1 2 3 4
5 6
7 8 9 10
11 12
13 14
15 16 17 18 19
20
Axl
1 2 3 4
5 6
7 8 9
11 12
13 14
15
Axl-like

B.

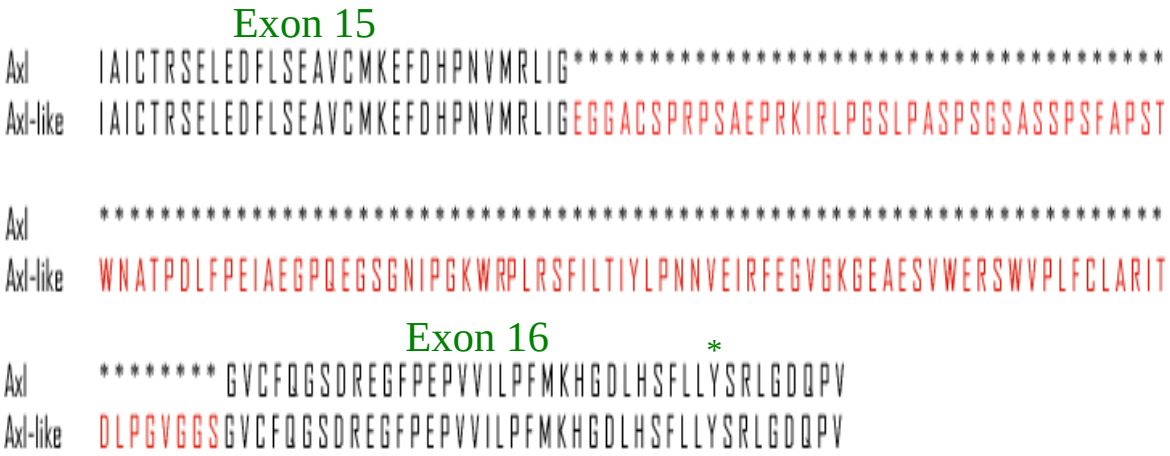
Exon 15
Axl
Axl-like
Axl
Axl-like
Exon 16
Axl
Axl-like

**Figure 1.4** Proposed action of AXL-LIKE on AXL. With normal dimerization of AXL, following stimulation and binding by its ligand GAS6, autophosphorylation occurs, followed by signaling through downstream pathways. This regulates cellular migration, adhesion, survival, and proliferation. In contrast, when AXL dimerizes with AXL-LIKE, lacking the tyrosine kinase domain, phosphorylation does not occur which disrupts subsequent signaling pathways and cellular processes.

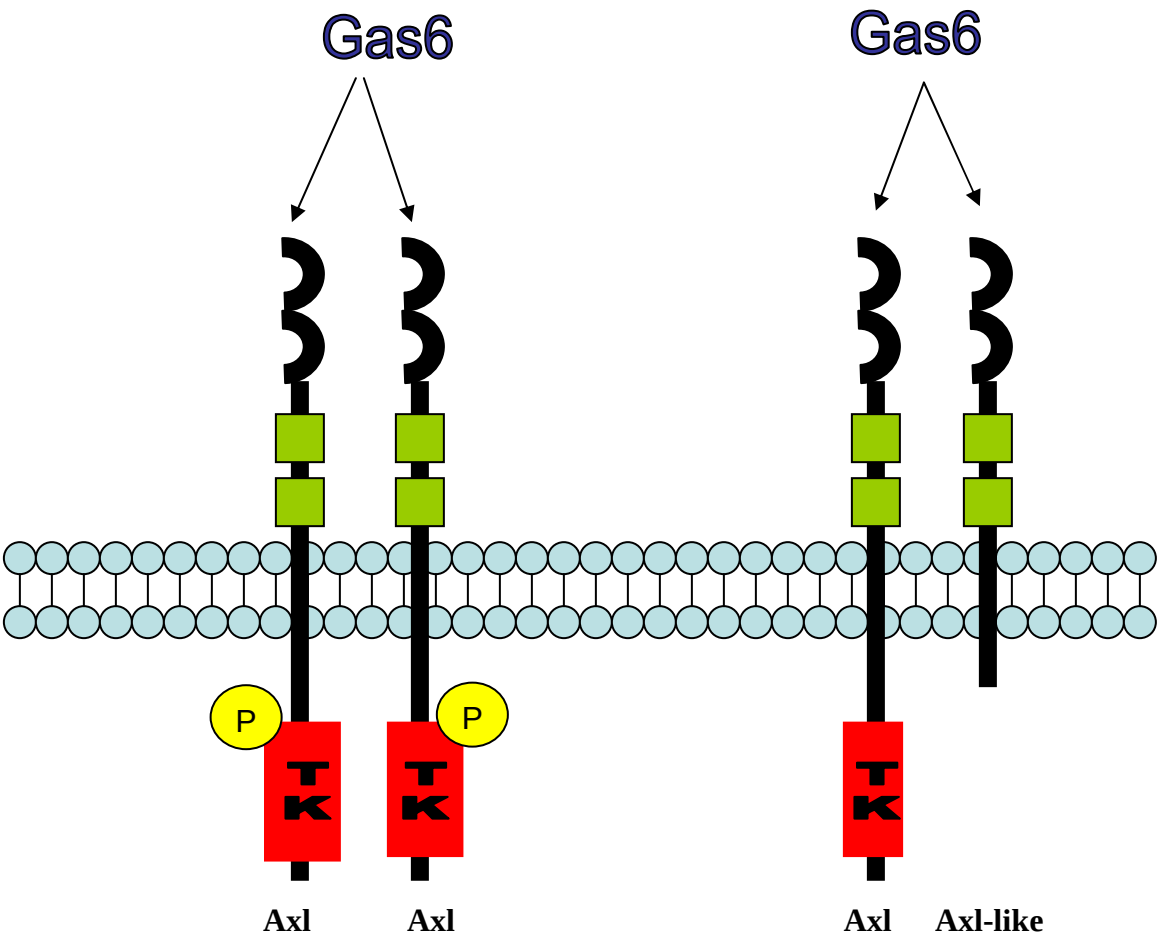


**Promotes Migration Adhesion Survival and Proliferation**

**Inhibits Migration and Adhesion**

**D. Rationale for current studies**

Triple deletion mutants of TAM receptors have been created in mice and exhibit decreased testis function and sperm production. This detrimental effect on reproduction in males provides support to study the expression and function of *Axl* in the developing testes. With the identification of a truncated isoform of *Axl* in the testes, we set out to determine whether *Axl-like* is expressed only in embryonic testes tissue or whether it is expressed in later times in development. Preliminary work using Northern blot hybridization techniques determined that *Axl-like* is expressed at much lower levels in the adult testes or other adult tissues compared to *Axl* (Figure 2.4). Animal studies were therefore designed to investigate the expression of *Axl-like* within the developing testes of the mouse. Prior studies (Wang et al., 2005) determined that AXL is expressed in developing testes in association with Sertoli cells. The high sequence homology between *Axl* and *Axl-like* suggested expression of both proteins in the testes. It is important to determine not only if both proteins are expressed in the testes but also the cell types in which they are expressed and whether they are co-expressed by the same cells. If there is interaction between the two proteins, this would suggest the potential that AXL-LIKE may regulate the expression or function of AXL (Figure 1.4).

Our studies have utilized cellular models to address the interaction of AXL and AXL-LIKE and to measure protein phosphorylation in cells transfected with *Axl* or *Axl-like* transcripts. We were unsuccessful in demonstrating a direct interaction between AXL and AXL-LIKE; however, our data indicate that AXL-LIKE does inhibit the increase in filopodia observed when AXL is overexpressed. This research provides

useful information concerning the role of AXL in promoting cytoskeletal changes that may enhance the metastasis of cancer cells and suggests a possible application of AXL-LIKE as a new therapeutic agent.

**E. Statement of hypothesis and specific aims**

Hypothesis

*Axl-like* is an alternatively spliced dominant negative form of *Axl* expressed in the testes and its purpose is to inhibit the physiological functions of AXL.

Specific aim I: To determine *Axl* and *Axl-like* mRNA expression in prenatal, early postnatal, and adult testis.

A. *Northern blot:* Adult murine tissues (brain, heart, spleen, lung, liver, kidney, skeletal muscle, and testis) were hybridized with radioactive probes specific to *Axl* and *Axl-like* in order to determine the tissue distribution for the two transcripts.

B. *Animals:* Parental mice underwent genotyping and wildtype mice were bred in the Comparative Medicine Department at East Carolina University. Total RNA was isolated from testes obtained from early postnatal (7dpp, 14dpp, and 21dpp) and adult mice, while total RNA was isolated from whole embryos obtained from prenatal mice (e15).

C. *RT-PCR:* Total RNA was isolated from the developing testes, reverse transcribed, and gene specific primers to *Axl* and *Axl-like* were designed and used to amplify each transcript from cDNA.

D. *Quantitative analysis of mRNA content:* Real-time PCR was performed on embryonic day 15, 7 dpp, 14 dpp, 21 dpp and adult testis total RNA using $RT^2$ SYBR Green/Fluorescein qPCR Master Mix. Results were analyzed according to the method of Livak and Schmittgen (2001).

Specific Aim II: To determine if AXL-LIKE functions through its interaction with AXL.

A. *Constructs:* Gene expression constructs were created with *Axl* cloned into a pcDNA 3.1/*myc*-His vector and *Axl-like* cloned into a p3XFLAG-CMV™-14 vector.

B. *Cellular transfections:* COS-7 cells were transiently transfected via electroporation with constructs containing empty GFP vector, empty Myc vector, empty Flag vector, *Axl*-Myc, *Axl-like*-Flag, or both *Axl*-Myc and *Axl-like*-Flag constructs.

C. *Cellular localization:* Cellular localization of AXL and AXL-LIKE in COS-7 transfectants was determined by indirect immunofluorescent visualization. The transfected cells were fixed and immunostained with anti-Myc and/or anti-Flag primary antibodies and the appropriate secondary antibodies. Cell nuclei were visualized by staining of DNA with DAPI.

D. *Filopodia analysis:* Transfected COS-7 cells were stained with anti-Myc and/or anti-Flag primary antibodies with the appropriate secondary antibody and visualized by indirect immunofluorescence. The total number of filopodia in transfected cells were counted and analyzed by imaging software.

E. *Mean cell area analysis:* The total cellular square area of transfected cells was measured and analyzed by imaging software.

F. *Interaction studies: Axl*-Myc and *Axl-like*-Flag were co-transfected into COS-7 cells to determine immunofluorescent co-localization using anti-Myc and anti-Flag primary antibodies. *Axl*-Myc or *Axl-like*-Flag transiently transfected COS-7 cells were analyzed to determine protein interaction using immunoprecipitation and co-immunoprecipitation of cell lysates with anti-Axl and anti-Flag antibodies on protein G beads followed by western blot analysis. Analysis of the total amount of AXL in cellular lysates by immunoblot was employed to determine the effect of AXL-LIKE on the expression of AXL.

G. *Phosphorylation studies: Axl*-Myc and *Axl-like*-Flag transiently transfected COS-7 cells were stimulated with GAS6 to determine whether overexpression of AXL-LIKE affects the phosphorylation state of AXL. Immunoprecipitation and co-immunoprecipitation with anti-Axl antibody on protein G beads and western blot analysis with anti-phospho-tyrosine antibodies were employed to detect phosphorylated protein.

# CHAPTER II: AXL AND AXL-LIKE mRNA EXPRESSION IN PRENATAL, EARLY POSTNATAL, AND ADULT TESTES

## A. Summary

The TAM (*Tyro3*, *Axl*, *Mer*) family of receptor kinases is known to play a role in spermatogenesis and is necessary for reproduction. Prior studies have evaluated the involvement of the TAM family in spermatogenesis in the developing murine testes using immunohistochemical, RT-PCR, and Northern blotting techniques. However, the relative mRNA levels of *Axl* in developing testes have not been assessed. A new protein termed *Axl-like* with high sequence homology to *Axl* but lacking the intrinsic tyrosine kinase domain was identified by a search of the NCBI-EST database. The *Axl-like* gene has not been studied previously. Preliminary experiments using Northern blotting techniques demonstrated *Axl* to be expressed in multiple tissues in adult mice, with high transcript levels present in the heart and testis tissue, while *Axl-like* transcript levels were below the level of detection in these tissues (Figure 2.4). The lack of detectable *Axl-like* transcript in adult tissues suggests that the transcript is found only in the early developmental stages of the mouse. The present study analyzes *Axl* and *Axl-like* expression at developmental milestone days in murine testes. These milestones are defined by the presence of specific cell types during development of the testes. Real-time PCR was performed to measure expression of these two genes normalized against the transcript level detected in the adult. Statistical analyses indicated that the expression of *Axl* was significantly higher on

7 days post partum (dpp) than on the other days measured. The relative level of *Axl-like* mRNA at 7dpp was significantly higher than at 21dpp, but not significantly different from e15 or 14dpp. The greater expression of *Axl* and *Axl-like* at 7dpp coincides with the time of the greatest number of Sertoli cells in the testes. The relative number of Sertoli cells decreases as the mouse ages and other testicular cell types increase. This pattern correlates with the gradual decrease in the expression levels of both *Axl* and *Axl-like* with testes development. The expression pattern of *Axl* and *Axl-like* is consistent with the hypothesis that there is a specific expression of these two genes in Sertoli cells of developing mouse testes. The expression of *Axl-like* in the early postnatal testes had not been investigated prior to these studies and these results may indicate that *Axl-like* is important in regulating the spermatogenic process.

**B. Introduction**

Sertoli and Leydig cells maintain homeostasis in the testis while germ cells preserve the population of spermatogenic cells to ensure the ability to reproduce. There are spermatogenic cells in varying stages of maturity within the testes during the time frame examined in this study. These cell types and processes involved in spermatogenesis were discussed in detail in Chapter I. This chapter will focus on the cellular components and events occurring within the murine testes from the prenatal period through early adulthood. Primordial germ cells of the testes are suspended in mitosis from the late prenatal time period until 7dpp. At this point (7dpp) primordial germ cells resume mitosis and begin their two meiotic divisions on their way to becoming

spermatids. Spermatids then undergo a process called spermiogenesis, which involves formational changes in order to develop into fully mature and functional sperm. These developmental processes require non-germline cell types in order to ensure the proper progression of spermatogenesis.

The prenatal mouse testis contains both Sertoli cells and primordial germ cells, which are precursors to the cells that ultimately will maintain the germ cell population throughout the life of the mouse. Sertoli cells have a variety of functions within the testes including synthesizing ABP, secreting inhibin or MIF, as well as phagocytosing apoptotic spermatogenic cells and residual bodies (Xiong et al., 2008). The spermatogonial cells are arrested in mitosis until 5dpp, when a cascade of cellular division ensues yielding a variety of different spermatogenic cell types. Spermatogenesis continues with Type A spermatogonia completing mitosis to yield identical daughter cells and/or Type B spermatogonia (Allen, 1918; Bellve et al., 1977). Type A spermatogonia maintain the germ cell population of the testes, while Type B spermatogonia divide and differentiate to give rise to primary spermatocytes. Primary spermatocytes undergo meiosis I to produce secondary spermatocytes, which then go through a second meiotic division to yield spermatids. Spermatids are then transformed into mature sperm by a process called spermiogenesis that includes nuclear condensation and elongation, formation of sperm specific structures, and removal of excess cytoplasm.

The cellular composition of the testis changes during the late fetal and the early postnatal period and is summarized in Table 1.1. Several milestone days were chosen for study because of the cell types present and the events occurring at that time of

development. Embryonic day 15 (e15) was chosen because spermatogonial cells are arrested in mitosis and the testes contain only primordial germ cells and Sertoli cells. By 5 days postpartum (dpp), mitosis has resumed and the development of germ cells into Type A and Type B spermatogonia has begun. By 14dpp, meiosis I has concluded yielding a large number of secondary spermatocytes in the testis. At 21dpp, meiosis II is completed and spermatids are ready to initiate spermiogenesis. Because of the requirement to continuously produce new sperm, the adult testes contains all cell types in various stages of mitosis, meiosis, and spermiogenesis. The adult was chosen as a basis for comparison of mRNA levels because the adult testis contains a complete population of differentiating cell types. These time points provide a preliminary insight into what cell types may express the proteins AXL and AXL-LIKE, because each time point contains a different percentage of the cell types found in the testes. For example, testis at 7dpp contain a population of 77% Sertoli cells and 23% spermatogonia, while at 21dpp there are only 28% Sertoli cells and 10% spermatogonia, with the largest cell type present being primary spermatocytes at 57% (Table 1.1). The following experiments were designed to correlate *Axl-like* expression in the testes with the presence of known populations of spermatogenic cell types. Knowledge of the expression pattern of *Axl-like* in the developing testis will facilitate determination of potential cell types that express *Axl-like* and permit design of future studies to examine its function in spermatogenesis.

Sertoli cells play an important part in regulating the environment within the seminiferous epithelium of the testes. It should be noted that Sertoli cells are capable of division only in prenatal and early postnatal stages of development (Orth, 1982). Orth et

al. (1988) determined that the spermatid number in adult rats is directly proportional to the number of Sertoli cells produced during the perinatal developmental period. That study utilized an antimitotic drug injected into the testes of newborn rats to halt the proliferation of Sertoli cells. Injections were given during a very small time frame when Leydig and germ cells were not undergoing division. Also, rapid clearance of the drug prevented other cell types from being affected. Adult rats treated with the antimitotic drug during the postpartum period contained 54% fewer Sertoli cells and 55% fewer round spermatids compared with untreated control animals. The fertility and sperm production of Sertoli cell-depleted rats was not assessed in this study. However, based on their findings, one can speculate that the Sertoli cell-depleted rat may still be able to produce mature sperm and reproduce but at a lower capacity. These findings suggest that the production of mature sperm is directly dependent upon Sertoli cells, and the proper functioning of Sertoli cells is important to maintain reproduction.

*Axl* and its family members, the TAM RTKs, have been studied in many different disease states and tissues, including the testes. TAM RTKs are localized to Sertoli cells and spermatogenic cells at differing staining intensities and time points in the late embryonic period and continuing to 56dpp (Wang et al., 2005). Prior immunohistochemical studies indicate that MER is primarily localized in the cytoplasm of primitive spermatogonia and Leydig cells of mice on days 3 and 7 postpartum. Weak staining was also observed in Sertoli cells at this time. By 14dpp, MER staining in spermatogonia is absent and Leydig cells are found to express MER most abundantly. Between 12.5 and 14.5dpc, TYRO3 was localized to the male genital ridge in primordial

germ cells and pre-Sertoli cells (Matsubara et al., 1996). At birth, TYRO3 localization was solely in Sertoli cells. TYRO3 is found only in Sertoli cells until 14dpp, at which time there is also staining in spermatocytes and round spermatids (Wang et al., 2005). AXL is localized predominantly to Sertoli cells within the testes (from 3dpp to 35dpp), with some slight staining in Leydig cells in the more mature mouse at 56dpp (Wang et al., 2005).

The function of the TAM family has also been shown to be important for normal spermatogenesis with the process being completely disrupted if all family members are deleted (Lu et al., 1999). *Mer* has been shown to be the main TAM receptor involved in the phagocytosis of apoptotic cells and residual bodies within the testes, while utilizing the other family members as supporting receptors in this process (Xiong et al., 2008). Matsubara et al. (1996) determined via *in situ* hybridization that primordial germ cell development, sexual differentiation, and Sertoli cell function is mediated by *Tyro3*. The function of *Axl* in the testes has not been established. In other tissues *Axl* induces cell survival, proliferation, and migration (Bellosta et al., 1995; Zhang et al., 1996; Heide et al., 1998). *Axl* has been determined to support other family members in the proper functioning of the testes (Lu et al., 1999; Xiong et al., 2008). The role of the AXL-LIKE protein in spermatogenesis, though originally identified in embryonic day 15 testes cDNA, has not been assessed. With its high sequence homology to *Axl*, one would hypothesize that it too may be involved in spermatogenesis. This study aims to determine the expression of *Axl-like* in prenatal, early postnatal, and adult testes by measuring the relative amounts of mRNA using real-time PCR methodology. Based on

previous studies, *Axl* is predominantly localized to Sertoli cells and we hypothesize that *Axl-like* will also exhibit a similar expression pattern. The expression pattern of *Axl-like* within developing testes is important to assess its function. Expression during fetal life would suggest a function in testes development and/or gene regulation, whereas expression in postnatal days might suggest a function in meiotic division of spermatocytes or a role in regulating the morphological changes associated with spermiogenesis.

**C. Experimental Procedures**

*Northern blot*

A cDNA probe to the 5′ end of *Axl* was prepared by PCR amplification in a 25 μl reaction volume containing 1 μl of DNA isolated from the *Axl* gene transcript, 1x *Ex Taq* Buffer (Takara Bio Inc., Japan), 500 μmol of each dNTP, 1.25 units of *Ex Taq* polymerase, and 1 μM of each primer. Amplification of *Axl* consisted of a "Hotstart" after denaturation at 95°C for 5 min, a long annealing at 55°C for 5 min, followed by 40 cycles at 95°C for 1 min, 55°C for 2 min, and 72°C for 1 min in a PTC-200 DNA Engine thermal cycler (MJ Research Inc., Watertown, MA) was performed. An extension time of 10 min at 72°C was added at the end of the final cycle followed by a holding temperature at 4°C until the reaction was removed from the machine. The entire sample was subjected to electrophoresis on an ethidium bromide-stained 2% low melting point (LMP) agarose gel. A band representing the *Axl* Northern probe is expected at ~550bp

(Figure 2.1 A). The primers for the *Axl* cDNA probe were Axl Oligos5'-1 and Axl Oligos 3'-7 (Table 2.1 for primer sequences).

A cDNA probe specific to the intronically expressed portion of *Axl-like* was amplified by PCR in a 50 μl reaction volume containing the same components as the *Axl* cDNA probe PCR reaction (see above). Amplification for *Axl-like* consisted of a denaturation at 94°C for 1 min, followed by a long annealing at 60°C for 5 min. Repeated amplification with 40 cycles at 94°C for 30 sec, 60°C for 30 sec, and 72°C for 30 sec in a PTC-200 DNA Engine thermal cycler (MJ Research Inc., Watertown, MA) was performed. An extension time of 10 min at 72°C was added following the final cycle and a holding temperature at 4°C was employed until the reaction was removed from the machine. The entire sample was electrophoresed on an ethidium bromide-stained 2% LMP agarose gel. A band representing the *Axl-like* Northern probe is expected at 139bp (Figure 2.1 B). The primers for the *Axl-like* cDNA probe were Axl-like5'-mid and Axl-like3'-2117 (Table 2.1).

A multiple tissue Northern blot membrane was purchased from Clontech Laboratories, Inc. (Mountain View, CA) containing 2 μg of adult murine tissue polyA+ RNA to brain, heart, lung, liver, spleen, skeletal muscle, kidney, and testis. The membrane was prehybridized by incubation at 68°C for 30 min with ExpressHyb solution (Clontech, Mountain View, CA). The radioactive hybridization probe was created using the High Prime DNA Labeling Kit (Roche Applied Science, Mannheim, Germany). The cDNA probe was first denatured by heating the 2% LMP agarose gel containing the *Axl* or *Axl-like* amplification product at 95°C for 2-5 min. The radioactive probe was

**Figure 2.1** PCR amplification of Northern blot cDNA probes. (A) An ethidium bromide stained 2% LMP agarose gel containing the PCR amplification product of a cDNA probe to *Axl* is shown. Expected amplification size is approximately 550bp (arrow), while smaller bands indicate non-specific amplification products. Lane 1, 100bp ladder, lane 2, *Axl* probe. (B) PCR amplification of a cDNA probe specific to *Axl-like* and electrophoresis on an ethidium bromide stained 2% LMP agarose gel. Expected amplification size is 139bp (arrow), while product below 100bp indicates primer dimer. Lane 1, 100bp ladder, Lane 2, *Axl-like* probe. Excess lanes depicting a separate, unrelated PCR were deleted to simplify the figure.

A.

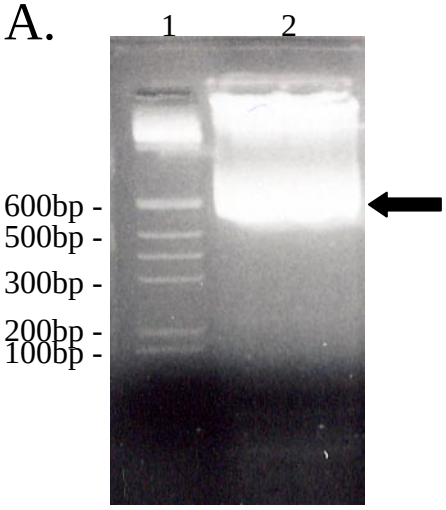
1
2
600bp -
500bp -
300bp -
200bp -
100bp -

B.

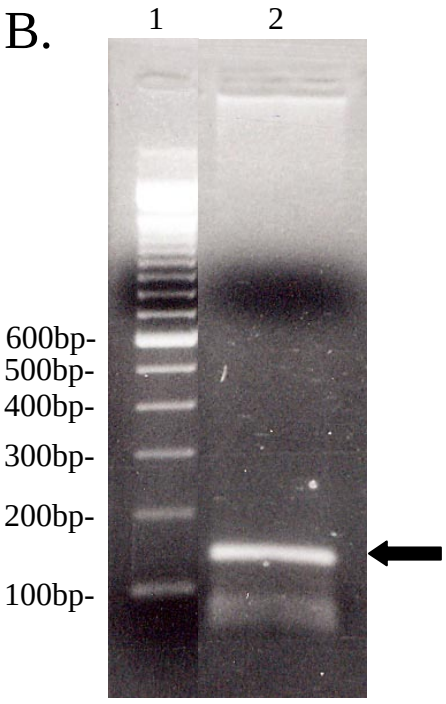
1
2
600bp-
500bp-
400bp-
300bp-
200bp-
100bp-

**Table 2.1** Primers used for Northern probes, genotyping, sex determination of embryos and real-time PCR.

| Primer Name | Sequence |
|---|---|
| Axl Oligos5'-1 | GCT GAC CCT ACT CTG GCT TCA AG |
| Axl Oligos3'-7 | GCA GGC TGT CAC AGA CAC AGT CA |
| Axl-like5'mid | GTG AGG GAG GAG CAT GTT CTC CCA GGC |
| Axl-like3'-2117 | CAG GGG TCG CAT TCC AAG TTG AGG GAG |
| AXL-Lu59 | AGA AGG GGT TAG ATG AGG AC |
| AXL-Lu60 | GCC GAG GTA TAG TCT GTC ACA G |
| AXL-Lu61 | TTT GCC AAG TTC TAA TTC CAT C |
| SRY5' | GAG AGC ATG GAG GGC CAT G |
| SRY3' | GAG TAC AGG TGT GCA GCT C |
| Axl-like5'ex14 | CTC AAG GTC GCT GTG AAG ACC ATG |
| Axl Oligos3'-6 | GCT TCT GGG AAA CCC TCT CTG TC |
| Axl Oligos5'-4 | GCG TGG TCC TTC GGT GTG ACA ATG |
| Axl Oligos3'-5 | GCT CCT TGA CGC AGG TAG TCG TA |
| Axl-like5'intron | GGA GGA GCA TGT TCT CCC AGG CCC |
| GAPDH(+) | ATG TGT CCG TCG TGG ATC TGA |
| GAPDH(-) | GAT GCC TGC TTC ACC ACC TT |

synthesized with Klenow polymerase by random priming of cDNA. Six μl of $dH_20$ and *Axl* or *Axl-like* PCR probe was combined with a mixture of 5 μl 5x buffer, 1 μl dGTP, 1 μl dCTP, 1 μl dTTP, and 5 μl $\alpha$-$^{32}$P dATP to yield a 25 μl total reaction volume. This 25 μl reaction was incubated at 37°C for 1 hr, followed by heating at 65°C for 3 min. The radioactive probe was then purified on a G50 micro-column by centrifugation for 2 min at 735 x g in order to separate the radioactive probes from the unincorporated nucleotides, and incubated with the membrane in ExpressHyb solution overnight at 68°C with shaking. The following day, the membrane was rinsed twice with 2x Sodium Chloride-Sodium Citrate (SSC) + 0.1% SDS, washed with the same solution three times for 15 min while shaking at room temperature, and finally washed twice with 0.2% SSC + 0.1% SDS for 15 min at 68°C while shaking. The blot was then exposed to Kodak BioMax XAR film (Rochester, NY) at -80°C for approximately 3 days (*Axl*) or for 2 weeks (*Axl-like*) with intensifying screens (Figure 2.4).

*Animals*

All the mice used in this study were produced in a breeding colony housed in the Comparative Medicine Department at East Carolina University and were maintained in accordance with the approved Animal Use Protocol W179c. Experimental animals were the progeny of a wildtype colony, confirmed by PCR, of an *Axl* knockout line derived from C57Black/6 and SV129 mice. Wild type parental mice were identified by genotyping (see later). These mice were kindly provided by Dr. Greg Lemke of The Salk

Institute (La Jolla, CA). Postpartum day 7 (7dpp), 14dpp, and 21dpp mice were anesthetized with isoflurane and then sacrificed by pentobarbital overdose (IP). Testes were immediately removed and placed in 1 ml of TRIzol® Reagent (Invitrogen Corporation) on ice. Embryonic day 15 (e15) mice were produced by mating adult wildtype mice. The time of coitus and fertilization (day 0) was assumed to be midnight after mating upon visual inspection of a plug in the female's vagina. Pregnant female mice were anesthetized with isoflurane and then sacrificed by cervical dislocation. Pups were excised from the uterus and decapitated to ensure death. Decapitated pups were then immediately placed in TRIzol® reagent on ice. Adult male mice were euthanized with $CO_2$ asphyxiation and then cervical dislocation was performed to ensure death. Testes were immediately placed in TRIzol® reagent on ice. Testis tissues were homogenized using a PRO 200 post mounted homogenizer (PRO Scientific Inc., Oxford, CT).

*Parent genotyping*

Tailsnips were recovered from weaned mice for genotyping to determine whether they were wildtype, heterozygous or homozygous *Axl* knockouts. Tailsnips were placed in a 1.5 ml eppendorf tube with 700 µl of Tail Lysis Buffer (100 mM Tris-HCl pH 8.5, 200 mM NaCl, 5 mM ethylenediaminetetraacetic acid (EDTA), 0.2% sodium dodecyl sulfate (SDS)). Next, 35 µl of 10 mg/ml fresh Proteinase K (in 50 mM Tris, pH 8.0) was added to the tube and incubated overnight at 55°C with gentle shaking. The next morning, 500 µl of phenol/chloroform was added and the tube shaken vigorously for 3

min at room temperature. The tube was then centrifuged at 16,000 x g for 6 min at room temperature. The aqueous phase was removed and transferred to a new 1.5 ml eppendorf tube. This step was repeated with 500 μl of chloroform. Next, 800 μl of isopropanol was added and the tube shaken by hand for 30 sec from a slow to fast speed. The DNA was recovered by centrifugation for 1 min at room temperature at 16,000 x g. The isopropanol layer was removed, and the pellet was washed with 100 μl of 70% ethanol and vortexed to remove SDS and phenol. The pellet was recovered by centrifugation (16,000 x g) for 1 min at room temperature. The last step was repeated using 100% ethanol. The pellet was allowed to air dry at room temperature for 2 min before being resuspended in 100 μl of Tris-EDTA pH 8.0 in a 1.5 ml eppendorf tube. The tube containing genomic DNA was placed at 55°C overnight before performing PCR.

PCR was performed in a 50 μl reaction volume containing 1 μl of DNA isolated from the tailsnip procedure described above, 1x *Ex Taq* Buffer (Takara Bio Inc., Japan), 500 μmol of each dNTP, 1.25 units of *Ex Taq* polymerase, and 0.2 μM of each primer. Amplification for *Axl* consisted of a "Hotstart" after denaturation at 94°C for 4 min, followed by 35 cycles of 94°C for 1 min, 52°C for 2 min, and 72°C for 3 min in a PTC-200 DNA Engine thermal cycler (MJ Research Inc., Watertown, MA). An extension time of 7 min at 72°C was added at the end of the final cycle followed by a holding temperature at 4°C until the reaction was removed from the machine. Approximately 15 μl of the final sample was separated by electrophoresis on an ethidium bromide-stained 2% agarose gel. A band representing the wildtype *Axl* gene product is expected at 350bp,

while a band representing the mutant gene of the *Axl* knockout is expected at 200bp (Figure 2.2). Heterozygous offspring would contain amplification products at both 350bp and 200bp. Lu59, Lu60, and Lu61 were the primers used for amplification of appropriate sized bands (Table 2.1 for primer sequences).

*Sex determination of embryos*

Murine embryos were needed to assess relative levels of e15 testes total RNA for analysis by real-time PCR of *Axl* and *Axl-like* gene transcripts. Visualization and isolation of the testes at embryonic day 15 (e15) is extremely difficult therefore the whole embryo was used to perform experiments. The sex of e15 pups was determined using cDNA to amplify the male specific *Sry* (sex-determining region Y) gene. Weanling DNA was used to validate this procedure by amplifiction of *Sry* from a known male weanling DNA with a comparison to that obtained from a known female weanling (Figure 2.3 A). Each PCR reaction mixture of 50 μl contained sample DNA (isolated by the method described in the parental genotyping section above), 1x *Ex Taq* Buffer (Takara Bio Inc., Japan), 500 μmol of each dNTP, 1.25 units of *Ex Taq* polymerase, and 1 μM of each primer. Amplification for *Sry* consisted of a "Hotstart" after a denaturation at 95°C for 5 min, followed by a long annealing step at 55°C for 5 min, and 36 cycles at 72°C for 1 min, 95°C for 1 min, and 55°C for 1 min in a PTC-200 DNA Engine thermal cycler (MJ Research Inc., Watertown, MA). An extension time of 10 min at 72°C was added at the end of the final cycle followed by a holding temperature of 4°C until the reaction was

**Figure 2.2** Genotyping of *Axl* heterozygous bred mice weanlings. Each lane represents the amplification product from tailsnip DNA isolations prepared from murine weanlings: lane 2, wildtype; lane 3, knockout; lane 4, heterozygote. Lane 1 indicates a 1kb ladder. The band at approximately 500bp in lane 4 represents non-specific amplification present in all heterozygous mice.

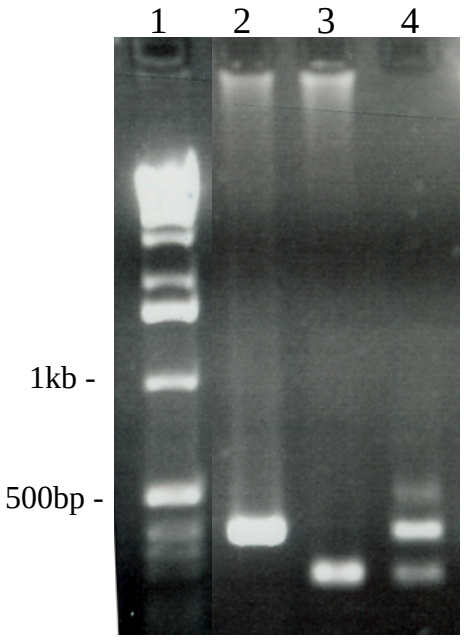
1
2
3
4
1kb -
500bp -

removed from the machine. Approximately 15 μl of the final sample was separated by electrophoresis on an ethidium bromide-stained 2% agarose gel. The *Sry* specific band (380bp) was only present in the males (Figure 2.3 A). Primers for *Sry* were SRY5' and SRY3' (Table 2.1), the same as that reported by Zwingman et al. (1993). It should be noted that if a female has chromosomes of XXY, or has testicular feminization, then she would also amplify the *Sry* gene. This 380bp band corresponds to the *Sry* amplification product reported by Zwingman et al. (1993) in pre-implanted embryos at the blastocyst stage. Non-specific products detected in the current study (Figure 2.3) are thought to be due to utilization of DNA from a tissue sample developed to a much later stage than Zwingman et al. (1993). The band immediately below the 380bp band (Figure 2.3 A) was also seen in the work of Zwingman et al. (1993).

For this study, embryos were excised from the uterus at day 15 and total RNA isolated as previously described. Total RNA was reverse transcribed and PCR was performed on the resulting cDNA. Primers amplifying *Sry* were utilized to determine sex of embryos. Figure 2.3 B shows the ethidium bromide stained 2% agarose gel with the *Sry* PCR amplification product found only in male mice. PCR did not detect an *Sry* transcript in cDNA from female pups at this early stage in development.

*RNA isolation and amplification*

RNA was isolated from tissue using TRIzol® Reagent according to the manufacturer's instructions. One milliliter of TRIzol® Reagent per 100 mg of tissue was used. Reverse Transcriptase (RT)-PCR was performed using an AffinityScript™

**Figure 2.3** Ability to detect *Sry* expression in *Axl* wildtype weanlings and day 15 embryos. (A) Male and female tailsnips first underwent genotyping to verify they were wildtype. PCR amplification was further performed on this DNA to determine if PCR amplification with primers specific to *Sry* could differentiate between male and female cDNA. This ethidium bromide stained 2% agarose gel contains the amplification products from that PCR. Lane 1, 100 bp ladder; lane 2, female weanling; lane 3, male weanling; lane 4, control PCR (no DNA). Arrow indicates a band at 380bp that is indicative of *Sry* amplification and is found only in the male weanling. The amplification product below the 380bp band was also reported by Zwingman et al. (1993) but was not further characterized. (B) Analysis of e15 pup cDNA after RNA isolation and further RT-PCR. Lane 1, 100 bp ladder; lane 2, unknown sex; lanes 3, 6, 8- male pups; lanes 4, 5, 7, 9- female pups.

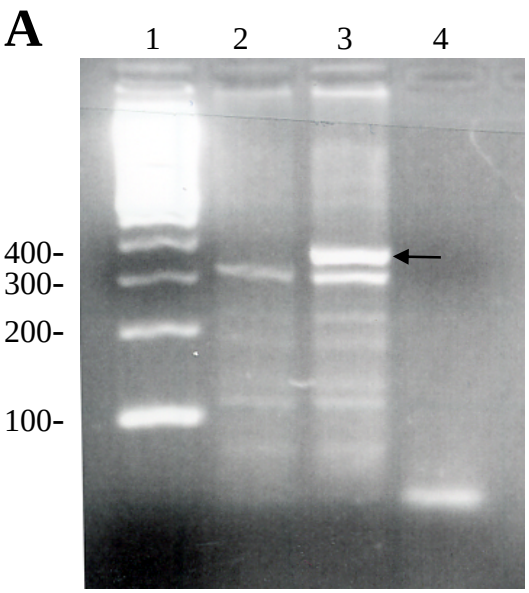
A
1
2
3
4
400-
300-
200-
100-

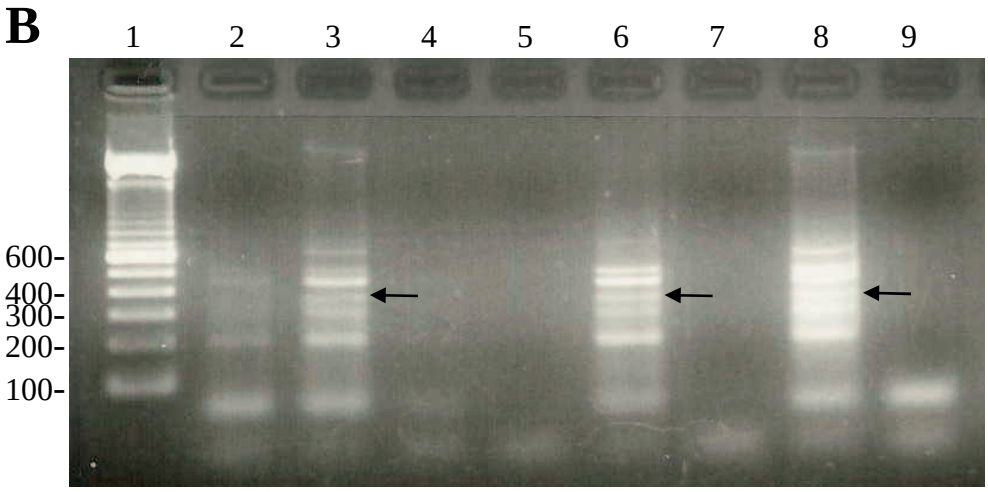
B
1
2
3
4
5
6
7
8
9
600-
400-
300-
200-
100-

Multi Temperature cDNA Synthesis Kit (Stratagene, Cedar Creek, TX) following the manufacturer's protocol. Briefly, 300 ng total RNA was used with random primers to amplify targeted cDNA sequences. Subsequent PCR reactions contained reverse-transcribed cDNA in a 50 μl reaction mixture containing 1x *Ex Taq* Buffer (Takara Bio Inc., Japan), 500 μmol of each dNTP, 1.25 units of *Ex Taq* polymerase, and 1 μM of each primer. Amplification for *Axl* and *Axl-like* consisted of a "Hotstart" after a denaturation at 94°C for 5 min, followed by a long annealing at 55°C for 5 min, and 40 cycles at 72°C for 1 min, 94°C for 30 sec, and 55°C for 30 sec in a PTC-200 DNA Engine thermal cycler (MJ Research Inc., Watertown, MA). An extension time of 10 min at 72°C was added at the end of the final cycle followed by a holding temperature of 4°C until the reaction was removed from the machine. Approximately 20 μl of the final sample was separated by electrophoresis on an ethidium bromide-stained 2% agarose gel. The created gene specific primers were able to amplify a fragment corresponding to *Axl* (161bp) and a separate fragment corresponding to *Axl-like* (250bp) in subsequent PCR analysis (Figure 2.5). Primers for *Axl* were Axl-like5'ex14 and Axl Oligos3'-6. Primers for *Axl-like* were Axl-like5'ex14 and Axl-like3'-2117 (Table 2.1 for primer sequences).

*Quantitative real-time PCR*

Three pools of six to eight pair of gonads for each age (7, 14, 21dpp), a single pair of adult testes, and three single decapitated male embryos at 15dpc were collected and total RNA was isolated using TRIzol® Reagent in the manner described previously. One μg of total RNA was then reverse transcribed using an AffinityScript™ Multi

Temperature cDNA Synthesis Kit following the manufacturer's protocol. For real-time PCR, samples were prepared in a final volume of 25 μl using a 96-well plate format with $RT^2$ SYBR Green/ Fluorescein qPCR Master Mix (SABiosciences Corporation, Frederick, MD), 400 nM of each forward and reverse primer, and 150 ng cDNA. PCR was performed on the iCycler iQ™ Optical Module (Bio-Rad Laboratories, Hercules, CA) using the following thermocycler conditions: stage 1, 95°C for 3 min, 1 cycle, stage 2, 95°C for 10 s and either 57°C, 60°C or 67°C (depending on the primer pair) for 45 s, 40 cycles. Melting curve analysis was used to monitor production of the appropriate PCR product, and samples were separated by electrophoresis on an ethidium bromide stained 2% agarose gel to confirm specificity. Each PCR was performed in triplicate with negative controls, where water was used in place of the reverse-transcribed template included for each primer pair. To correlate the cycle threshold (Ct) values from the sample amplification plot to target copy number, standard curves were composed of eight threefold dilutions of sample cDNA at a starting concentration of 30 ng. Gene specific primers to *Axl*, *Axl-like*, and *GAPDH* were created within parameters for real-time PCR. *Axl* primers were Axl Oligos5'-4 and Axl Oligos3'-5. *Axl-like* primers were Axl-like5'intron and Axl-like3'-2117. *GAPDH* primers were GAPDH(+) and GAPDH(-) (Table 2.1).

Relative mRNA values for real-time PCR experiments were calculated using the method described by Livak and Schmittgen (2001). The point at which the PCR product is first detected above a fixed threshold is termed cycle threshold (Ct) and was determined in triplicate for each sample to account for pipetting error. A melting curve

analysis was performed with each sample and primer pair to confirm amplification of only the expected product. To determine the relative amount of gene specific transcript present in the cDNA of each day of tissue sampling, their respective Ct values were first normalized by subtracting the reported Ct value of the gene of interest from the internal control, GAPDH (e.g. Ct = Ct *Axl* – Ct *GAPDH*)$_{\text{Time X}}$. Time X indicates day observed (e15, 7dpp, 14dpp, 21dpp). This equation yields the first ΔCt. The second ΔCt comes from the normalization of the values from the gene of interest and reference gene against a control time point, which for this experiment was selected to be the adult. The equation (Ct = $Ct_{avg}$ *Axl* – $Ct_{avg}$ *GAPDH*)$_{\text{Time 0}}$, where time 0 refers to adult Ct averages from three separate mouse testes mRNA performed in triplicate, yields this result. Relative concentration was determined (relative concentration= $2^{-\Delta\Delta Ct}$), where ΔΔCt = (Ct *Axl* – Ct *GAPDH*)$_{\text{Time X}}$ – ($Ct_{avg}$ *Axl* – $Ct_{avg}$ *GAPDH*)$_{\text{Time 0}}$. The amplification efficiency of the primers was determined by performing the Ct slope method. Three-fold serial dilutions of mRNA template (30 ng to 0.01 ng) were amplified with each primer, and analysis of the results by linear standard curve were employed (Excel) where $E_X = 10^{(-1/slope)} - 1$. Since the amplification efficiency was close to 100% (GAPDH: 98%, Axl: 97%, and Axl-like: 95%), the use of "2" in the equation was valid to determine relative concentration. The "2" indicates that perfect doubling of the transcript of interest occurs during each amplification cycle of the PCR. Graphs of real time-PCR results present in the results section indicate the mean fold change of the expression of the target gene (*Axl* or *Axl-like*) relative to the internal control (GAPDH) and adult transcript expression levels for each time point examined.

*Statistical analysis*

Determination of statistical significance from the real-time PCR results was performed on Number Crunchers Statistical System 2000. One-way ANOVA, Newman-Keuls, Bonferroni, Duncan's, and Fisher's LSD multiple-comparison test, were performed. All means were considered different at $p<0.05$.

**D. Results**

*Northern blot hybridization experiments determined Axl was expressed in multiple adult murine tissues while the Axl-like transcript was barely detectable.*

A multiple tissue Northern blot containing polyA+ RNA from adult murine tissues was probed for the *Axl* and *Axl-like* transcripts to determine tissue expression. Figure 2.4 A demonstrates that the radioactive *Axl* cDNA probe hybridizes strongly to RNA isolated from the heart and testes, with less hybridization to the brain, spleen, lung, liver, and kidney samples. The *Axl* transcript was not detectable in skeletal muscle. Figure 2.4 B indicates the same membrane stripped and reprobed for *Axl-like*. While distinct bands were not detected in the *Axl-like* Northern, diffuse hybridization was observed with a tissue distribution similar to that for *Axl*. The lack of hybridization of *Axl-like* in adult murine tissues suggests that the *Axl-like* transcript is found only in embryonic and developing tissues, where it was first identified.

*Amplification of Axl and Axl-like gene products by RT-PCR.*

Before quantitative mRNA analysis by real-time PCR could be performed, the ability to amplify appropriate size products from cDNA was confirmed. Since the sequence of the *Axl-like* transcript differs from that of *Axl* due to a read-through into an intron, it was necessary that the intronically expressed sequence could be amplified. Two samples of total RNA were isolated from pups on 7dpp, 14dpp, and 21dpp. Each sample represented a pool of 6-8 pairs of testes from males of the same litter. This total RNA was then treated with reverse transcriptase and random primers to yield cDNA. PCR was

**Figure 2.4-** Northern blot of Axl and Axl-like. (A) A multiple tissue Northern blot membrane was hybridized with a radioactive cDNA probe that recognizes the 5′ end of *Axl* and exposed for 3 days. Since the *Axl* and *Axl-like* transcripts are identical in this region, this probe hybridizes to both transcripts. Expected transcript size is about 4.1kb (not including the polyA tail). The heart and testes RNAs hybridized the probe most abundantly, while the brain, spleen, lung, liver, and kidney RNAs contained lower levels of hybridization. *Axl* hybridization was not observed in the skeletal muscle. (B) The Northern blot in (A) was stripped and reprobed with a radioactive cDNA probe that hybridizes to the intronically expressed portion of *Axl-like* and therefore does not cross-react with the *Axl* message and exposed for 2 weeks. No distinct bands indicating *Axl-like* were observed, although an expected hybridization product should be around 2.7kb (not including the polyA tail). Lanes indicated contain tissues from adult murine organs: lane 1, heart; lane 2, brain; lane 3, spleen; lane 4, lung; lane 5, liver; lane 6, skeletal muscle; lane 7, kidney; and lane 8, testes.

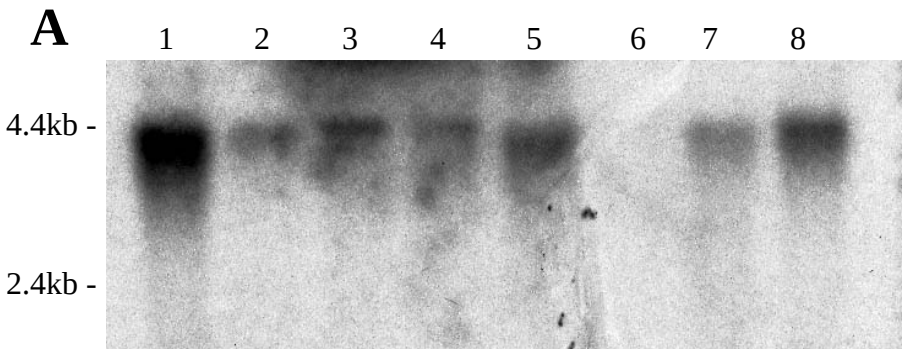
A
1 2 3 4 5 6 7 8
4.4kb -
2.4kb -

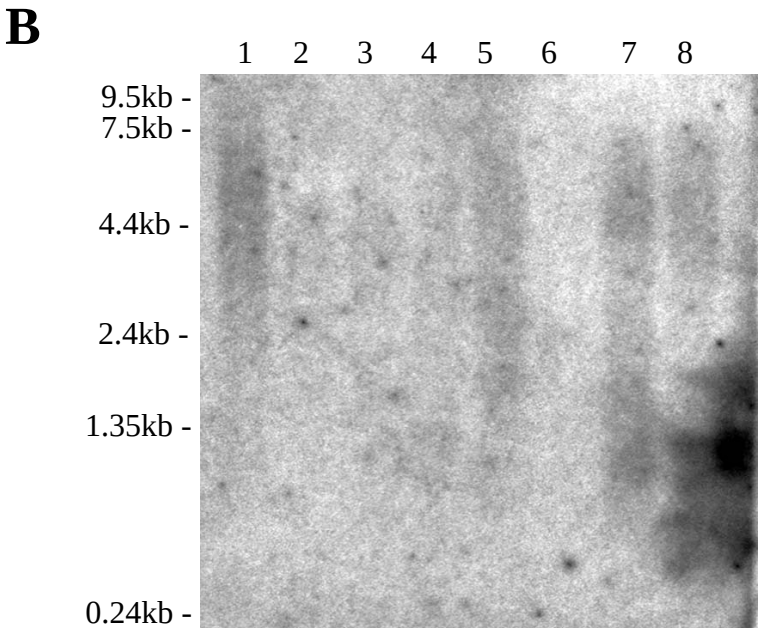
B
1 2 3 4 5 6 7 8
9.5kb -
7.5kb -
4.4kb -
2.4kb -
1.35kb -
0.24kb -

performed using primer pairs in which the sequence of the 5′ primer is found in both *Axl* and *Axl-like* whereas the 3′ primer is isoform specific. The 5′ primer was constructed from sequence at the 3′ end of exon 14 (Figure 2.5 A). The sequence of the 3′ primer for *Axl* is located in exon 16 while that for Axl-like is located in the intron that is expressed only in *Axl-like* (Figure 2.5 A). The expected amplification product is 161bp for *Axl* (Figure 2.5 B, even numbered lanes) and 250bp for *Axl-like* (Figure 2.5 B, odd numbered lanes). If amplification of the transcripts were from genomic DNA, a product of 2.6kb for *Axl* would be amplified, encompassing both the intron between exons 14 and 15, and that between exons 15 and 16. For *Axl-like*, an amplification product of 2.3kb, including the intron between exon 14 and 15, would be observed if the transcript were from genomic DNA. No larger amplification products were observed at these sizes indicating that the *Axl* and *Axl-like* transcripts being amplified in these reactions are not from genomic DNA. The appropriate sized bands were detected using the mouse cDNA samples, which confirms specific sequence amplification of both the *Axl* and *Axl-like* gene products is possible using early postnatal testes.

*Axl and Axl-like expression is correlated with the number of Sertoli cells within the testes.*

Real-time PCR experiments were performed using multiple RNA samples isolated from tissues recovered from e15, 7dpp, 14dpp, 21dpp, and adult. These days were chosen because of the specific cellular makeup of the testes on each day (Table 1.1). Primers were created to amplify unique sequences within the *Axl* and *Axl-like* gene transcripts

**Figure 2.5** Amplification of *Axl* and *Axl-like* in developing mouse testes. (A) This cartoon depicts *Axl* and *Axl-like* transcripts in murine testes cDNA. Arrows above the exons indicate the location of primers used for amplification. The open arrow at the end of the *Axl* transcript indicates continuation of the expressed sequence in *Axl*. The black diamond at the end of exon 15 of *Axl-like* indicates a stop codon. (B) This gel shows the amplification product with *Axl* and *Axl-like* primers from a PCR of two separate groups of 7dpp (lanes 2, 3, 10, 11), 14dpp (lanes 4, 5, 12, 13), and 21dpp (lanes 6, 7, 14, 15) testes cDNA. Lane 1 indicates a 100bp ladder, while lanes 8 and 9 indicate negative controls (no cDNA). Even numbered lanes have been amplified for the presence of *Axl* (red arrow) at 161bp, while odd numbered lanes have been amplified for the presence of *Axl-like* (blue arrow) at approximately 250bp.

**A**

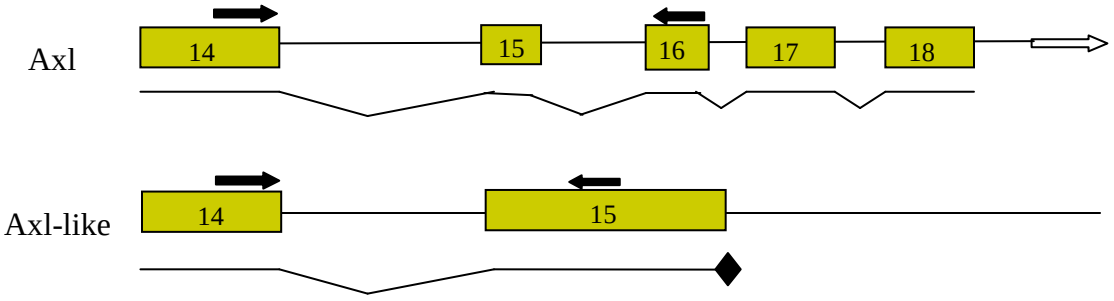
Axl
14
15
16
17
18
Axl-like
14
15

**B**

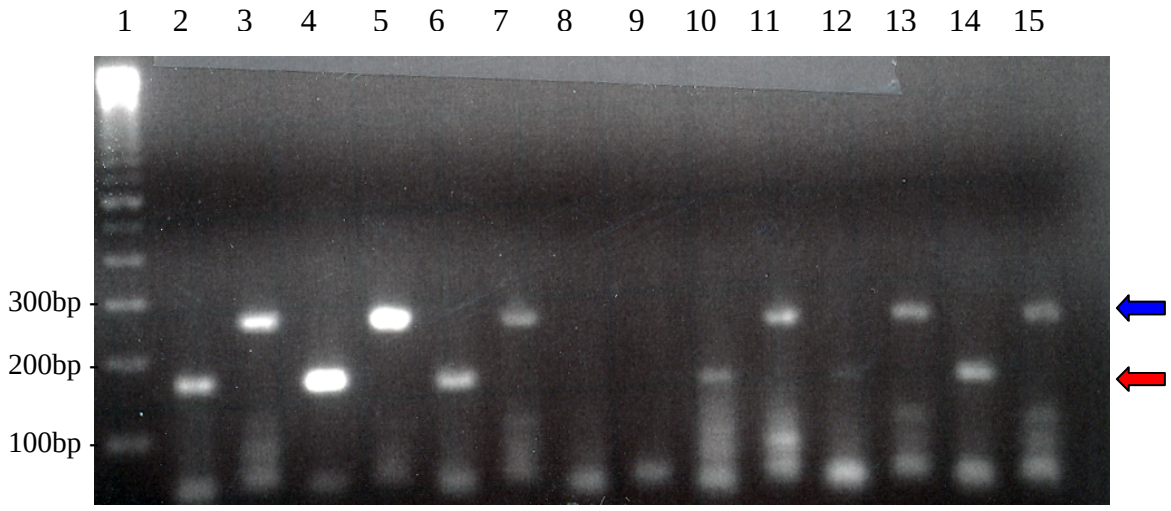
1 2 3 4 5 6 7 8 9 10 11 12 13 14 15
300bp
200bp
100bp

(Table 2.1). GAPDH was used as an internal control to adjust for differences in the amount of sample cDNA used and the relative expression value calculated using the method of Livak and Schmittgen (2001). The pattern of *Axl* expression observed (Figure 2.6) demonstrated that the greatest ($p \leq 0.05$) expression level occurred at 7dpp, followed by a decline as the mice matured. There was no difference in *Axl* expression among the other days examined. The expression of *Axl-like* displayed the same trend of declining expression levels as mice matured, with the highest mRNA levels found at 7dpp. A significant difference was detected between 7dpp and 21dpp mRNA levels (Figure 2.7). There was no statistical significance found among the other groups compared. It should be noted that the Fisher's LSD multiple-comparison test also indicated a significant difference in *Axl-like* results between e15 and 21dpp. There was also a significant difference seen between 7dpp and 14dpp in the *Axl-like* results. The other multiple-comparison tests performed (Newman-Keuls, Bonferroni, and Duncan's) did not confirm this significance and therefore these tests were felt to be more accurate since three of the four multiple-comparison tests yielded the same result.

**Figure 2.6** Real-time PCR analysis of *Axl* in developing murine testes tissue. Multiple determinations of *Axl* relative mRNA concentration levels were normalized against *GAPDH* and compared to mRNA level in the adult testes. Multiple total RNA isolations were from the testes at each of the indicated days: e15, 7dpp, 14dpp, 21dpp, and adult. Gene specific primers were created to amplify *Axl* specific sequence. Relative mRNA values were calculated as described by Livak and Schmittgen (2001). There is a significant difference in the amount of mRNA present in 7dpp compared to the other days analyzed. There is not a significant difference among the other days analyzed. $p<0.05$*.

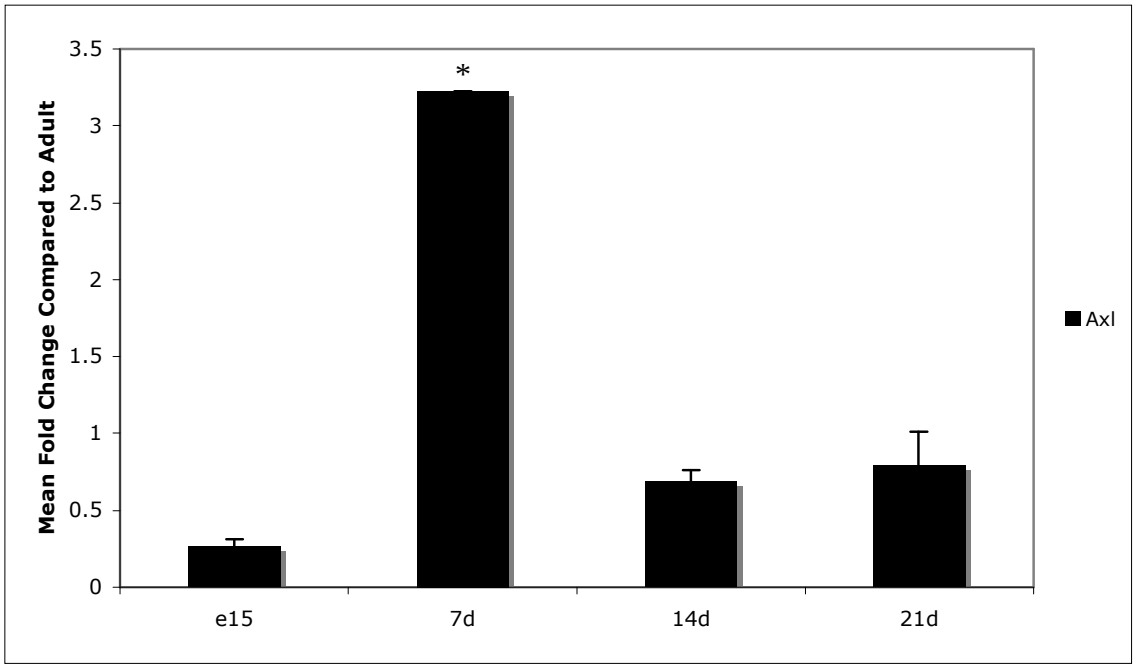
Mean Fold Change Compared to Adult
3.5
3
2.5
2
1.5
1
0.5
0
*
e15
7d
14d
21d
Axl

**Figure 2.7** Real-time PCR analysis of *Axl-like* in developing murine testes tissue. Multiple determinations of *Axl-like* mRNA concentration levels were normalized against *GAPDH* and compared to adult testis mRNA levels. Multiple total RNA isolations were from testes at each of the indicated days: e15, 7dpp, 14dpp, 21dpp, and adult. Gene specific primers were created to amplify an *Axl-like* specific sequence. Relative mRNA values were calculated as described by Livak and Schmittgen (2001). There is a significant difference in the amount of mRNA present in 7dpp compared to 21dpp and adult. There is not a significant difference between other groups. $p<0.05$*.

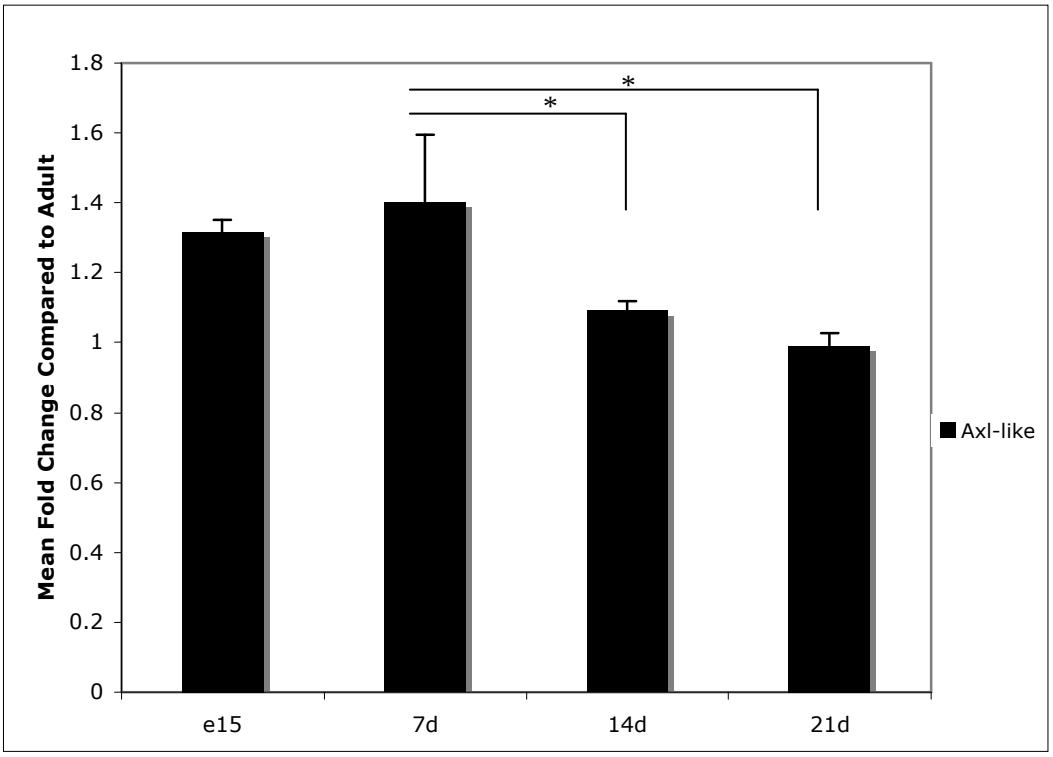
Mean Fold Change Compared to Adult
1.8
1.6
1.4
1.2
1
0.8
0.6
0.4
0.2
0
*
*
e15
7d
14d
21d
Axl-like

**E. Discussion**

The current study investigated the relative levels of the *Axl* and *Axl-like* gene transcripts in prenatal, early postnatal, and adult testes utilizing real-time PCR. Previous studies (Chan et al., 2000; Wong and Lee, 2002; Wang et al., 2005) have examined expression of members of the TAM family using a variety of techniques. This is the first study to utilize real-time PCR.

Wang et al. (2005) investigated the immunohistochemical staining pattern of TAM family members in developing mouse testis. Important to this study was the staining pattern Wang et al. (2005) observed for AXL. In early developing mouse testis, specifically 3-35dpp, staining was observed only in Sertoli cells. All other cell types present at these days contained no AXL staining. While in more mature testes, 56dpp, staining for AXL was present in a stage dependent manner in Sertoli cells, and staining was also visible in some Leydig cells. With regard to Sertoli cells there was stronger expression observed at stages I-VI, where there are spermatocytes and round spermatids, than at stages IX-XII, where there are no round spermatids and reduced numbers of spermatocytes. In these later stages, IX-XII, no mature elongated spermatids are present, and therefore no genes or proteins associated with these cell types are present in the seminiferous epithelium at this stage. The definition and importance of stages of the seminiferous epithelium were previously discussed and are summarized in Table 1.2. Stage dependent AXL staining of Sertoli cells suggests that AXL may have a role in Sertoli cell phagocytosis of residual bodies from developing spermatids.

There are two forms of Leydig cells present in the seminiferous epithelium, spindle-shaped Leydig cells with spindle-shaped nuclei and polygonal Leydig cells with round nuclei. The spindle-shaped Leydig cells are progenitor cells, while the polygonal Leydig cells indicate a newly formed early adult Leydig cell (Baillie, 1964). The progenitor cells express steroidogenic enzymes, are capable of producing androgens, but contain a non-functional form of the LH receptor possessing only an ectodomain (Hardy et al., 1990; Tena-Sempere et al., 1994). The newly formed early adult Leydig cells contain steroidogenic enzymes, LH receptors, and have 40% of the capacity to secrete testosterone as that of a mature Leydig cell (Prince, 1984). The newly formed Leydig cell also contains the highest capacity for secreting androstenedione, a precursor to testosterone and estrogen, when compared to immature and mature adult Leydig cells. Intense staining for AXL was present in the spindle-shaped Leydig cells, but not in the polygonal Leydig cells (Wang et al., 2005). Localization of AXL primarily in Sertoli cells supports the hypothesis that AXL is involved in the control of Sertoli cell function as it provides physical or nutritive support to the developing spermatogenic cells.

Chan et al. (2000) performed RT-PCR and Northern blot experiments to evaluate expression of the TAM family members, as well as their ligand, GAS6, using a variety of rodent cell lines. *Tyro3* and *Mer* were expressed in all cell lines as determined by RT-PCR. GAS6 was also found to be present in all cell lines, with the most expression found in the Sertoli cell line. *Tyro3* and GAS6 findings were confirmed by Northern blot. Surprisingly, *Axl* expression was not observed by either of these techniques. This may be due to cellular changes associated with developing stable cells or differences in

methodology among investigators. These results are in contrast to our study, as well as that of Wang et al. (2005), which clearly indicate the association of AXL with the Sertoli cells of the testes.

We detected a correlation between the relative mRNA levels of *Axl* and *Axl-like* gene transcripts with the number of Sertoli cells present the testes. For both genes, there was an increase observed in the level of each transcript from embryonic day 15 to 7dpp followed by a significant decrease at the other time points. Day 7 postpartum corresponds to the time with the highest percentage of Sertoli cells within developing murine testes. Kluin et al. (1984) determined that the Sertoli cell population at 7dpp is five times that of the adult mouse. The current study also demonstrated that as the mouse matures, the relative mRNA levels of both the *Axl* and *Axl-like* transcript decline. This pattern is similar to that observed for Sertoli cells during the time period studied. The percentage of Sertoli cells in the developing testis at e15 is unknown. Our data suggests that the proportion of Sertoli cells present at this day is not as high as that found at 7dpp. Our findings are supported by experiments performed by Wong and Lee (2002). They utilized Northern blotting and densitometry to determine relative total RNA levels of TAM family members in developing BALB/c mice testes for 5dpp to 90dpp. They reported a decrease in *Axl* and *Tyro3* expression following the resumption in mitosis. GAS6 expression was unchanged during this time period.

The correlation of *Axl* and *Axl-like* with Sertoli cells may be of functional importance. Sertoli cells have been shown to maintain the homeostasis of the somatic environment by endocytosing and degrading residual bodies and apoptotic spermatogenic

cells (Russell and Clermont, 1977; Chemes, 1986; Pineau et al., 1991; Miething, 1992). Xiong et al. (2008) determined that if all three TAM family members were mutated, then the phagocytic function of Sertoli cells was significantly inhibited. In addition, these authors reported that *Mer* was primarily responsible for triggering phagocytosis by Sertoli cells, though all three family members are participants in the binding of Sertoli cells to apoptotic spermatogenic cells. Apoptotic cells contain phosphotidylserine residues on their surface, which bind directly to phagocytotic cells containing the phosphotidylserine receptor or indirectly though soluble proteins such as the ligands for the TAM family of receptors, GAS6 and Protein S (Nakano et al., 1997; Xiong et al., 2008). The binding of apoptotic cells to Sertoli cells in mice with mutations in one or two of the TAM family members was similar to that of wildtype mice. However, Sertoli cells from triple mutant mice lacking all members of the TAM family were severely deficient in their ability to bind apoptotic cells. When *Mer* alone was mutated, phagocytosis was significantly inhibited. When *Tyro3* or *Axl* was mutated, this inhibition did not occur (Xiong et al., 2008). Double mutants of *Mer/Tyro3* or *Mer/Axl* elicited the same inhibition of phagocytosis, though not in a cooperative manner (the amount of inhibition did not increase). The role of *Axl* in phagocytosis appears to be less significant than *Mer*; however, *Axl* and *Tyro3* are still important for the proper maintenance of reproductive capacities by supporting the proper functioning of *Mer*. Of interest is the observation that the clearance of apoptotic cells by dendritic cells in the brain is mediated predominantly by *Axl* and *Tyro3* rather than by *Mer* (Behrens et al., 2003; Seitz et al., 2007).

In summary, we have utilized real-time PCR as a method of quantifying the relative levels of *Axl* and *Axl-like* mRNA within the testes of prenatal, early postnatal, and adult mice. The level of transcript correlates with the proportion of Sertoli cells present within the testes at specific developmental days, suggesting that Sertoli cells primarily express *Axl* and *Axl-like*. Future work should include other analysis methods, such as *in situ* hybridization, to determine specific localization of the *Axl-like* message in Sertoli cells or other cell types comprising the developing testes. One difficulty with *in situ* hybridization is designing a probe specific for *Axl-like* that will not cross-react with *Axl* or other transcripts. The *Axl-like* transcript contains the intronically expressed sequence not found in *Axl*, therefore designing a probe in this region should be sufficient to alleviate any cross-reaction with *Axl*. A more significant consideration is that germ cells store mRNA transcripts to pass on to future developing spermatogenic cells making it difficult to correlate the biological function of proteins with the presence of their gene transcript. Detection of an mRNA transcript in a cell type may not indicate that it is actively transcribed at that particular developmental stage, making interpretation of results more complicated. Based on the similar relative mRNA expression patterns of *Axl* and *Axl-like* described in this study, I would predict that the localization of *Axl-like* by *in situ* hybridization would be comparable to that observed with *Axl*. Such a finding would further support a role of *Axl-like* in maintaining or regulating the function of *Axl* within the testes.

Another means of investigating the localization of AXL-LIKE in the testis would be to create an antibody to this protein. Currently, no antibody to AXL-LIKE exists, but

designing a specific reagent should not be difficult given the sequence differences between the two proteins. An antibody that recognizes the intronically expressed portion of AXL-LIKE should not cross-react with AXL. There is also a minor difference in the sequence of AXL-LIKE at the C-terminal end of the protein that may be adequate for antibody production. An antibody to AXL-LIKE would allow future research to be performed in assessing the endogenous expression of AXL-LIKE in different cellular systems and *in vivo*, as well as testing its functionality without overexpression (which may alter its normal function). The work performed in this current study is significant because *Axl-like* had not been assessed in the early postnatal testes, nor has its association with testicular cells been demonstrated. This work also confirms the findings of other investigators using real time PCR, an approach that has not been used previously.

# CHAPTER III: AXL-LIKE FUNCTION THROUGH THE INTERACTION WITH AXL

## A. Summary

There are several truncated kinase proteins expressed within the testes: FERT (Keshet et al., 1990), HCK-TR (Bordeleau and Leclerc, 2008), and *c-kit* (Sakamoto et al., 2004). Since AXL-LIKE appears to be a truncated version of AXL, the present study attempted to determine if AXL-LIKE is acting in a dominant negative fashion toward the native function of AXL within a cellular system. Constructs expressing the full-length transcripts of *Axl* and *Axl-like* were created. These constructs were transfected into COS-7 cells and the effects of overexpression were measured by immunohistochemistry, immunoprecipitation, and Western blotting techniques. Overexpression of AXL in COS-7 cells significantly increased the number of filopodia present on the cellular surface. This phenotype was inhibited by the co-expression of AXL-LIKE in these cells. Cells transfected with AXL were significantly smaller than control cells. Co-transfection with both AXL and AXL-LIKE reduced cell size even further. This finding further supports the hypothesis that AXL-LIKE is regulating a function of AXL, such as in motility or adhesion. Immunoprecipitation experiments demonstrated that AXL-LIKE does not directly interact nor form a complex with AXL. However, the introduction of AXL-LIKE constructs into COS-7 cells diminished the amount of AXL *in vitro* suggesting that although there is not direct interaction between these proteins, there may be an indirect affect of AXL-LIKE upon AXL function.

## B. Introduction

AXL is overexpressed in multiple types of cancers. This suggests that reducing or eliminating AXL expression may be a useful therapy for the malignancy. Prior studies indicate that overexpression of AXL in a variety of cells is associated with an invasive phenotype which may lead to acceleration in the spread of cancer cells within tissues (Shieh et al., 2005; Vajkoczy et al., 2006; Lay et al., 2007). The action of AXL may be reduced by limiting ligand availability. One method to do this is to introduce soluble ectodomains into the extracellular environment. Prior studies demonstrate that AXL can undergo proteolytic cleavage to create soluble ectodomains in murine and human cells and that this mechanism acts to regulate deactivation of phosphorylation pathways (O'Bryan et al., 1995; Costa et al., 1996; Budagian et al., 2005a). Costa et al. (1996) found that stimulating dormant NIH3T3 cells with GAS6 caused an increase in DNA synthesis. When those same cells overexpressed the AXL ectodomain at various concentrations, DNA synthesis was inhibited in a dose-dependent manner. Sainaghi et al. (2005) investigated the effect of soluble AXL ectodomains on the GAS6 mitogenic effect in the prostate carcinoma cells lines, DU-145 and PC3. Treatment of these cell lines with soluble ectodomains reduced the ability of GAS6 to induce stimulation and proliferation. Given the similarity in the sequences of AXL and AXL-LIKE, it is possible that AXL-LIKE may regulate the function of AXL. Before one can determine that AXL-LIKE has a direct affect upon AXL, their interaction with each other must be determined.

In addition to forming homodimers, Axl has been demonstrated to heterodimerize with IL-15Rα (Budagian et al., 2005), a cytokine that inhibits apoptosis (Bulfone-Paus et

al., 1997). Although the ability of AXL to heterodimerize with other members of its family has not been studied, other receptor tyrosine kinase families, such as EGFR, have been reported to display heteromeric interactions within their family (Tzahar et al., 1996; Graus-Porta et al., 1997). Angelillo-Scherrer et al. (2005) have reported that in order to maintain GAS6 stimulated phosphorylation/activation in thrombocytic pathways, at least one, if not all, of the TAM family members are needed. Since the sequence of *Axl-like* is so similar to *Axl*, it is probable that they too will dimerize with one another. In this study, the interaction of AXL and AXL-LIKE was determined using immunofluorescence and immunoprecipitation methodology. This work is significant because it is the first assessment of the interaction and regulation of AXL *in vitro* with an endogenously expressed truncated isoform of itself, AXL-LIKE.

## C. Experimental Procedures

*Antibodies and Reagents*

Mouse monoclonal anti-c-Myc antibody was purchased from BD Clontech (Mountain View, CA). Goat polyclonal anti-Axl antibody was purchased from Santa Cruz Biotechnology, Inc (Santa Cruz, CA). Rabbit polyclonal anti-Flag antibody was purchased from Sigma-Aldrich (St. Louis, MO). FITC-conjugated donkey anti-mouse and anti-goat secondary antibodies, as well as Texas Red-conjugated donkey anti-rabbit secondary antibodies were purchased from Jackson ImmunoResearch Laboratories, Inc (West Grove, PA).

*Generation of Axl and Axl-like constructs*

*Axl* cDNA was provided by the Janssen lab in Heidelberg, Germany. The *Axl* cloning strategy is summarized in Figure 3.1 A. Briefly, *Axl* full-length cDNA was subcloned into pGEM® T-vector (Promega Corporation, Madison, WI) using primers (Table 3.1) (Integrated DNA Technologies, Coralville, IA) that created a 5′ BamHI restriction cleavage site (Axl-100 5'BH1) and a 3′ EcoRI restriction cleavage site (Axl-100 3'ER1-2) (Figure 3.2 A). Following ligation, the full length *Axl* cDNA was excised using BamHI and EcoRI (Invitrogen Corporation, Carlsbad, CA) (Figure 3.2 B). The excised DNA fragment was then ligated into a pcDNA 3.1/*myc*-His vector (Invitrogen Corporation, Carlsbad, CA). The Axl-Myc construct was digested with the restriction enzyme PstI to confirm appropriate fragment sizes (Figure 3.2 C). Sequencing confirmed identity of the construct.

*Axl-like* could not be amplified as a full-length cDNA. This was thought to be due to low transcript abundance. The occurrence of a native EcoRV site at bp908 allowed for the cloning of two separate pieces of the transcript and then ligation to form the whole sequence. The strategy for cloning *Axl-like* is shown in Figure 3.1 B. The 5′ half of *Axl-like* (907bp) was amplified from *Axl* cDNA using a 5′ primer containing an EcoRI restriction enzyme site and a 3′ primer retaining the native EcoRV site (Figure 3.3 A). This amplification product was then ligated into pGEM T-vector before being excised by digestion with the EcoRI and EcoRV restriction enzymes (Figure 3.3 B, lane 2) followed by ligation into the p3XFLAG-CMV™-14 expression vector (Sigma-Aldrich,

**Figure 3.1** Cloning strategy for *Axl*-Myc and *Axl-like*-Flag constructs. (A) Cartoon depicting the cloning strategy of *Axl* into the pcDNA3.1/myc-His vector. *Axl* cDNA was amplified by PCR to attach BamHI and EcoRI restriction cleavage sites to the 5′ and the 3′ end, respectively (a). This PCR product was passaged through T-vector (b), digested with BamHI and EcoRI, and cloned into the pcDNA3.1/myc-His vector to produce the final expression vector (c). The Myc protein tag is located at the C-terminus of the *Axl* sequence. (B) Cartoon depicting the cloning strategy of *Axl-like* into the p3XFLAG-CMV-14 vector. The 5′ fragment of *Axl-like* was amplified by PCR to place an EcoRI restriction cleavage site at the 5′ end (a). This amplification product was ligated into the p3XFLAG-CMV-14 vector, and the resultant construct was digested with EcoRV and BamHI (b) to open the vector in order to insert the 3′ fragment of *Axl-like*. The 3′ fragment of *Axl-like* was synthesized by the Genscript Corp (Piscataway, NJ) with a BamHI restriction cleavage site placed at the 3′ end and ligated to a pUC-57 vector (c). The Axl-like3′-pUC57 construct was then digested with EcoRV and BamHI (d) and the released DNA fragment ligated into the p3XFLAG-CMV-14 recombinant construct containing the 5′ half of *Axl-like* to produce a full-length *Axl-like*-Flag construct (e). The Flag amino acid tag is located at the C-terminus of the *Axl-like* sequence.

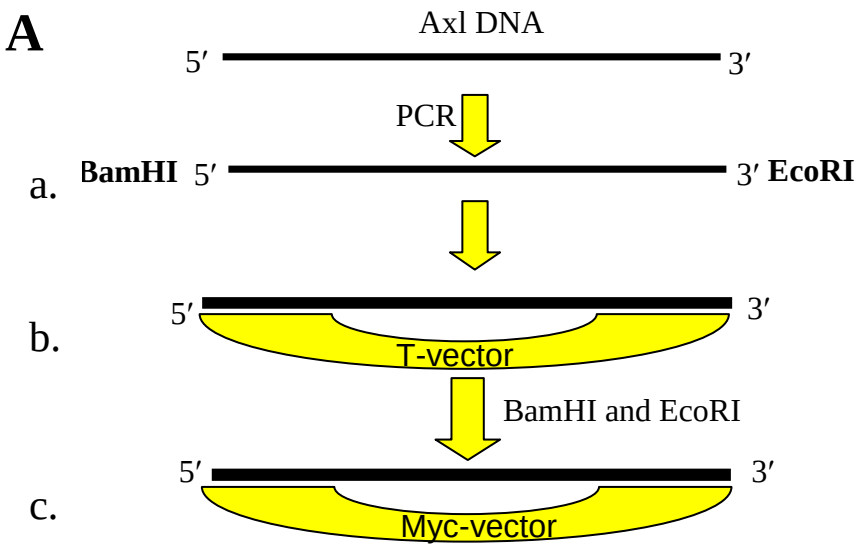
A
Axl DNA
5′
3′
PCR
a.
BamHI
5′
3′
EcoRI
b.
5′
3′
T-vector
BamHI and EcoRI
c.
5′
3′
Myc-vector

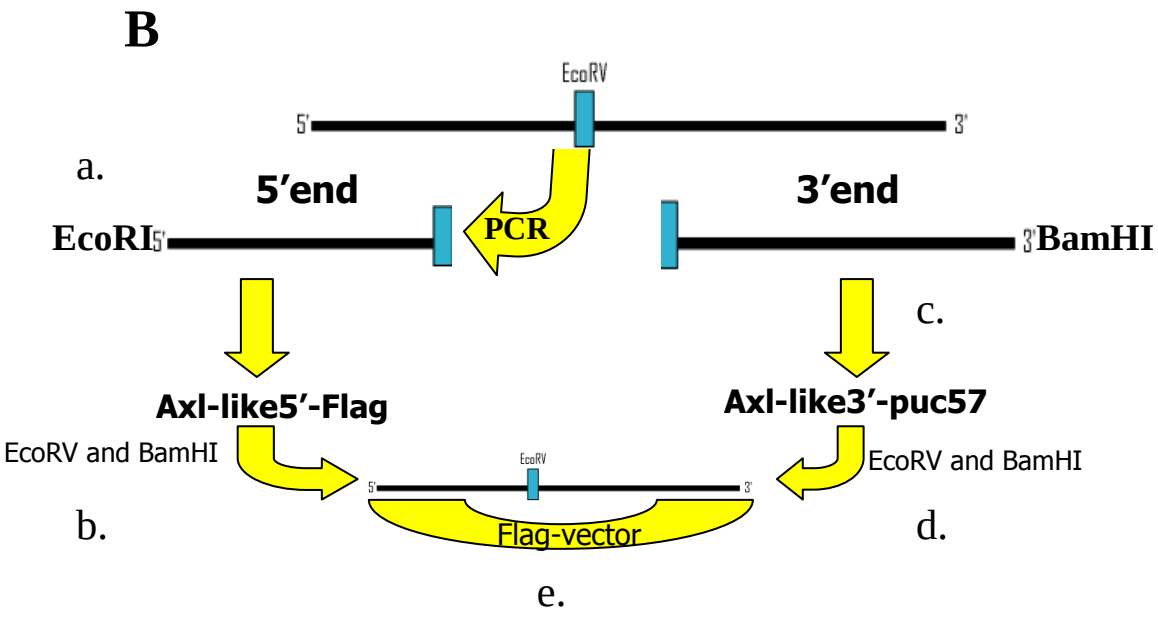
B
EcoRV
5′
3′
a.
5′end
3′end
EcoRI
5′
PCR
3′
BamHI
c.
Axl-like5′-Flag
Axl-like3′-puc57
EcoRV and BamHI
EcoRV and BamHI
EcoRV
5′
3′
b.
Flag-vector
d.
e.

**Figure 3.2** Cloning of *Axl* into the pcDNA3.1/myc-His vector. (A) PCR of *Axl* transcript from cDNA provided by the Janssen lab. Lane 1, 1kb ladder; lanes 2-4, *Axl* cDNA PCR; lane 5, control PCR with no plasmid DNA. The expected size of the amplification product is 2.7kb. (B) BamHI and EcoRI digest of *Axl* in T-vector (passaging vector). Lane 1, 1kb ladder; lanes 2-4, *Axl*-T-vector constructs. Expected fragment sizes are 3.1kb (T-vector) and 2.7kb (*Axl* insert, arrow). (C) PstI digest of *Axl*-Myc construct. Lane 1, 1kb ladder; lanes 2-9, *Axl*-Myc digests of DNA prepared from individual clones; lane 10, control digest with no DNA. Expected fragment sizes are 4.8kb, 1.6kb, 1.4kb, 150bp, and 113bp. The two smaller fragment sizes are not visible in this gel.

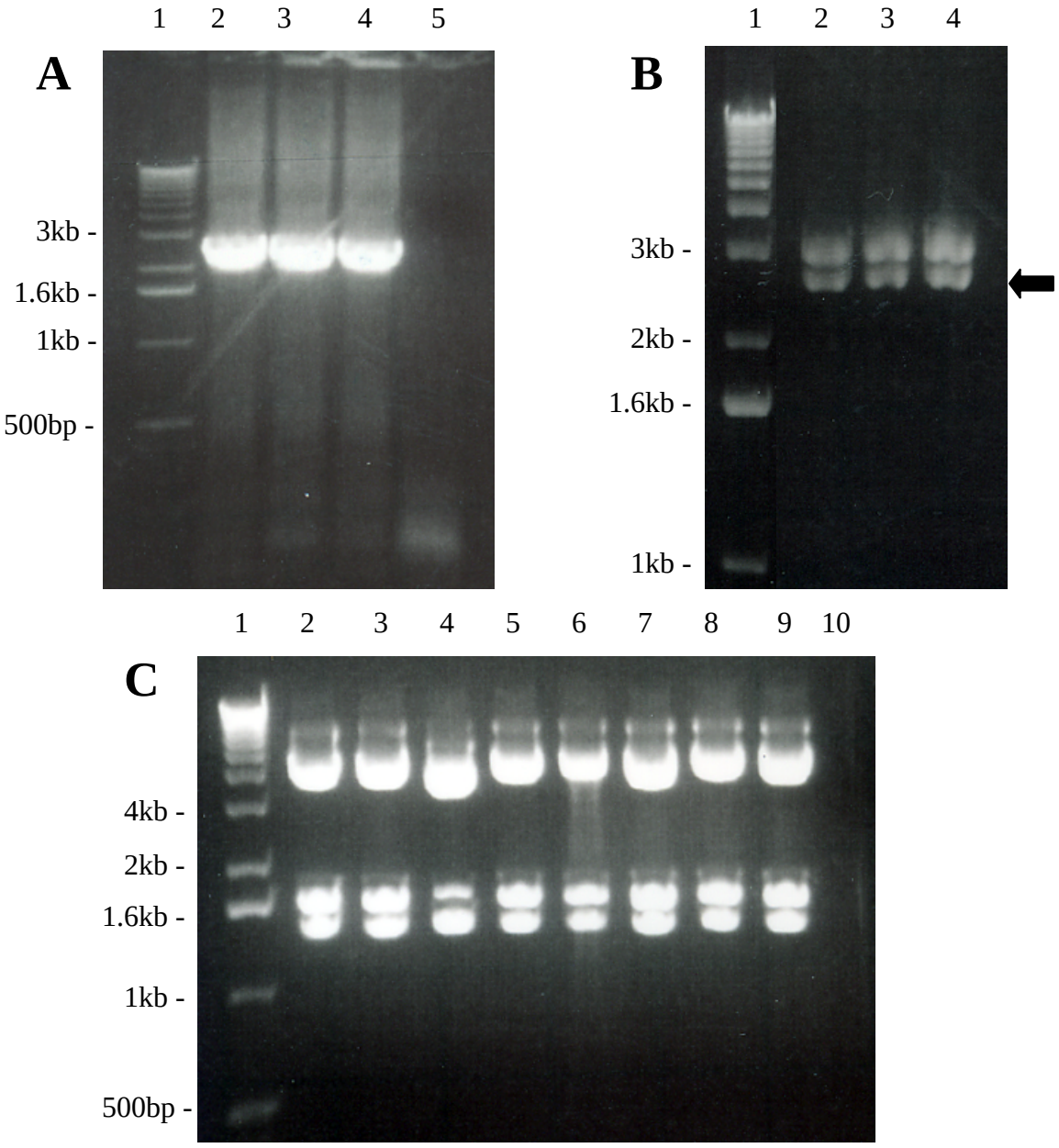
A
1 2 3 4 5
3kb -
1.6kb -
1kb -
500bp -
B
1 2 3 4
3kb -
2kb -
1.6kb -
1kb -
C
1 2 3 4 5 6 7 8 9 10
4kb -
2kb -
1.6kb -
1kb -
500bp -

**Figure 3.3** Cloning of *Axl-like* into the p3XFLAG-CMV-14 vector. (A) Ethidium bromide stained agarose gel depicting the PCR amplification of the *Axl-like* 5′ fragment from *Axl* cDNA provided by the Janssen lab. Lane 1, 1kb ladder; lanes 2 and 3, Axl-like5′ PCR. Expected amplification size is 908bp. (B) Passaging of Axl-like5′ and 3′ through separate vectors. Lane 1- 1kb ladder, lane 2- Axl-like5′-T-vector digested with EcoRI and EcoRV; lane 3, Axl-like3′-pUC57 digested with EcoRV and BamHI; Lane 4, control digest. Expected product sizes are 3.1kb (T-vector), 2.7kb (pUC57 vector), 1.3kb (Axl-like3′), and ~1kb (Axl-like5′). (C) Axl-like5′ ligated into the p3XFLAG-CMV-14 vector. Lane 1, 1kb ladder; lanes 2-5, Axl-like5′-Flag digested with EcoRI and EcoRV; and lane 6, control digest. Expected bands are 6.3kb (p3XFLAG-CMV-14 vector) and 908bp (Axl-like5′). (D) Full-length *Axl-like* in the p3XFLAG-CMV-14 vector. Lane 1, 1kb ladder; lanes 2 and 3, full length *Axl-like*-Flag construct digested with BamHI and EcoRI; lane 4, control digest. Expected digestion products at 6.3kb (p3XFLAG-CMV-14 vector) and 2.3kb (full length *Axl-like* transcript) are shown. This figure was taken from a gel that contained multiple lanes of potential full-length clones digested with BamHI and EcoRI. Incorrect clone digestions were removed to simplify the figure; however, samples shown in each panel were analyzed on the same gel.

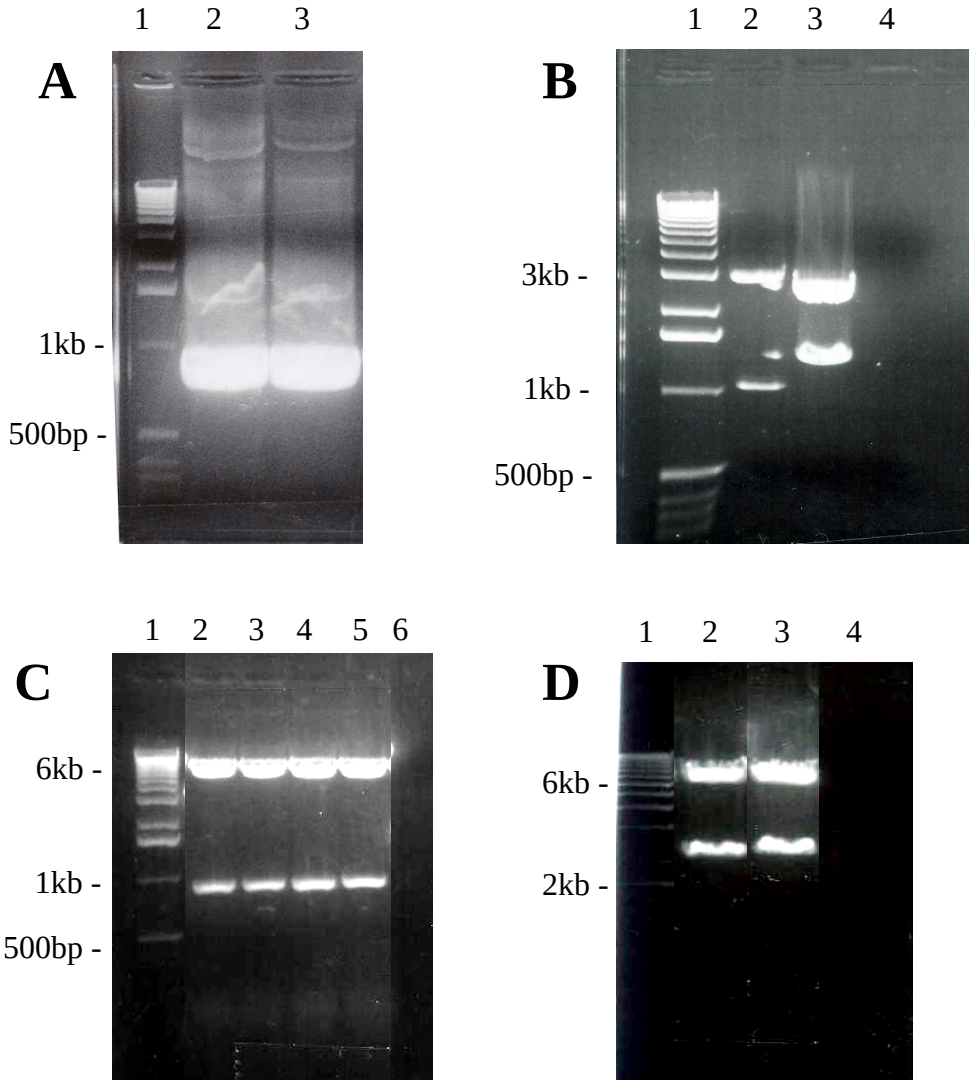
1 2 3
A
1kb -
500bp -
1 2 3 4
B
3kb -
1kb -
500bp -
1 2 3 4 5 6
C
6kb -
1kb -
500bp -
1 2 3 4
D
6kb -
2kb -

**Table 3.1** Primers used for cloning of *Axl* and *Axl-like* into expression vectors.

| Primer Name | Sequence |
|---|---|
| Axl-100 5'BH1 | GCG CGG ATC CAT GGG CAG GGT CCC GCT GGC CTG G |
| Axl-100 3'ER1-2 | GCG CGA ATT CGG CTC CGT CCT CCT GCC CTG GAG G |
| Axl-like 5'ER1 | GCG CGA ATT CAT GGG CAG GGT CCC GCT G |
| Axl-like A3' | CTG CTG CTG CAG GAT ATC CG |

St. Louis, MO). Proper ligation was confirmed by digesting the *Axl-like*5′-Flag construct with EcoRI and EcoRV (Figure 3.3 C). It was not possible to isolate the 3′ half of *Axl-like* (1360bp) using Polymerase Chain Reaction (PCR). Therefore this sequence was synthesized by GenScript Corporation (Piscataway, NJ) and cloned into a pUC57 vector retaining the native 5′ EcoRV site and including the addition of a 3′ BamHI restriction enzyme site. The synthesized 3′ half of *Axl-like* was excised from the pUC57 vector (Figure 3.3 B, lane 3), and inserted into the *Axl-like*5′-Flag construct at the EcoRV and BamHI restriction sites, thus creating a full-length *Axl-like*-Flag construct. The *Axl-like*-Flag construct was digested with BamHI and EcoRI to confirm presence of the appropriate construct (Figure 3.3 D).

*Cell culture and transfection*

COS-7 cells (an African Green monkey kidney cell line, kindly provided by Dr. Warren Knudson and Dr. Edward Seidel from East Carolina University, NC) were grown in Dulbecco's Modified Eagle Medium (DMEM) containing 10% Fetal Bovine Serum (FBS), 10,000 units/ml of penicillin, and 10,000 μg/ml streptomycin in a humidified air-5% $CO_2$ atmosphere at 37°C. *Axl*-Myc, empty Myc vector, *Axl-like*-Flag, empty Flag vector, and/ or empty GFP vectors were transfected into COS-7 cells, using the AMAXA Nucleofector Kit V (Cologne, Germany) according to the manufacturer's instructions. Briefly, approximately 1x $10^6$ cells were transfected with 4 μg of endotoxin-free DNA constructs via electroporation using program A-024 on an Amaxa machine. Cells were

plated in 6-well dishes and allowed to adhere overnight at 37°C in a humidified 5% $CO_2$ atmosphere before being subjected to further experimentation.

*Immunofluorescence*

COS-7 cells were transfected via electroporation with GFP, Myc, *Axl*-Myc, Flag, *Axl-like*-Flag constructs individually or co-transfected with *Axl*-Myc and *Axl-like*-Flag constructs or with GFP and *Axl-like*-Flag. Transfected cells were grown on glass coverslips and fixed with 2% paraformaldehyde in 1x Phosphate Buffered Saline (PBS) for 7 min at room temperature. Excess fixative was removed with three washes of Tris Buffered Saline- 0.1% Triton X-100 (TBST) for 5 min at room temperature. Cells were blocked with 2% Bovine Serum Albumin (BSA) in TBST for 1 hr at room temperature and then incubated separately for 2 hrs at room temperature in the dark with primary antibodies against Myc, Flag, or Axl. The Myc and Flag antibodies were diluted 1:200 and the Axl antibody was diluted 1:100 in TBST containing 2% BSA. After washing three times with TBST, cells were incubated for 1 hr in the dark at room temperature with donkey anti-rabbit Texas Red-conjugated secondary antibody (1:400) to detect Flag, donkey anti-mouse FITC-conjugated secondary antibody (1:200) to detect Myc, or donkey anti-goat FITC-conjugated secondary antibody (1:200) to detect *Axl*. All coverslips were rinsed a final three times with TBST and mounted on glass microscope slides using Vectashield mounting media containing 4, 6-Di-Amidino-2-Phenyl-Indole dihydrochloride (DAPI) (Vector Laboratories, Burlingame, CA). Images were captured on a Nikon Eclipse (E600) Y-FL epifluorscence microscope equipped with camera

controller (Hamamatsu, Japan). Images were analyzed with MetaMorph software (Molecular Devices, Sunnyvale, CA).

*Phosphorylation and immunoprecipitation studies*

COS-7 cells were transfected with no vector, empty Myc vector, empty Flag vector, *Axl*-Myc, or *Axl-like*-Flag using the Amaxa electroporation kit as described above. Cells were lysed in a cell lysis buffer containing 50 mM Tris-HCl pH 7.5, 15 mM EGTA, 100 mM NaCl, 1% sodium deoxycholate and 0.1% Triton X-100 along with protease inhibitor cocktail (Sigma-Aldrich, St. Louis, MO) at a concentration of 1:10, phosphatase inhibitor cocktail III (containing NaF, $Na_3VO_4$, $Na_4P_2O_7 \cdot 10H_2O$, and β-glycerophosphate) (EMD Chemicals Inc, Gibbstown, NJ) at a concentration of 1:100, and PMSF (phenylmethanesulphonylfluoride) (3 μl per 1.5 ml). The cells were collected and needle aspirated three times using a 25-gauge needle. The cell lysate was incubated on ice for 10 min, followed by centrifugation at 16,000 x g for 10 min at 4°C. The supernatant was then transferred to a new tube. A BCA (bicinchoninic acid) protein assay (Thermo Fisher Scientific Inc, Rockford, IL) was then performed to determine protein concentration of the lysate. One hundred micrograms of cellular lysate was used per immunoprecipitation reaction. The 100 μg of lysate was precleared by the addition of 20 μl protein G beads, rotated for 30 min at 4°C and followed by centrifugation at ~750 x g for 5 min at 4°C. Two micrograms of antibody (AXL or Normal Goat IgG) was added to the lysate and rotated for 2 hrs at 4°C. Thirty microliters of washed Protein G beads were then added to the lysate/antibody mixture and were allowed to rotate overnight at

4°C. The following day, the tubes were centrifuged at ~750 x g for 5 min at 4°C to pellet the beads and the supernatant was moved to a new tube. The beads were rinsed three times with 1x PBS with PMSF, followed by centrifugation at ~750 x g for 2 min at 4°C. The protein complexes were eluted from the beads by addition of 2x sodium dodecyl sulfate (SDS) with 10% dithiothreitol (DTT), followed by heating at 95°C for 10 min, and subsequent centrifugation at 2,000 x g for 5 min at room temperature. For each IP, the elution was halved allowing 50 μg (of the 100 μg total starting protein) to be subjected to Western blot.

If phosphorylation affects were to be studied, COS-7 cells were transfected with empty Myc vector, *Axl*-Myc, empty Flag vector, or *Axl-like*-Flag via electroporation as described above. Cells were allowed to adhere overnight in DMEM media containing 10% FBS. The following day the media was removed, washed twice with 1x PBS and serum free DMEM media was introduced and cells incubated overnight at 37°C in a humidified 5% $CO_2$ incubator. The following morning, media was removed and replaced with serum free media containing 350 ng/ml human recombinant GAS6 (Amgen, Thousand Oaks, CA) and allowed to sit at 37°C for 30 min. Following stimulation by GAS6, cells were rinsed with 1x PBS and then lysed, followed by immunoprecipitation as mentioned above.

*Western blot analysis*

Immunoprecipitated proteins (50 μg) were separated on a 10% poly-acrylamide Tris-glycine gel and transferred to a polyvinylidene fluoride (PVDF) membrane. The

membrane was blocked in 2% donkey serum in Tris buffered saline (TBS) (for AXL primary antibody), 5% milk in TBST (for Myc, Flag, and β-actin primary antibodies), or 5% BSA in TBST (for phospho-tyrosine antibody) for 1 hr at room temperature. Membranes were briefly rinsed with TBST to remove any excess blocking solution (for Myc and Flag antibodies only). The membranes were incubated overnight at 4°C with anti-c-Myc or anti-Flag primary antibodies in 1% BSA in TBS at a concentration of 1:1000; anti-Axl primary antibody in 2% donkey serum in TBS at a concentration of 1:500; anti-Phospho-tyrosine primary antibody in 5% BSA in TBST at a concentration of 1:1000; or anti-β-actin primary antibody in 5% milk in TBST at a concentration of 1:1000. Following three washes in TBST for 10 min each, the membranes were incubated with either anti-mouse, anti-goat, or anti-rabbit IgG-HRP (Jackson ImmunoResearch Laboratories, Inc) secondary antibody diluted 1:40,000 in 1% BSA (c-Myc and Flag), 5% BSA (phospho-tyrosine), or TBST (Axl) for 1 hr at room temperature. Secondary antibody was diluted 1:20,000 in 5% milk and incubated on the membrane for 1 hr at room temperature for the β-actin blot. Unbound antibody was then removed with three washes in TBST for 10 min each. Antibody bound to proteins on the PVDF membrane was detected using SuperSignal® West Pico Chemiluminescent Substrate (Pierce Biotechnology, Rockford, IL) for 5 min.

Densitometry of blots was measured on a Chemidoc XRS (Bio-Rad, Hercules, CA). The Volume Analysis Report tool of the equipment software was used to determine the area and density measurements of bands of interest. These results were multiplied to determine the intensity of the bands. The experimental values were normalized against

the value of *β-actin* (internal standard). Statistical analysis was performed using pair wise t-tests in Excel (Microsoft Corporation, Redmond, WA), with significance set to $p<0.05$.

*Morphometric analysis*

Images captured on the Nikon Eclipse (E600) Y-FL epifluorescence microscope were analyzed with MetaMorph imaging software. For filopodial analysis, images of 50 cells of each transient transfection type, GFP, *Axl*-Myc, *Axl-like*-Flag, or *Axl*-Myc/*Axl-like*-Flag were captured with a Hamamatsu camera. Filopodia were visualized by immunofluorescent staining of transfected COS-7 cells with the appropriate primary and secondary antibodies. The number of filopodia on the cellular surface was counted and analyzed by ANOVA and pair-wise t-tests using SPSS (Statistical Package for the Social Sciences). Significance was set at $p<0.05$.

Cells were transiently transfected with GFP, *Axl*-Myc, *Axl-like*-Flag, or *Axl*-Myc*/Axl-like*-Flag and the square area measured. 50 images of each cellular transfection type were captured with a Hamamatsu camera and analyzed with MetaMorph imaging software. The circumference of each immunofluorescently labeled cell was identified and the cellular square area determined. Data were analyzed by ANOVA and pair-wise t-tests using SPSS and Excel.

**D. Results**

*AXL and AXL-LIKE co-localize in COS-7 cells.*

Before the role of *Axl-like* in regulating *Axl* function could be evaluated, it was necessary to determine whether the two proteins are associated with each other. One way to accomplish this is by transfecting COS-7 cells with both constructs and evaluating their cellular localization. It was necessary to use epitope-tagged proteins because an antibody against AXL-LIKE is not available. Therefore, expression constructs were designed in order to express AXL fused to the Myc epitope tag and AXL-LIKE fused to the Flag epitope. *Axl*-Myc or *Axl-like*-Flag were transfected into COS-7 cells to determine cellular compartment localization. AXL-Myc appeared to be mainly localized to the cellular membrane with some perinuclear staining, while AXL-LIKE weakly stained the cell membrane but was mainly localized to the cytoplasm (Figure 3.4 A). Subsequently, COS-7 cells were co-transfected with *Axl*-Myc and *Axl-like*-Flag constructs. Immunofluorescence revealed that AXL and AXL-LIKE appear to co-localize within the same subcellular compartment in COS-7 cells (Figure 3.4 B). Interestingly, the localization pattern of AXL, when co-expressed with AXL-LIKE, was observed more strongly in the cytoplasm than the cell membrane. This redistribution of AXL to the cytoplasm in co-transfected cells suggests that AXL-LIKE is causing a sequestration of AXL within the cell. This finding is an initial step to support the hypothesis that AXL and AXL-LIKE bind to each other within the cell. The apparent co-localization of two proteins provides support that there is a possible interaction between

**Figure 3.4** Immunofluorescent co-localization of *Axl*-Myc and *Axl-like*-Flag fusion proteins after COS-7 cellular transfection. (A) Cells were transfected with either *Axl*-Myc or *Axl-like*-Flag constructs as described in experimental procedures. AXL-Myc appears to be mainly localized to the cellular membrane (white arrow), while AXL-LIKE staining is predominantly cytoplasmic, as indicated by the staining pattern of vesicular bodies. (B) Panels indicate an example of a COS-7 cell co-transfected with both *Axl*-Myc and *Axl-like*-Flag constructs. The first image indicates the co-transfected cell visualized for AXL-Myc with an anti-Myc primary antibody and FITC secondary (green). The middle image indicates the same cell also transfected with the *Axl-like*-Flag construct and visualized with an anti-Flag primary antibody and Texas Red secondary (red). The last image shows the merged image where the blue color indicates DAPI, which is a marker for DNA. The localization pattern of AXL in singly transfected cells compared to those that were co-transfected (panel A compared to B) changes from cell membrane to cytoplasmic suggesting that AXL-LIKE may sequester AXL and prevent it from reaching the cellular membrane. Size bars indicate 10 μm.

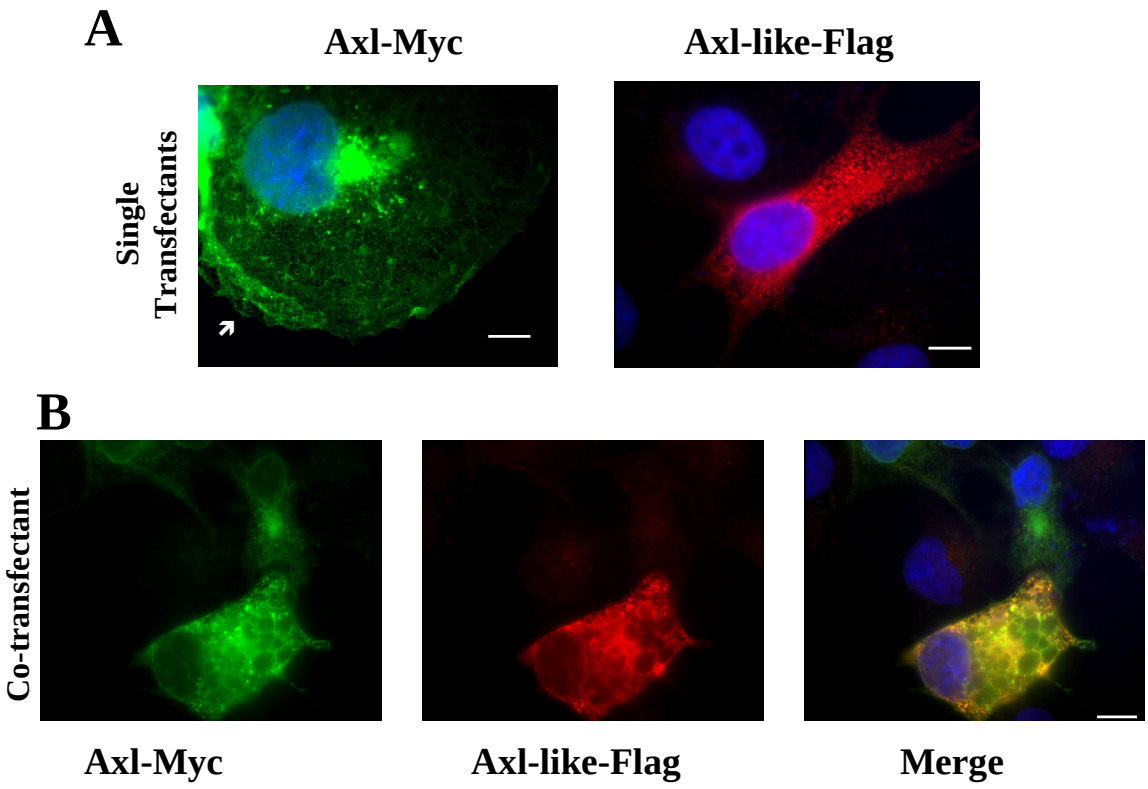
A
Axl-Myc
Axl-like-Flag
Single Transfectants
B
Co-transfectant
Axl-Myc
Axl-like-Flag
Merge

the proteins within the cell. Another way to test for direct interaction is using co-immunoprecipitation techniques. This experiment is discussed in more detail at a later time.

*Effect of AXL-LIKE on the AXL phenotype in COS-7 cells.*

COS-7 cells were either singly transfected with an empty GFP vector (control) (Figure 3.5 A), *Axl*-Myc (Figure 3.5 B), or *Axl-like*-Flag vector (Figure 3.5 C), or co-transfected with *Axl*-Myc and *Axl-like*-Flag constructs (Figure 3.5 D). Transfection of *Axl*-Myc construct into COS-7 cells results in a quantifiable increase in the number of filopodia present on the cellular surface compared with cells transfected with *Axl-like*-Flag or co-transfected with *Axl*-Myc and *Axl-like*-Flag. The co-overexpression of *Axl-like*-Flag in cells overexpressing *Axl*-Myc reversed the phenotype exhibited by cells transfected only with *Axl*-Myc. Figure 3.6 A is a graph depicting the mean number of filopodia present on the cellular surface of the corresponding transfected cell, while Figure 3.6 B shows the statistical analysis results. These findings support the hypothesis that Axl-like interferes with the function of *Axl in vitro*.

In addition to the increase in filopodia, total cell surface area decreased when COS-7 cells were co-transfected with *Axl*-Myc and *Axl-like*-Flag. Figure 3.7 A depicts graphed results of the mean square area of transfected cells. Of significance is the finding that transfection with either or both of the constructs reduced cell size compared with GFP control. Transfection alone did appear to play a role in the diminished square area of the cells. Because GFP was the only "empty" construct used in these

**Figure 3.5** Overexpression of the *Axl*-Myc construct in COS-7 cells causes an increase in the number of filopodia present on the cellular surface. COS-7 cells were transfected with constructs via electroporation as described. Cells were transfected with GFP (A), *Axl*-Myc (B), *Axl-like*-Flag (C), or *Axl*-Myc and *Axl-like*-Flag (D). The cells transfected with *Axl*-Myc were stained with an anti-Myc primary antibody and a FITC secondary antibody (green). Those transfected with *Axl-like*-Flag were stained with an anti-Flag primary antibody and a Texas Red secondary antibody (red). Cells co-transfected with both constructs were stained with both Myc and Flag primary antibodies, and images were captured with both channels of the microscope (D). The overexpression of AXL-Myc produced cells with an increase in filopodial protrusions (arrow in B) from the cell surface, while those also expressing AXL-LIKE-Flag inhibited the increase in filopodia (D). Size bars indicate 10 μm.

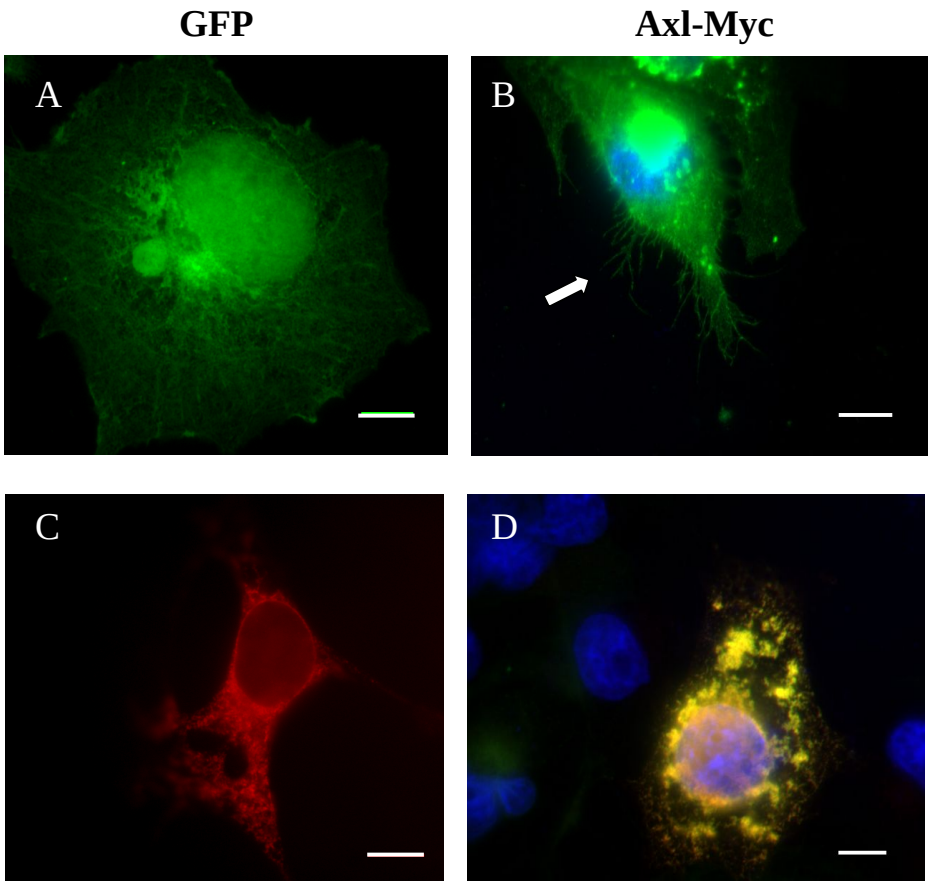
GFP
Axl-Myc
A
B
C
D
Axl-like-Flag
Axl-Myc
Axl-like-Flag

**Figure 3.6** Overexpression of AXL causes an increase in the number of filopodia present on the cellular surface. COS-7 cells were transfected with GFP, *Axl*-Myc, *Axl-like*-Flag, or *Axl*-Myc/*Axl-like*-Flag constructs, visualized by immunofluorescent staining, and the number of filopodia on each transfected cell was counted. The mean number of filopodia per cell is graphed in (A), while the paired t-test analysis results from the graph above are depicted in (B). Number of cells counted per transfection is 50. Significant differences are considered to be $p<0\ .05$ and are indicated by asterisk (*) in B.

**A**

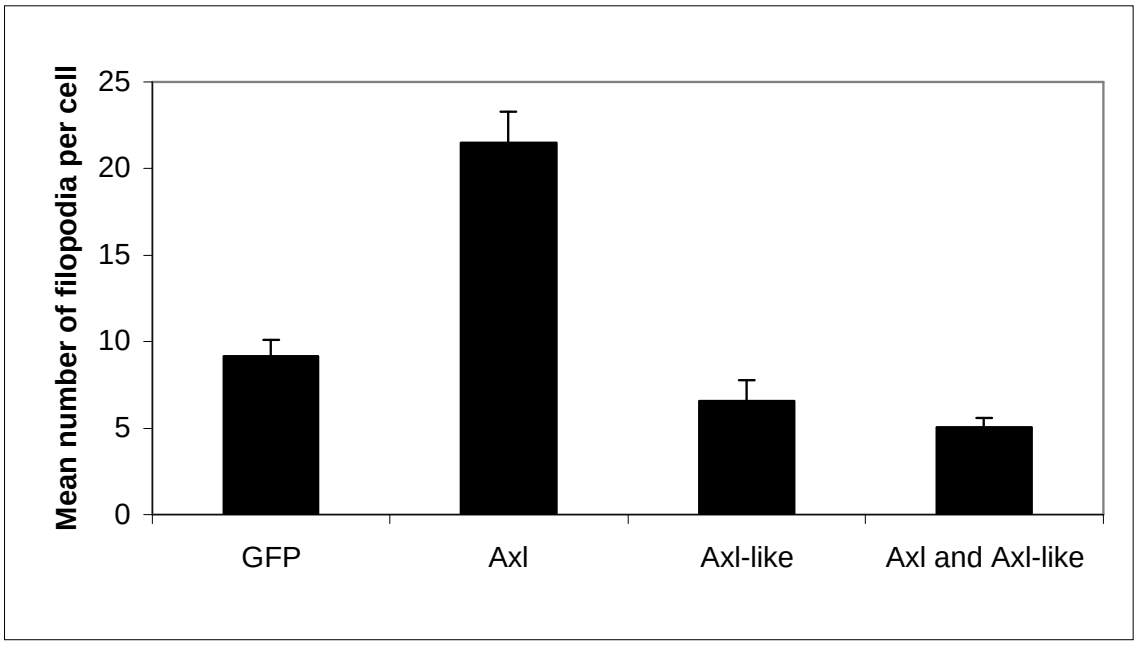


**B**

| Pair | Significance |
|---|---|
| GFP vs. Axl | <0.001* |
| GFP vs. Axl-like | 0.131 |
| GFP vs. Axl and Axl-like | 0.001* |
| Axl vs. Axl and Axl-like | <0.001* |
| Axl-like vs. Axl and Axl-like | 0.206 |
| Axl vs. Axl-like | <0.001* |

**Figure 3.7** Square area of transfected COS-7 cells was significantly diminished when transfected with *Axl-like*. (A) Cells were singly transfected with either GFP, *Axl*-Myc, or *Axl-like*-Flag construct or co-transfected with *Axl*-Myc and *Axl-like*-Flag constructs. After immunofluorescent staining with primary antibodies against Myc and/or Flag, the circumference of each labeled cell was identified, and the cell area was analyzed using MetaMorph software. Cell number analyzed was 50 per transfection type. The single transfection of either *Axl*-Myc or *Axl-like*-Flag into COS-7 cells caused a similar decrease in the cell area. (B) Paired t-test analysis was performed and significance was $p<0.05$*.

**A**

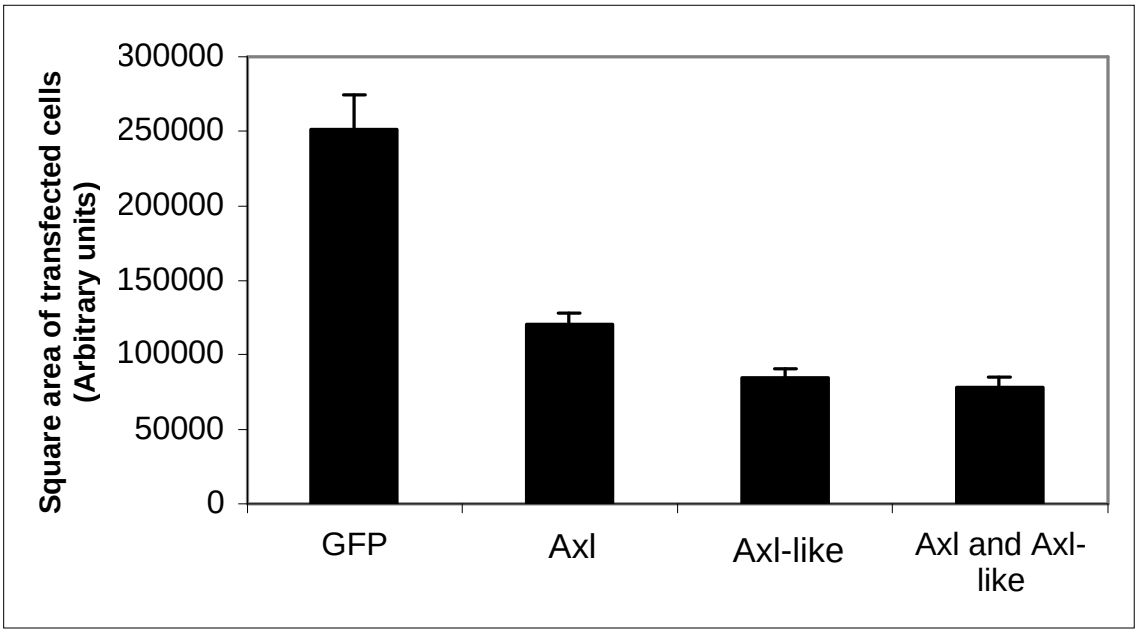


**B**

| Pair | Significance |
|---|---|
| GFP vs. Axl | <0.001* |
| GFP vs. Axl-like | <0.001* |
| GFP vs. Axl and Axl-like | <0.001* |
| Axl vs. Axl and Axl-like | <0.001* |
| Axl-like vs. Axl and Axl-like | 0.505 |
| Axl vs. Axl-like | 0.001* |

experiments, it seems that the *Axl*-Myc and *Axl-like*-Flag constructs were not well tolerated by the cell. The effect of this decrease in cell size with these constructs on our results is unknown. However, the fact that cells co-transfected with *Axl* and *Axl-like* are smaller in size than cells expressing *Axl* alone support the hypothesis that *Axl-like* is acting to inhibit the phenotype of *Axl in vitro*.

*AXL and AXL-LIKE are not associated.*

Immunofluorescence studies demonstrated co-localization of AXL and AXL-LIKE *in vitro*. This co-localization supports the hypothesis that AXL and AXL-LIKE do interact with each other but it does not reveal if that interaction is through direct association with one another. To determine if there is interaction between the two proteins, COS-7 cells, which endogenously express AXL, were singly transfected with either the *Axl*-Myc or *Axl-like*-Flag construct. The following day cells were lysed and subjected to immunoprecipitation with an antibody against the tyrosine kinase domain of AXL. This antibody does not recognize the AXL-LIKE protein, therefore it will immunoprecipitate transiently expressed AXL-LIKE only if it is associated with endogenous AXL polypeptide. Cell lysates were precipitated using the AXL antibody and precipitated proteins were separated by electrophoresis, transferred to a PVDF membrane and stained with the Flag antibody (Figure 3.8 A). A Flag stained protein was not detected in *Axl-like* transfected cells suggesting that AXL and AXL-LIKE do not interact but does not preclude these two proteins influencing common downstream signaling pathways.

**Figure 3.8** AXL-LIKE does not co-immunoprecipitate with AXL in COS-7 cells. COS-7 cells were transfected with the *Axl-like*-Flag construct. Cell lysate was prepared as described in the experimental procedures, and incubated with AXL antibody bound to protein G sepharose beads. Lanes indicate the transfected cellular lysate (lane L), unbound protein (lane Unb), and bound protein (lane IP) immuno-blotted with an anti-Flag antibody. The AXL-LIKE-Flag protein should migrate at around 80kDa (arrow). Usually a doublet is visible; a doublet is also seen with AXL, where the lower band corresponds to the partially glycosylated form. There is a clear indication the *Axl-like*-Flag construct is found in the lysate and unbound, but there appears to be very minor if any interaction of AXL-LIKE and AXL as indicated by the lack of IP in lane 3. The lower band in lanes 1 and 2 (arrowhead) indicate a cross-reaction with the Flag construct and the AXL antibody. This band was also observed in empty Flag vector transfections into COS-7 cells. The band in lane 3 indicates light chain IgG.

**IP: Axl**
**Blot: Flag**

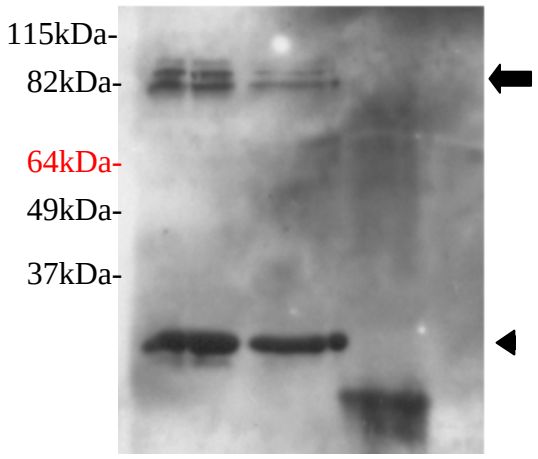

*Introduction of Axl-like diminishes the amount of endogenous AXL present within cells*

*Axl*-Myc transfectants were subjected to the same protocol as the *Axl-like*-Flag transfectants (Figure 3.9 A). Total cell lysates and proteins immunoprecipitated by an AXL antibody were evaluated for AXL content using electrophoresis followed by immunoblotting using the same AXL antibody. Stained proteins on each blot were quantified by densitometry (Figure 3.9 B). Each experiment was repeated at least 3 times. Low but detectable levels of AXL protein (~120kDa) were present in total cell lysates (Figure 3.9 A, lane 7) and precipitated proteins (Figure 3.9 A, lane 9) from COS-7 cells. Transfection of COS-7 cells with the *Axl*-Myc construct resulted in an increase in the amount of AXL present in both the total lysates (Figure 3.9 A, lane 1) and precipitated proteins (Figure 3.9 A, lane 3). In contrast, transfection with the *Axl-like* construct decreased the level of AXL detected in lysates (Figure 3.9 A, lane 4) and immunoprecipitations (Figure 3.9 A, lane 6) from COS-7 cells suggesting that AXL-LIKE may interfere with the expression of AXL through a yet as undetermined mechanism. This finding and the prior observation that co-transfection of *Axl* and *Axl-like* results in an apparent decrease in AXL localization at the plasma membrane suggest a regulatory role for AXL-LIKE in the function of AXL. AXL-LIKE may function to target AXL to degradative pathways instead of recycling pathways.

*Role of AXL-LIKE in regulation of the cellular protein phosphorylation of AXL.*

Data from this dissertation indicate that expression of AXL-LIKE affects the amount of AXL expressed and its cellular localization. In addition, co-expression of

**Figure 3.9**- Expression of AXL decreases when AXL-LIKE is introduced into COS-7 cells. (A) COS-7 cells were singly transfected with *Axl*-Myc, *Axl-like*-Flag, or no construct, lysates prepared and protein immunoprecipitated as described in the experimental procedures. The upper panel shows levels of AXL staining by immunoblot of proteins isolated from the different single transfections of COS-7 cells. The first three lanes indicate *Axl*-Myc transfections (lanes 1-3), the middle three lanes contain *Axl-like*-Flag transfectants (lanes 4-6), while the last three lanes indicate untransfected cells (lanes 7-9). Lanes labeled with "L" contain total cellular lysate from each transfection (40 μg); lanes indicated by "Unb" contain unbound proteins; while lanes indicated by "IP" demonstrate immunoprecipitation (50 μg) with the AXL antibody. The untransfected lanes indicate the endogenous amount of AXL (~120kDa) within COS-7 cells. There is overexpression of AXL when the *Axl*-Myc construct is introduced (lane 1 compared to lane 7), and there seems to be a decrease in the levels of AXL present when *Axl-like*-Flag construct is introduced (lane 4 compared to lane 7). The lower panel depicts the same membrane stripped and reprobed for actin to ensure that equal amounts of protein were loaded in each lane. The lower band in the IP lanes represents cross-reaction of the secondary antibody with heavy chain IgG. (B) The graph indicates the intensity of the AXL staining (uppermost band) in the lysate. (C) Statistical analysis of the intensity of AXL staining in the lysates of the transfectants. Pairs analyzed are shown in the first column, while pair-wise t-test analysis results are shown in the second column. $p<0.05$*

**A**

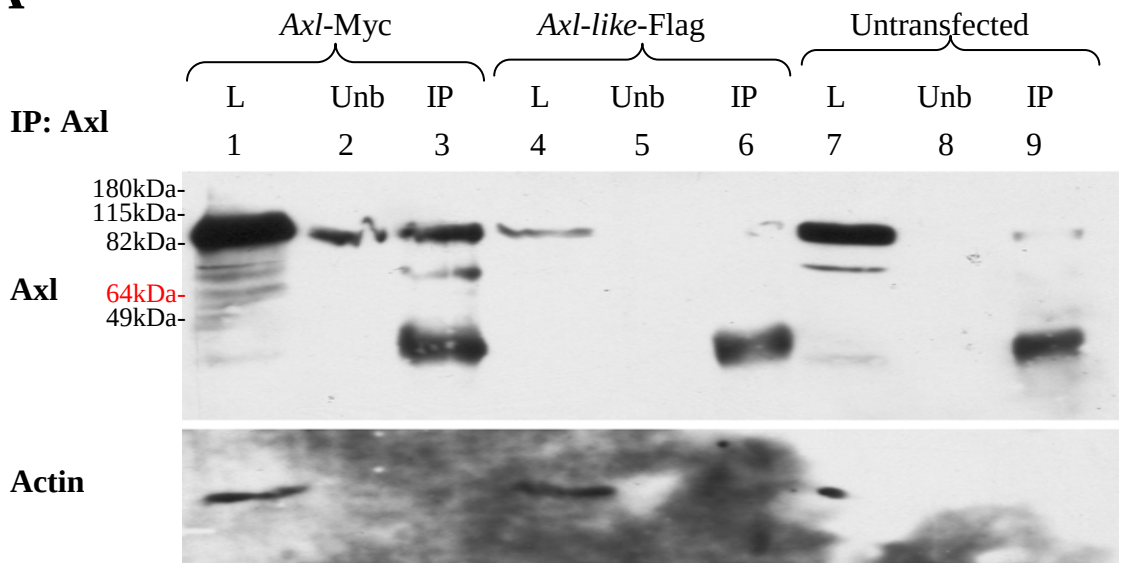


**B**

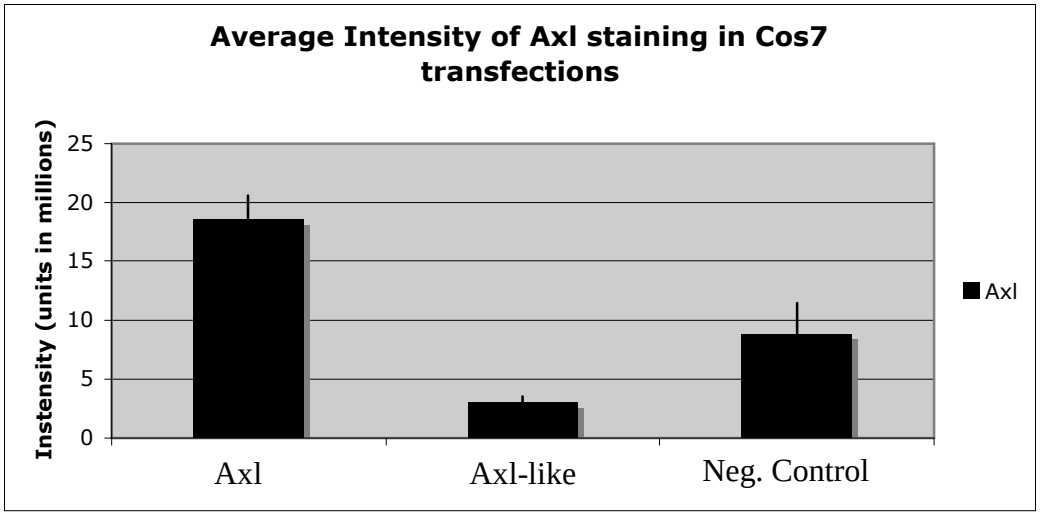


**C**

| Pair | Significance |
|---|---|
| Axl-Myc to Axl-like-Flag | 0.006* |
| Axl-Myc to Negative Control | 0.003* |
| Axl-like-Flag to Negative Control | 0.081 |

AXL-LIKE with AXL abrogates the increase in filopodia caused by expression of AXL alone. AXL is a receptor tyrosine kinase that dimerizes upon stimulation with a ligand. This results in autophosphorylation of the cytoplasmic portion of each receptor and subsequent phosphorylation of proteins involved in intracellular signaling pathways. One mechanism by which AXL-LIKE may regulate AXL is through these phosphorylation events since heterodimerization of AXL and AXL-LIKE (lacks tyrosine kinase) would inhibit AXL phosphorylation and associated signaling pathways. Accordingly, experiments were performed to examine phosphorylation in COS-7 cells treated with GAS6, an AXL specific ligand. COS-7 cells were transfected with empty Myc or Flag vectors as controls, and *Axl*-Myc or *Axl-like*-Flag constructs and stimulated with GAS6. Lysates were precipitated with AXL antibody, and phosphorylated proteins were detected using a tyrosine phosphate antibody (PY20) in the three pools: total, unbound, and IP. Overexpression of *Axl*-Myc resulted in the detection of a phosphorylated protein in the cell lysate, while *Axl-like*-Flag transfectants showed no change in phosphorylation status when stimulated with the GAS6 ligand (Figure 3.10 A). This increase in phosphorylation was only observed in the AXL-Myc lysate lane (Figure 3.10 A, lane 4). The size of the phosphorylated protein was approximately 120 kD, which is about the same size as full-length AXL, however it is not AXL because no phosphorylated protein was detected in the IP lane (Figure 3.10 A, lane 6). The other half of the IP elution was subjected to confirmatory Western blot staining with the AXL antibody to ensure the IP had functioned properly (Figure 3.10 B). Results indicated that all IPs, except for the Myc IP, were successful. The phosphorylation data indicates that the overexpression of *Axl*-Myc

**Figure 3.10-** Introduction of *Axl*-Myc causes an increase in phosphorylation of an unidentified protein. (A) COS-7 cells were transfected with empty Myc vector (lanes 1-3), *Axl*-Myc (lanes 4-6), empty Flag vector (lanes 7-9), or *Axl-like*-Flag (lanes 10-12). Following stimulation with GAS6, lysates were prepared for immunoprecipitation with an AXL antibody, followed by immunoblotting with the phospho-tyrosine specific antibody PY20 (upper panel). The introduction of *Axl*-Myc resulted in the detection of a phosphorylated protein (lane 4) in the total cell lysate as compared to the other transfectants. The blot was stripped and reprobed with β-actin (lower panel) to ensure equal protein loading. Lanes depicted by "L" indicate lysates (20 μg); lanes with "Unb" indicate unbound protein; and lanes with "IP" indicate bound protein (50 μg). (B) AXL Western blot indicating the AXL IPs, subjected to PY20 staining in panel A, were successful. Each transfection is indicated above the lane. All IP lanes contained 50 μg protein. (C) Graphical representation of the ratio of PY20 positive 120kDa band to actin staining in the cellular lysate lanes as determined by densitometry.

**A**

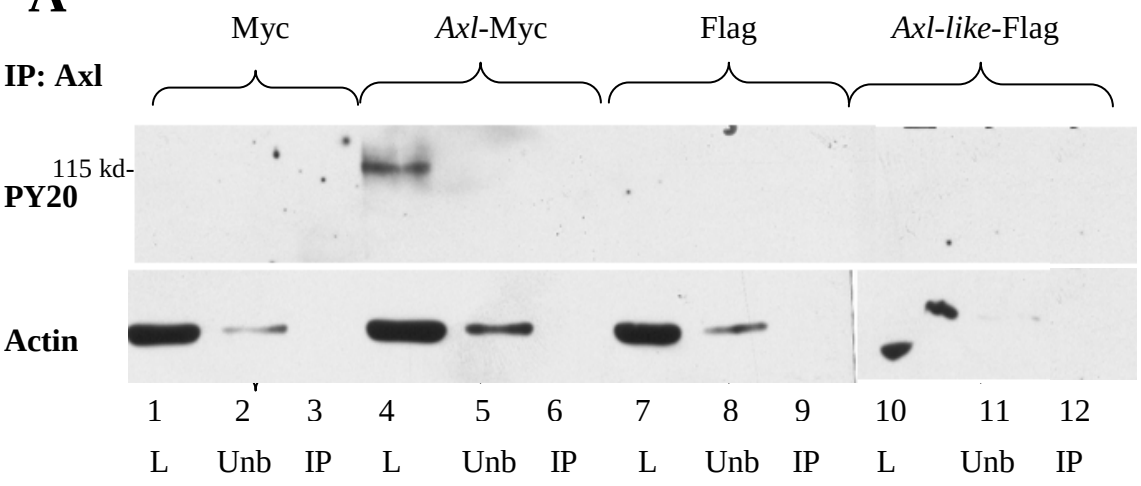
Myc
Axl-Myc
Flag
Axl-like-Flag
IP: Axl
115 kd-
PY20
Actin
1 2 3 4 5 6 7 8 9 10 11 12
L Unb IP L Unb IP L Unb IP L Unb IP

**B**

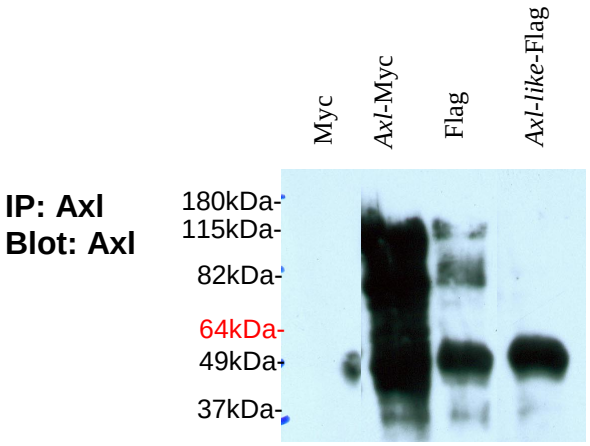
Myc
Axl-Myc
Flag
Axl-like-Flag
IP: Axl
Blot: Axl
180kDa-
115kDa-
82kDa-
64kDa-
49kDa-
37kDa-

**C**

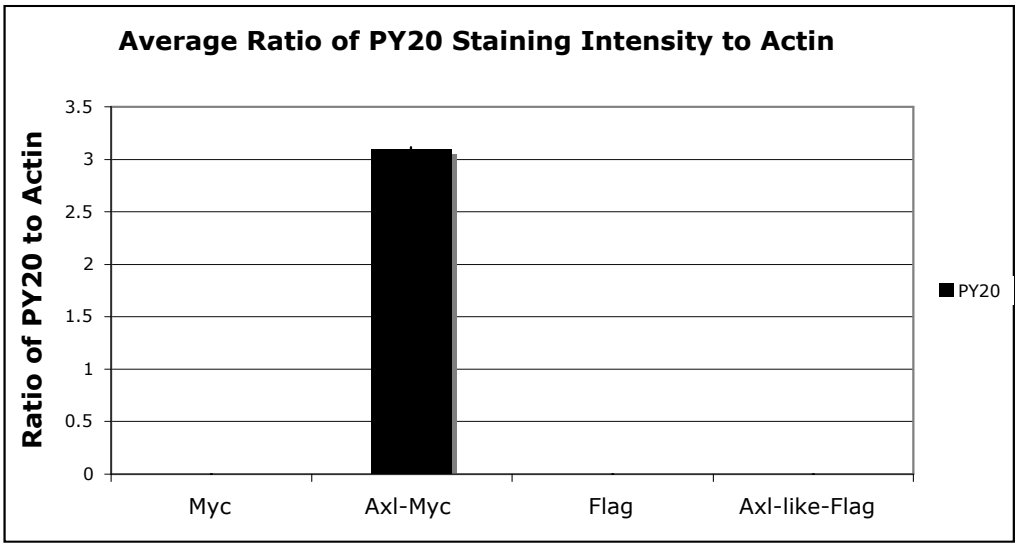
Average Ratio of PY20 Staining Intensity to Actin
Ratio of PY20 to Actin
3.5
3
2.5
2
1.5
1
0.5
0
Myc
Axl-Myc
Flag
Axl-like-Flag
PY20

increased the phosphorylation of a protein other than AXL. In contrast, introduction of the *Axl-like*-Flag construct had no affect on protein phosphorylation as expected (Figure 3.10 A, lanes 10-12). This finding confirms that AXL-LIKE plays no role in the phosphorylation of AXL, but may interfere in the downstream signaling pathways of AXL.

**E. Discussion**

AXL is a well-studied protein since it is found in multiple tissues and performs numerous functions within cellular systems, however AXL-LIKE has not been well characterized. This is likely due to its specificity for the testis and expression only in early developmental stages. The current study used epitope-tagged whole sequence constructs in order to study the effects of AXL-LIKE upon AXL in an *in vitro* model system. The fact that we were unable to amplify a full-length *Axl-like* transcript from an endogenous source may be due to the fact that *Axl-like* is found in the embryonic day 15 testes cDNA and we were using whole embryonic day 15 cDNA. The transcript of *Axl-like* may be present in quantities too low to efficiently amplify using PCR. Nevertheless, once the *Axl-like* transcript was obtained by other means, we were able to evaluate the effect of AXL-LIKE upon AXL *in vitro*.

Intracellular co-localization of AXL and AXL-LIKE support the hypothesis that these two proteins may interact with each other, although immunoprecipitation experiments indicate that this interaction is neither direct nor do these proteins reside in the same complex. It is important to remember these proteins localize to different

cellular compartments when introduced independently of each other (Figure 3.4). AXL was localized mainly to the cellular membrane, while AXL-LIKE was localized to a cytoplasmic compartment. This finding is similar to that found by Hu et al. (2006). They studied receptor tyrosine kinases of the ERBB family, specifically that of ERBB2. Full-length ERBB2 is localized to the cellular membrane, but its truncated form HERSTATIN, which lacks the functional tyrosine kinase domain, is localized within a cytoplasmic compartment. When co-transfected, HERSTATIN sequestered a large fraction of ERBB2 within the cytoplasm. The mechanism of this alteration in location is that formation of an ERBB2 and HERSTATIN complex inhibits ERBB2 from completing its transit through the endoplasmic reticulum (ER) and localizing to the cellular membrane. This prevents association with other family members and participation in signaling pathways. This is one possible mechanism to explain the effect of AXL-LIKE on AXL *in vitro*. This mechanism is consistent with the differential localization of co-transfectants compared to single transfectants (Figure 3.4) and with the reduction in mature AXL in the cell when AXL-LIKE is introduced (Figure 3.9 A). Future experiments may address this mechanism by transfecting cells with both constructs and then staining with AXL and ER-protein specific antibodies. Co-localization would support the sequestration hypothesis. In addition, treatment with Brefeldin A, a fungal antibiotic that specifically inhibits ER to Golgi transport, can be used to determine whether the blockage caused by AXL-LIKE occurs post Golgi. If AXL-LIKE is inhibiting transport of AXL using a mechanism similar to ERBB2/HERSTATIN, there should be no change in unprocessed protein (as compared to

Figure 3.9 A, lane 4) or localization of AXL (as compared to Figure 3.4 B) in co-transfected cells treated with Brefeldin A compared to untreated cells.

Soluble receptors for the TAM family of RTKs have been reported. These soluble receptors are produced by proteolytic cleavage of the membrane associated protein and release of an ectodomain (O'Bryan et al., 1995; Costa et al., 1996; Budagian et al., 2005a; Sather et al., 2007). Soluble TAM ectodomains bind to native receptor ligands such as GAS6 and serve as a "ligand sink," effectively reducing stimulation of functional receptors in the membrane (Budagian et al., 2005a; Sather et al., 2007). In most cases, proteolytic cleavage, not alternative splicing, produces the soluble ectodomains.

Vajkoczy et al. (2006) reported that a construct of *Axl* that lacked the intrinsic tyrosine kinase domain (AXL-DN: a man-made version of *Axl-like*) acts as a dominant-negative receptor to inhibit the migration and invasion of a gliomal cell line compared to cells containing wildtype *Axl*. In addition, AXL-DN cells appeared to round up, lose their cell-to-cell contacts, and exhibit a reduction in the number of filopodia (Vajkoczy et al., 2006). The morphological characteristics induced by AXL-DN are similar to those reported here for cells co-transfected with *Axl* and *Axl-like*, specifically the diminished number of filopodia and reduced cell size seen when AXL-LIKE was expressed in cells overexpressing AXL. This was partially seen in COS-7 cells transfected only with *Axl-like*, where a decrease in the mean square area of cells solely containing endogenous AXL was observed, while the change in the number of filopodia was not significant.

Data from this study are consistent with those of Zhang et al. (2008) who reported that introduction of a tyrosine kinase domain deletion mutant of *Axl* (dnAxl) into highly invasive breast cancer cell lines possessing high endogenous AXL levels abrogated GAS6 stimulated tyrosine phosphorylation and decreased motility and invasiveness. Ultimately the overexpression of dnAxl caused cells containing high endogenous AXL expression to convert from highly invasive breast cancer cells to a weak or non-invasive type with a spherical phenotype (Zhang et al., 2008).

Although our findings show that there was not an interaction between AXL and AXL-LIKE, there was a significant decrease in the amount of fully mature AXL present in the cell lysates when the *Axl-like*-Flag construct was transfected into COS-7 cells compared to cells transfected with the *Axl*-Myc construct. Data from Chapter II demonstrated that AXL localization changed from membrane associated to cytoplasmic when cells were co-transfected with both *Axl*-Myc and *Axl-like*-Flag constructs. The redistribution of AXL may represent sequestration of AXL in the ER causing a decrease in the amount of fully processed AXL present within the cell. Another possible explanation is that AXL-LIKE is causing AXL to be shifted to an intracellular degradative pathway. Following ligand binding to TAM receptors, activation of downstream signaling pathways, followed by receptor endocytosis occurs. Two pathways can then be initiated. In one pathway, the receptors pass from early to late endosomes, and finally enter recycling endosomes. The recycling endosome takes the receptor back to the cellular membrane to allow for repeated signaling events. In the other pathway, the late endosome transfers the receptor to a lysosome and marks it for

degradation. It is possible that the introduction of AXL-LIKE is causing an increase in the targeting of AXL for lysosomal degradation. One way to test this is by inhibiting lysosomal degradation with the addition of chlorquine. If AXL-LIKE is causing AXL to be degraded, Western blot analysis of lysates from untransfected cells and cells singly transfected with *Axl-like*, both treated with chlorquine, will show similar levels of full-length AXL (such as in Figure 3.9 A, lane 7) rather than a decrease (Figure 3.9 A, lane 7 compared to lane 4). This would indicate that AXL-LIKE is targeting AXL for the degradative pathway instead of the recycling pathway.

Smith et al. (1993) reported that when a truncated form of the insulin receptor (lacking the tyrosine kinase domain) is introduced into Rat 1 fibroblasts, there was a decrease in the amount of ATP-dependent, clathrin-coated, endocytosis of this receptor compared to the full-length insulin receptor. They also found that there appeared to be an alteration in the recycling pathway of insulin bound to the truncated receptors. They hypothesized that, when bound to the truncated receptor, insulin is preferentially recycled or retroendocytosed by a process that includes brief internalization, to allow the ligand to dissociate from the receptor, and a quick return to the cell membrane. This theory does not seem likely in the case of AXL and AXL-LIKE because AXL-LIKE appeared to be predominantly localized in a cytoplasmic compartment unlike the truncated insulin receptor (Figure 3.4 A). If AXL-LIKE were unable to be efficiently endocytosed, an overabundance of this receptor at the membrane would be observed.

Overexpression of AXL in COS-7 cells, by introduction of the *Axl*-Myc construct, resulted in phosphorylation of an unidentified protein (Figure 3.10 A). AXL and TYRO3

overexpression causes ligand-independent dimerization and autophosphorylation (Taylor et al., 1995; Burchert et al., 1998). In the current study, although the size of the protein phosphorylated in the lysate (Figure 3.10 A, lane 4) was approximately the same as AXL (120-140 kD), failure to precipitate the protein with an AXL antibody indicated that it is not AXL, although successful AXL IP was confirmed by Western blot analysis (Figure 3.10 B). The lack of precipitation of the phosphorylated protein may be caused by masking of the antibody epitope or GAS6 stimulation in this system may result in barely detectable levels of AXL activation but enough to yield signaling in downstream pathways.

AXL is involved in a variety of downstream signaling pathways such as: PI3K and C1-TEN, which both function in the AKT pathway, to promote cellular survival as well as actin reorganization and cell migration; the PLC pathway, which regulates $Ca^{2+}$ signaling; GRB2, which stimulates the MAPK pathway to promote proliferation; and SRC/LCK, which play a role in proliferation, actin reorganization and cellular migration (Fridell et al., 1996; Braunger et al., 1997; Goruppi et al., 1997; Allen et al., 2002; Hafizi et al., 2002). With the known interaction of AXL in the activation of these pathways, any of these cascades could be activated by overexpression of AXL and subsequently result in an increase in phosphorylation. Since overexpression of AXL was shown to increase the number of filopodia *in vitro*, it is possible that the PI3K/RAS/MAPK/hsp25 pathway is being stimulated in these cells.

Allen et al. (2002) showed that GAS6 stimulated AXL expressing NLT GnRH neuronal cells to reorganize their actin cytoskeleton with the increased production of

lamellipodia and membrane ruffles. However, this cytoskeletal remodeling was significantly hindered when AXL signaling through the RAC/p38 MAPK/ MAPKAPK2/hsp25 pathway was inhibited by introduction of AXL extracellular domain (ECD). These experiments demonstrate the linkage between AXL and regulation of the actin cytoskeleton and support our results showing a cytoskeletal phenotype when AXL-LIKE is expressed in AXL overexpressing cells. We were unable to co-transfect *Axl* and *Axl-like* into an adequate number of cells expressing both constructs to study the protein effects by Western blot. Based on our findings, however, I would expect that cells co-transfected with both *Axl* and *Axl-like* would act similarly to the cells transfected with *Axl-like* alone. Phosphorylation would be inhibited, or at least diminished as compared to cells overexpressing only *Axl*.

Budagian et al. (2005) reported that AXL heterodimerizes with IL-15Rα. This study showed that AXL interacted with IL-15Rα to stimulate the activation of NF-κB resulting in increased cellular survival. AXL has also been reported to stimulate the PI3K/AKT/NF-κB pathway (Demarchi et al., 2001). Interestingly, Budagian et al.'s (2005) study utilized *Axl* dominant negative constructs (lacking the tyrosine kinase domain) to determine whether the phosphorylation of IL-15Rα after association with its ligand, IL-15, is mediated through AXL. Co-immunoprecipitation studies indicated that the AXL-DN construct and the full-length AXL bind to IL-15Rα, indicating that the extracellular domain of AXL is necessary and sufficient for dimerization with IL-15Rα. They also determined that phosphorylation of AXL and IL-15Rα, when stimulated with IL-15 (the ligand for IL-15Rα) or GAS6 (the ligand of AXL), was only produced with

the full-length AXL. There was no phosphorylation of either protein observed with the AXL-DN construct. Our findings are not comparable with those of Budagian et al. (2005), however, because no phosphorylation of AXL was detected upon stimulation with GAS6 in our cell line, COS-7, which differs from that used by Budagian, L939 fibroblasts. No phosphorylated protein was detected corresponding to the known size of IL-15Rα. Therefore, IL-15Rα is likely not the mediator of the observations in our study.

In summary, we have utilized constructs of endogenous proteins to test their interaction and function in a cellular environment. Our study points to AXL-LIKE as a potential regulator of AXL *in vitro*. This protein should be targeted in future studies to determine its mechanism of inhibition of the AXL signaling cascade network and if this effect is specifically localized to the testes. The ability of AXL-LIKE to inhibit the increased number of filopodia formed by AXL overexpressing cells suggests that it might be possible to inhibit the metastasis of cancer in patients by introducing AXL-LIKE into tumors overexpressing AXL and may lead to more effective tumor treatment without the concern of metastasis.

# CHAPTER IV: GENERAL DISCUSSION

The TAM family of receptor tyrosine kinases has been implicated in a wide range of functions in multiple tissues within the body. In this study, we aimed to determine the localization and function of a possible new member of the TAM family, which we have termed *Axl-like*. The high sequence homology of *Axl* with *Axl-like* supports our hypothesis that the two proteins interact with one another and that AXL-LIKE may work to regulate a function of AXL. Chapter II examined the expression of *Axl* and *Axl-like* in prenatal, early postnatal, and adult testes, while Chapter III examined the potential interaction and function of the two proteins in cultured cells.

Data described in Chapter II indicate a correlation between the expression of *Axl* and *Axl-like* relative mRNA levels with the percentage of Sertoli cells within the developing testes at the days examined. This observation suggests an association of these proteins with, and possible localization in, Sertoli cells. The highest expression was observed at 7dpp, which also corresponds to the day of highest abundance of Sertoli cells. This finding is consistent with the prior report by Wang et al. (2005), which found AXL to be localized to only the Sertoli cells of early postnatal mice. These results were similar to other data obtained from the study of the TAM family as described by several investigators (Lu et al., 1999; Wong and Lee, 2002). Wong and Lee (2002) utilized Northern blot experiments with total testes RNA to assess the postnatal developmental expression levels for each TAM family member. *Axl* and *Tyro3* transcript levels were found to decline as the mouse matured, while *Mer* transcript levels increased until 20dpp

and then steadily decreased until 90dpp (Wong and Lee, 2002). The similar expression of *Axl-like* and *Axl* suggests that *Axl-like* may also be predominantly expressed in Sertoli cells. Further studies using immunohistochemical and/or *in situ* hybridization methodologies are required to confirm the hypothesized cellular location of *Axl-like*. Northern blot hybridization techniques were used to examine the expression of *Axl* and *Axl-like* RNA in a variety of adult murine tissues (Figure 2.3). A strong signal for *Axl* was detected in heart and testis, with weaker hybridization in brain, liver, lung, spleen, and kidney. *Axl* was not detected in skeletal muscle. *Axl-like* RNA was barely detectable in any of the adult tissues analyzed. Therefore, *Axl-like* is primarily expressed by the early postnatal testes and its expression decreases with age.

The study of protein interaction is best performed directly in tissues of organisms, but when that is not possible cell culture experiments with endogenous proteins as well as introduced constructs are readily accepted as adequate measures of interaction. In the current studies, direct examination of endogenous AXL-LIKE expression and interaction with other proteins is not feasible because there is not an antibody available specific to this protein. Chapter III discusses the cloning of *Axl* and *Axl-like* constructs, as well as their interaction and affect on cellular morphology. Myc and Flag cloning vectors were chosen because they use epitope tags that are smaller in size than fusion proteins, such as GFP, where the protein is very large and may interfere with normal signaling events. Our results indicate that although AXL and AXL-LIKE do not interact with each other, AXL-LIKE may still interfere with the normal signaling pathways activated by AXL. When AXL was overexpressed in cells there was an increase in the number of filopodia;

however, when AXL-LIKE was introduced into a cell also overexpressing AXL, that phenotype was inhibited. These results are similar to reports by other investigators (Allen et al., 2002; Vajkoczy et al., 2006; Zhang et al., 2008) using dominant negative constructs of AXL, which are similar in structure to AXL-LIKE (lacking the tyrosine kinase domain).

This study provides additional information concerning possible mechanisms regulating the function of AXL *in vivo* and *in vitro*. While these data indicate that AXL-LIKE suppresses the increase in filopodia observed when AXL is overexpressed *in vitro*, the mechanism of action remains unclear regarding which pathway is responsible. It would be interesting to study the effects of AXL-LIKE in a cancer model. Since AXL is overexpressed in many different cancers, it is possible that those patients may have improper expression or function of AXL-LIKE. Defective AXL-LIKE may cause misregulation of AXL thus leading to an increased disposition toward cancer or cancer metastasis. Conversely, if AXL-LIKE is not involved in cancer, it could be used as a treatment for cancer patients, inhibiting AXL and its role in the invasive phenotype associated with metastatic spread of cancer.

Support for this approach is the findings of Sainaghi et al. (2005). These investigators reported that prostate carcinoma cell lines expressing AXL undergo dose dependent proliferation in response to GAS6 stimulation. The proliferation of these cancer cells is reduced by the addition of AXL ectodomains (similar to AXL-LIKE in structure) to the media.

Vajkoczy et al. (2006) reported a 2-fold increase in expression of *Axl* in several human glioma cell lines compared with normal tissue. Introduction of a dominant-negative construct of AXL lacking the intracellular tyrosine kinase domain (AXL-DN) markedly decreased growth by 30 to 50% compared to wildtype (AXL-WT) or mock treated cells, respectively. In addition, tumor growth in nude mice was suppressed 85% when cells contained the dominant negative construct. Cell mobility assays confirmed that the AXL-DN tumor cells were less invasive than their wildtype counterparts. These studies support the possibility that AXL-LIKE may suppress the function of AXL and prevent cancer metastasis. Widespread expression in the body will, however, make inhibition of AXL in specific tissues difficult and treatment of the entire organism may be detrimental.

The consequences of reduced *Axl* expression in various tissues has been investigated using single, double, or triple mutants for the TAM family members. Although mice possessing mutations for all three TAM family members are viable at birth, they begin to show pathology in lymph nodes, spleen, and thymus at around 4 weeks after birth (Lu and Lemke, 2001) and in the testes as early as 3 weeks after birth (Lu et al., 1999). Additional problems were associated with aberrant proliferation of B and T cells, including the development of autoimmunity. Double knockouts of various TAM family members exhibited less severe phenotypes while single mutants displayed little autoimmunity. This suggests that inhibiting *Axl* alone *in vivo* may not have serious detrimental effects on normal tissue function. Investigation of *Axl-like* in a cancer model

is one area of potential future research, however, further examination of its role in spermatogenesis is also needed.

The studies described in this dissertation indicate a correlation between the levels of *Axl-like* mRNA expression and the percentage of Sertoli cells present within the developing testes. This is the first report of the expression or function of *Axl-like* beyond the detection of its transcript in embryonic day 15 male testes. The correlation of *Axl-like* with Sertoli cells allows new areas of research to be explored, especially with regard to the potential interaction of AXL and AXL-LIKE within the developing testes. This study also demonstrated that although AXL and AXL-LIKE do not bind to each other, AXL-LIKE might be involved in regulating the function of AXL. The introduction of AXL-LIKE into a cellular model overexpressing AXL causes an inhibition of the production of filopodia by these cells, a common precursor to increased cell motility. This inhibition of the phenotype of AXL *in vitro* by AXL-LIKE should be assessed further in a cancer model. If AXL-LIKE limits cell motility in such a model, then it could be a potential new avenue of therapy for cancer patients. A new approach to regulate the invasion promoting ability of AXL *in vivo* in cancer patients with tumors overexpressing *Axl* without detrimentally affecting other areas of the body would be innovative.

# REFERENCES


Adams, I. R., & McLaren, A. (2002). Sexually dimorphic development of mouse primordial germ cells: Switching from oogenesis to spermatogenesis. *Development, 129*(5), 1155-1164.

Allen, E. (1918) Studies on cell division in the albino rat. *Journal of Morphology, 31,* 133-185.

Allen, M. P., Linseman, D. A., Udo, H., Xu, M., Schaack, J. B., Varnum, B., Heidenreich, K. A., & Wierman, M.E. (2002). Novel mechanism for gonadotropin-releasing hormone neuronal migration involving GAS6/Ark signaling to p38 mitogen-activated protein kinase. *Molecular and Cellular Biology, 22*(2), 599-613.

Angelillo-Scherrer, A., Burnier, L., Flores, N., Savi, P., DeMol, M., Schaeffer, P., Herbert, J. M., Lemke, G., Goff, S.P., Matsushima, G. K., Earp, H. S., Vesin, C., Hoylaerts, M. F., Plaisance, S., Collen, D., Conway, E. M., Wehrle-Haller, B., & Carmeliet, P. (2005). Role of GAS6 receptors in platelet signaling during thrombus stabilization and implications for antithrombotic therapy. *The Journal of Clinical Investigation, 115*(2), 237-246.

Baillie, A. H. (1964). Further observations on the growth and histochemistry of Leydig tissue in the postnatal prepubertal mouse testis. *Journal of Anatomy, 98,* 403-418.

Baker, P. J., & O'Shaughnessy, P. J. (2001). Role of gonadotrophins in regulating numbers of Leydig and Sertoli cells during fetal and postnatal development in mice. *Reproduction, 122*(2), 227-234.

Behrens, E. M., Gadue, P., Gong, S. Y., Garrett, S., Stein, P. L., & Cohen, P. L. (2003). The mer receptor tyrosine kinase: Expression and function suggest a role in innate immunity. *European Journal of Immunology, 33*(8), 2160-2167.

Behrens, J., Mareel, M. M., Van Roy, F. M., & Birchmeier, W. (1989). Dissecting tumor cell invasion: Epithelial cells acquire invasive properties after the loss of uvomorulin-mediated cell-cell adhesion. *The Journal of Cell Biology, 108*(6), 2435-2447.

Bellosta, P., Costa, M., Lin, D. A., & Basilico, C. (1995). The receptor tyrosine kinase ARK mediates cell aggregation by homophilic binding. *Molecular and Cellular Biology, 15*(2), 614-625.

Bellve, A. R., Cavicchia, J. C., Millette, C. F., O'Brien, D. A., Bhatnagar, Y. M., & Dym, M. (1977). Spermatogenic cells of the prepuberal mouse. isolation and morphological characterization. *The Journal of Cell Biology, 74*(1), 68-85.

Biesecker, L. G., Giannola, D. M., & Emerson, S. G. (1995). Identification of alternative exons, including a novel exon, in the tyrosine kinase receptor gene Etk2/tyro3 that explain differences in 5' cDNA sequences. *Oncogene, 10*(11), 2239-2242.

Bordeleau, L. J., & Leclerc, P. (2008). Expression of hck-tr, a truncated form of the src-related tyrosine kinase hck, in bovine spermatozoa and testis. *Molecular Reproduction and Development, 75*(5), 828-837.

Braunger, J., Schleithoff, L., Schulz, A. S., Kessler, H., Lammers, R., Ullrich, A., Bartram, C. R., & Janssen, J. W. (1997). Intracellular signaling of the Ufo/Axl receptor tyrosine kinase is mediated mainly by a multi-substrate docking-site. *Oncogene, 14*(22), 2619-2631.

Brinster, R. L. (2007). Male germline stem cells: From mice to men. *Science, 316*(5823), 404-405.

Budagian, V., Bulanova, E., Orinska, Z., Duitman, E., Brandt, K., Ludwig, A., Hartmann, D., Lemke, G., Saftig, P., & Bulfone-Paus, S. (2005). Soluble axl is generated by ADAM10-dependent cleavage and associates with GAS6 in mouse serum. *Molecular and Cellular Biology, 25*(21), 9324-9339.

Budagian, V., Bulanova, E., Orinska, Z., Thon, L., Mamat, U., Bellosta, P., Basilico, C., Adam, D., Paus, R., & Bulfone-Paus, S. (2005). A promiscuous liaison between IL-15 receptor and axl receptor tyrosine kinase in cell death control. *The EMBO Journal, 24*(24), 4260-4270.

Bulfone-Paus, S., Ungureanu, D., Pohl, T., Lindner, G., Paus, R., Ruckert, R., Krause, H., & Kuzendorf, U. (1997). Interleukin-15 protects from lethal apoptosis in vivo. *Nature Medicine, 3*(10), 1124-1128.

Burchert, A., Attar, E. C., McCloskey, P., Fridell, Y. W., & Liu, E. T. (1998). Determinants for transformation induced by the axl receptor tyrosine kinase. *Oncogene, 16*(24), 3177-3187.

Ceresa, B. P., Kao, A. W., Santeler, S. R., & Pessin, J. E. (1998). Inhibition of clathrin-mediated endocytosis selectively attenuates specific insulin receptor signal transduction pathways. *Molecular and Cellular Biology, 18*(7), 3862-3870.

Chan, M. C., Mather, J. P., McCray, G., & Lee, W. M. (2000). Identification and regulation of receptor tyrosine kinases rse and mer and their ligand GAS6 in testicular somatic cells. *Journal of Andrology, 21*(2), 291-302.

Chemes, H. (1986). The phagocytic function of Sertoli cells: A morphological, biochemical, and endocrinological study of lysosomes and acid phosphatase localization in the rat testis. *Endocrinology, 119*(4), 1673-1681.

Chen, Y. M., Lee, N. P., Mruk, D. D., Lee, W. M., & Cheng, C. Y. (2003). Fer kinase/FerT and adherens junction dynamics in the testis: An in vitro and in vivo study. *Biology of Reproduction, 69*(2), 656-672.

Cobb, J., & Handel, M. A. (1998). Dynamics of meiotic prophase I during spermatogenesis: From pairing to division. *Seminars in Cell & Developmental Biology, 9*(4), 445-450.

Costa, M., Bellosta, P., & Basilico, C. (1996). Cleavage and release of a soluble form of the receptor tyrosine kinase ARK in vitro and in vivo. *Journal of Cellular Physiology, 168*(3), 737-744.

Demarchi, F., Verardo, R., Varnum, B., Brancolini, C., & Schneider, C. (2001). GAS6 anti-apoptotic signaling requires NF-kappa B activation. *The Journal of Biological Chemistry, 276*(34), 31738-31744.

Dettin, L., Ravindranath, N., Hofmann, M. C., & Dym, M. (2003). Morphological characterization of the spermatogonial subtypes in the neonatal mouse testis. *Biology of Reproduction, 69*(5), 1565-1571.

D'Eustachio, P., Colman, D. R., & Salzer, J. L. (1988). Chromosomal location of the mouse gene that encodes the myelin-associated glycoproteins. *Journal of Neurochemistry, 50*(2), 589-593.

Dolci, S., Pellegrini, M., Di Agostino, S., Geremia, R., & Rossi, P. (2001). Signaling through extracellular signal-regulated kinase is required for spermatogonial proliferative response to stem cell factor. *The Journal of Biological Chemistry, 276*(43), 40225-40233.

Dym, M., & Fawcett, D. W. (1970). The blood-testis barrier in the rat and the physiological compartmentation of the seminiferous epithelium. *Biology of Reproduction, 3*(3), 308-326.

Ebner, V. von. (1871). Untersuchungen uber den Bau der Samenkanalchen und die Entwicklung der Spermatozoiden bei den Saugethieren und beim Menschen. (Inquiries about the construction of the canal's semen and the development of sperm in the Saugethieren and humans.)

Ford, C. E., Evans, E. P., Burtenshaw, M. D., Clegg, H. M., Tuffrey, M., & Barnes, R. D. (1975). A functional 'sex-reversed' oocyte in the mouse. *Proceedings of the Royal Society of London.Series B, Containing Papers of a Biological Character.Royal Society, 190*(1099), 187-197.

Fridell, Y. W., Jin, Y., Quilliam, L. A., Burchert, A., McCloskey, P., Spizz, G., Varnum, B., Der, C., & Liu, E. T. (1996). Differential activation of the Ras/extracellular-signal-regulated protein kinase pathway is responsible for the biological consequences induced by the axl receptor tyrosine kinase. *Molecular and Cellular Biology, 16*(1), 135-145.

Goruppi, S., Ruaro, E., Varnum, B., & Schneider, C. (1997). Requirement of phosphatidylinositol 3-kinase-dependent pathway and src for GAS6-axl mitogenic and survival activities in NIH 3T3 fibroblasts. *Molecular and Cellular Biology, 17*(8), 4442-4453.

Graus-Porta, D., Beerli, R. R., Daly, J. M., & Hynes, N. E. (1997). ErbB-2, the preferred heterodimerization partner of all ErbB receptors, is a mediator of lateral signaling. *The EMBO Journal, 16*(7), 1647-1655.

Grimes, M. L., Beattie, E., & Mobley, W. C. (1997). A signaling organelle containing the nerve growth factor-activated receptor tyrosine kinase, TrkA. *Proceedings of the National Academy of Sciences of the United States of America, 94*(18), 9909-9914.

Griswold, M. D., Heckert, L., & Linder, C. (1995). The molecular biology of the FSH receptor. *The Journal of Steroid Biochemistry and Molecular Biology, 53*(1-6), 215-218.

Hafizi, S., Alindri, F., Karlsson, R., & Dahlback, B. (2002). Interaction of axl receptor tyrosine kinase with C1-TEN, a novel C1 domain-containing protein with homology to tensin. *Biochemical and Biophysical Research Communications, 299*(5), 793-800.

Hafizi, S., Gustafsson, A., Stenhoff, J., & Dahlback, B. (2005). The ran binding protein RanBPM interacts with axl and sky receptor tyrosine kinases. *The International Journal of Biochemistry & Cell Biology, 37*(11), 2344-2356.

Hafizi, S., Ibraimi, F., & Dahlback, B. (2005). C1-TEN is a negative regulator of the Akt/PKB signal transduction pathway and inhibits cell survival, proliferation, and migration. *The FASEB Journal: Official Publication of the Federation of American Societies for Experimental Biology, 19*(8), 971-973.

Hafizi, S., & Dahlbäck, B. (2006). Signalling and functional diversity within the axl subfamily of receptor tyrosine kinases. *Cytokine & Growth Factor Reviews, 17*(4), 295-304.

Hardy, M. P., Kelce, W. R., Klinefelter, G. R., & Ewing, L. L. (1990). Differentiation of Leydig cell precursors in vitro: A role for androgen. *Endocrinology, 127*(1), 488-490.

Heide, I., Sokoll, A. C., Henz, B. M., Nagel, S., Kreissig, K., Grutzkau, A., Grabbe, J., Wittig, B., & Neubauer, A. (1998). Regulation and possible function of axl expression in immature human mast cells. *Annals of Hematology, 77*(5), 199-205.

Herbst, J. J., Opresko, L. K., Walsh, B. J., Lauffenburger, D. A., & Wiley, H. S. (1994). Regulation of postendocytic trafficking of the epidermal growth factor receptor through endosomal retention. *The Journal of Biological Chemistry, 269*(17), 12865-12873.

Hoschuetzky, H., Aberle, H., & Kemler, R. (1994). Beta-catenin mediates the interaction of the cadherin-catenin complex with epidermal growth factor receptor. *The Journal of Cell Biology, 127*(5), 1375-1380.

Hu, P., Zhou, T., Qian, L., Wang, J., Shi, M., Yu, M., Yang, Y., Zhang, X., Shen, B., & Guo, N. (2006). Sequestering ErbB2 in endoplasmic reticulum by its autoinhibitor from translocation to cell surface: An autoinhibition mechanism of ErbB2 expression. *Biochemical and Biophysical Research Communications, 342*(1), 19-27.

Itman, C., Mendis, S., Barakat, B., & Loveland, K. L. (2006). All in the family: TGF-beta family action in testis development. *Reproduction, 132*(2), 233-246.

Janssen, J. W., Schulz, A. S., Steenvoorden, A. C., Schmidberger, M., Strehl, S., Ambros, P. F., & Bartram, C.R. (1991). A novel putative tyrosine kinase receptor with oncogenic potential. *Oncogene, 6*(11), 2113-2120.

Jenkins, R. B., Kimmel, D. W., Moertel, C. A., Schultz, C. G., Scheithauer, B. W., Kelly, P. J., & Dewald, G. W. (1989). A cytogenetic study of 53 human gliomas. *Cancer Genetics and Cytogenetics, 39*(2), 253-279.

Kabbani, N. (2008). Proteomics of membrane receptors and signaling. *Proteomics, 8*(19), 4146-4155.

Kelly, K. L., & Ruderman, N. B. (1993). Insulin-stimulated phosphatidylinositol 3-kinase. association with a 185-kDa tyrosine-phosphorylated protein (IRS-1) and localization in a low density membrane vesicle. *The Journal of Biological Chemistry, 268*(6), 4391-4398.

Kerr, J. B., & de Kretser, D. M. (1974). Proceedings: The role of the Sertoli cell in phagocytosis of the residual bodies of spermatids. *Journal of Reproduction and Fertility, 36*(2), 439-440.

Keshet, E., Itin, A., Fischman, K., & Nir, U. (1990). The testis-specific transcript (ferT) of the tyrosine kinase FER is expressed during spermatogenesis in a stage-specific manner. *Molecular and Cellular Biology, 10*(9), 5021-5025.

Kierszenbaum, A. L. (2006). Tyrosine protein kinases and spermatogenesis: Truncation matters. *Molecular Reproduction and Development, 73*(4), 399-403.

Kierszenbaum, A. L., Rivkin, E., & Tres, L. L. (2003). Acroplaxome, an F-actin-keratin-containing plate, anchors the acrosome to the nucleus during shaping of the spermatid head. *Molecular Biology of the Cell, 14*(11), 4628-4640.

Kluin, P. M., Kramer, M. F., & de Rooij, D. G. (1984). Proliferation of spermatogonia and Sertoli cells in maturing mice. *Anatomy and Embryology, 169*(1), 73-78.

Lawson, C., Goupil, S., & Leclerc, P. (2008). Increased activity of the human sperm tyrosine kinase SRC by the cAMP-dependent pathway in the presence of calcium. *Biology of Reproduction, 79*(4), 657-666.

Lawson, K. A., Dunn, N. R., Roelen, B. A., Zeinstra, L. M., Davis, A. M., Wright, C. V., Korving, J. P., & Hogan, B. L. (1999). Bmp4 is required for the generation of primordial germ cells in the mouse embryo. *Genes & Development, 13*(4), 424-436.

Lay, J. D., Hong, C. C., Huang, J. S., Yang, Y. Y., Pao, C. Y., Liu, C. H., Lai, Y. P., Lai, G. M., Cheng, A. L., Su, I. J., & Chuang, S. E. (2007). Sulfasalazine suppresses drug resistance and invasiveness of lung adenocarcinoma cells expressing AXL. *Cancer Research, 67*(8), 3878-3887.

Leblond, C. P., & Clermont, Y. (1952). Definition of the stages of the cycle of the seminiferous epithelium in the rat. *Annals of the New York Academy of Sciences, 55*(4), 548-573.

Lemke, G., & Rothlin, C. V. (2008). Immunobiology of the TAM receptors. *Nature Reviews. Immunology, 8*(5), 327-336.

Li, E., & Hristova, K. (2006). Role of receptor tyrosine kinase transmembrane domains in cell signaling and human pathologies. *Biochemistry, 45*(20), 6241-6251.

Linger, R. M., Keating, A. K., Earp, H. S., & Graham, D. K. (2008). TAM receptor tyrosine kinases: Biologic functions, signaling, and potential therapeutic targeting in human cancer. *Advances in Cancer Research, 100*, 35-83.

Liu, E., Hjelle, B., & Bishop, J. M. (1988). Transforming genes in chronic myelogenous leukemia. *Proceedings of the National Academy of Sciences of the United States of America, 85*(6), 1952-1956.

Livak, K. J., & Schmittgen, T. D. (2001). Analysis of relative gene expression data using real-time quantitative PCR and the 2(-delta delta C(T)) method. *Methods, 25*(4), 402-408.

Lu, Q., Gore, M., Zhang, Q., Camenisch, T., Boast, S., Casagranda, F., Lai, C., Skinner, M. K., Klein, R., Matsushima, G. K., Earp, H. S., Goff, S. P., & Lemke, G. (1999). Tyro-3 family receptors are essential regulators of mammalian spermatogenesis. *Nature, 398*(6729), 723-728.

Lu, Q., & Lemke, G. (2001). Homeostatic regulation of the immune system by receptor tyrosine kinases of the tyro 3 family. *Science, 293*(5528), 306-311.

Manfioletti, G., Brancolini, C., Avanzi, G., & Schneider, C. (1993). The protein encoded by a growth arrest-specific gene (GAS6) is a new member of the vitamin K-dependent proteins related to protein S, a negative coregulator in the blood coagulation cascade. *Molecular and Cellular Biology, 13*(8), 4976-4985.

Matsubara, N., Takahashi, Y., Nishina, Y., Mukouyama, Y., Yanagisawa, M., Watanabe, T., Nakano, T., Nomura, K., Arita, H., Nishimune, Y., Obinata, M., & Matsui, Y. (1996). A receptor tyrosine kinase, sky, and its ligand gas 6 are expressed in gonads and support primordial germ cell growth or survival in culture. *Developmental Biology, 180*(2), 499-510.

McCloskey, P., Fridell, Y. W., Attar, E., Villa, J., Jin, Y., Varnum, B., & Liu, E. T. (1997). GAS6 mediates adhesion of cells expressing the receptor tyrosine kinase axl. *The Journal of Biological Chemistry, 272*(37), 23285-23291.

Miething, A. (1992). Germ-cell death during prespermatogenesis in the testis of the golden hamster. *Cell and Tissue Research, 267*(3), 583-590.

Nagano, T., & Suzuki, F. (1976). The postnatal development of the junctional complexes of the mouse Sertoli cells as revealed by freeze-fracture. *The Anatomical Record, 185*(4), 403-417.

Nakano, T., Ishimoto, Y., Kishino, J., Umeda, M., Inoue, K., Nagata, K., Ohashi, K., Mizuno, K., & Arita, H. (1997). Cell adhesion to phosphatidylserine mediated by a product of growth arrest-specific gene 6. *The Journal of Biological Chemistry, 272*(47), 29411-29414.

Nebel, B. R., Amarose, A. P., & Hacket, E. M. (1961). Calendar of gametogenic development in the prepuberal male mouse. *Science, 134*, 832-833.

Ner, S. S. (1992). HMGs everywhere. *Current Biology: CB, 2*(4), 208-210.

Niemi, M., & Kormano, M. (1965). Cyclical changes in and significance of lipids and acid phosphatase activity in the seminiferous tubules of the rat testis. *The Anatomical Record, 151*, 159-170.

Nyquist, S. E., Acuff, K., & Mollenhauer, H. H. (1973). Residual bodies and their components. I. Isolation methods. *Biology of Reproduction, 8*(1), 119-124.

Oakberg, E. F. (1956). A description of spermiogenesis in the mouse and its use in analysis of the cycle of the seminiferous epithelium and germ cell renewal. *The American Journal of Anatomy, 99*(3), 391-413.

Oakberg, E. F. (1956). Duration of spermatogenesis in the mouse and timing of stages of the cycle of the seminiferous epithelium. *The American Journal of Anatomy, 99*(3), 507-516.

O'Bryan, J. P., Fridell, Y. W., Koski, R., Varnum, B., & Liu, E. T. (1995). The transforming receptor tyrosine kinase, axl, is post-translationally regulated by proteolytic cleavage. *The Journal of Biological Chemistry, 270*(2), 551-557.

O'Bryan, J. P., Frye, R. A., Cogswell, P. C., Neubauer, A., Kitch, B., Prokop, C., Espinosa, R., 3rd, Le Beau, M. M., Earp, H. S., & Liu, E.T. (1991). Axl, a transforming gene isolated from primary human myeloid leukemia cells, encodes a novel receptor tyrosine kinase. *Molecular and Cellular Biology, 11*(10), 5016-5031.

Ohno, S., Kaplan, W. D., & Kinosita, R. (1957). Heterochromatic regions and nucleolus organizers in chromosomes of the mouse, mus musculus. *Experimental Cell Research, 13*(2), 358-364.

Ohno, S. (1970). Morphological aspects of meiosis and their genetical signifance. In: Advances in Experimental Medicine and Biology. The Human Testis, edited by E. Rosenberg and C. A. Paulsen. New York: Plenum, 1970, vol. 10, p. 115-125.

Orian-Rousseau, V., Chen, L., Sleeman, J. P., Herrlich, P., & Ponta, H. (2002). CD44 is required for two consecutive steps in HGF/c-met signaling. *Genes & Development, 16*(23), 3074-3086.

Orth, J. M. (1982). Proliferation of Sertoli cells in fetal and postnatal rats: A quantitative autoradiographic study. *The Anatomical Record, 203*(4), 485-492.

Orth, J. M., Gunsalus, G. L., & Lamperti, A. A. (1988). Evidence from Sertoli cell-depleted rats indicates that spermatid number in adults depends on numbers of Sertoli cells produced during perinatal development. *Endocrinology, 122*(3), 787-794.

O'Shaughnessy, P. J., Baker, P. J., & Johnston, H. (2005). Neuroendocrine regulation of Leydig cell development. *Annals of the New York Academy of Sciences, 1061*, 109-119.

Palmer, S. J., & Burgoyne, P. S. (1991). In situ analysis of fetal, prepuberal and adult XX----XY chimaeric mouse testes: Sertoli cells are predominantly, but not exclusively, XY. *Development, 112*(1), 265-268.

Pineau, C., Le Magueresse, B., Courtens, J. L., & Jegou, B. (1991). Study in vitro of the phagocytic function of Sertoli cells in the rat. *Cell and Tissue Research, 264*(3), 589-598.

Prince, F. P. (1984). Ultrastructure of immature Leydig cells in the human prepubertal testis. *The Anatomical Record, 209*(2), 165-176.

Qian, X., Karpova, T., Sheppard, A. M., McNally, J., & Lowy, D. R. (2004). E-cadherin-mediated adhesion inhibits ligand-dependent activation of diverse receptor tyrosine kinases. *The EMBO Journal, 23*(8), 1739-1748.

Regaud, C. (1901). Etudes sur la structure des tubes seminiferes et sur la spermatogenese chez les mammiferes. (Studies on the structure of seminiferous tubules and spermatogenesis in mammals) *Archives d'anatomie microscopique et de morpholgie experimentale, 4*, 101-156 & 231-380.

Ren, Y., & Savill, J. (1998). Apoptosis: The importance of being eaten. *Cell Death and Differentiation, 5*(7), 563-568.

Rescigno, J., Mansukhani, A., & Basilico, C. (1991). A putative receptor tyrosine kinase with unique structural topology. *Oncogene, 6*(10), 1909-1913.

Roosen-Runge, E. C. (1955). Quantitative studies on spermatogenesis in the albino rat. III. Volume changes in the cells of the seminiferous tubules. *The Anatomical Record, 123*(4), 385-398.

Russell, L. D., & Clermont, Y. (1977). Degeneration of germ cells in normal, hypophysectomized and hormone treated hypophysectomized rats. *The Anatomical Record, 187*(3), 347-366.

Sainaghi, P. P., Castello, L., Bergamasco, L., Galletti, M., Bellosta, P., & Avanzi, G. C. (2005). GAS6 induces proliferation in prostate carcinoma cell lines expressing the axl receptor. *Journal of Cellular Physiology, 204*(1), 36-44.

Sakamoto, A., Yoneda, A., Terada, K., Namiki, Y., Suzuki, K., Mori, T., Ueda, J., & Watanabe, T. (2004). A functional truncated form of c-kit tyrosine kinase is produced specifically in the testis of the mouse but not the rat, pig, or human. *Biochemical Genetics, 42*(11-12), 441-451.

Sasaki, T., Knyazev, P. G., Clout, N. J., Cheburkin, Y., Gohring, W., Ullrich, A., Timpl, R., & Hohenester, E. (2006). Structural basis for GAS6-axl signalling. *The EMBO Journal, 25*(1), 80-87.

Sather, S., Kenyon, K. D., Lefkowitz, J. B., Liang, X., Varnum, B. C., Henson, P. M., & Graham, D. K. (2007). A soluble form of the mer receptor tyrosine kinase inhibits macrophage clearance of apoptotic cells and platelet aggregation. *Blood, 109*(3), 1026-1033.

Schulz, A. S., Schleithoff, L., Faust, M., Bartram, C. R., & Janssen, J. W. (1993). The genomic structure of the human UFO receptor. *Oncogene, 8*(2), 509-513.

Seitz, H. M., Camenisch, T. D., Lemke, G., Earp, H. S., & Matsushima, G. K. (2007). Macrophages and dendritic cells use different Axl/Mertk/Tyro3 receptors in clearance of apoptotic cells. *Journal of Immunology, 178*(9), 5635-5642.

Sekido, R., Bar, I., Narvaez, V., Penny, G., & Lovell-Badge, R. (2004). SOX9 is up-regulated by the transient expression of SRY specifically in Sertoli cell precursors. *Developmental Biology, 274*(2), 271-279.

Sharpe, C., Lawrence, N., & Martinez Arias, A. (2001). Wnt signalling: A theme with nuclear variations. *BioEssays : News and Reviews in Molecular, Cellular and Developmental Biology, 23*(4), 311-318.

Shieh, Y. S., Lai, C. Y., Kao, Y. R., Shiah, S. G., Chu, Y. W., Lee, H. S., & Wu, C. W. (2005). Expression of axl in lung adenocarcinoma and correlation with tumor progression. *Neoplasia, 7*(12), 1058-1064.

Smith, R. M., Sasaoka, T., Shah, N., Takata, Y., Kusari, J., Olefsky, J. M., & Jarett, L. (1993). A truncated human insulin receptor missing the COOH-terminal 365 amino acid residues does not undergo insulin-mediated receptor migration or aggregation. *Endocrinology, 132*(4), 1453-1462.

Steinfeld, R., Van Den Berghe, H., & David, G. (1996). Stimulation of fibroblast growth factor receptor-1 occupancy and signaling by cell surface-associated syndecans and glypican. *The Journal of Cell Biology, 133*(2), 405-416.

Tam, P. P., & Snow, M. H. (1981). Proliferation and migration of primordial germ cells during compensatory growth in mouse embryos. *Journal of Embryology and Experimental Morphology, 64*, 133-147.

Taylor, I. C., Roy, S., & Varmus, H. E. (1995). Overexpression of the sky receptor tyrosine kinase at the cell surface or in the cytoplasm results in ligand-independent activation. *Oncogene, 11*(12), 2619-2626.

Tena-Sempere, M., Zhang, F. P., & Huhtaniemi, I. (1994). Persistent expression of a truncated form of the luteinizing hormone receptor messenger ribonucleic acid in the rat testis after selective Leydig cell destruction by ethylene dimethane sulfonate. *Endocrinology, 135*(3), 1018-1024.

Tobias, P. V. (1956). Chromosomes, sex-cells, and evolution in a mammal. London: Percy, Lund, Humphries.

Tougard, C., Picart, R., & Tixier-Vidal, A. (1977). Cytogenesis of immunoreactive gonadotropic cells in the fetal rat pituitary at light and electron microscope levels. *Developmental Biology, 58*(1), 148-163.

Tzahar, E., Waterman, H., Chen, X., Levkowitz, G., Karunagaran, D., Lavi, S., Ratzkin, B. J., & Yarden, Y. (1996). A hierarchical network of interreceptor interactions determines signal transduction by neu differentiation factor/neuregulin and epidermal growth factor. *Molecular and Cellular Biology, 16*(10), 5276-5287.

Vajkoczy, P., Knyazev, P., Kunkel, A., Capelle, H. H., Behrndt, S., von Tengg-Kobligk, H., Kiessling, F., Eichelsbacher, U., Essig, M., Read, T. A., Erber, R., & Ullrich, A. (2006). Dominant-negative inhibition of the axl receptor tyrosine kinase suppresses

brain tumor cell growth and invasion and prolongs survival. *Proceedings of the National Academy of Sciences of the United States of America*, *103*(15), 5799-5804.

van de Wetering, M., & Clevers, H. (1992). Sequence-specific interaction of the HMG box proteins TCF-1 and SRY occurs within the minor groove of a watson-crick double helix. *The EMBO Journal, 11*(8), 3039-3044.

Visconti, P. E., Bailey, J. L., Moore, G. D., Pan, D., Olds-Clarke, P., & Kopf, G. S. (1995). Capacitation of mouse spermatozoa. I. correlation between the capacitation state and protein tyrosine phosphorylation. *Development, 121*(4), 1129-1137.

Visconti, P. E., Moore, G. D., Bailey, J. L., Leclerc, P., Connors, S. A., Pan, D., Olds-Clarke, P., & Kopf, G. S. (1995). Capacitation of mouse spermatozoa. II. protein tyrosine phosphorylation and capacitation are regulated by a cAMP-dependent pathway. *Development, 121*(4), 1139-1150.

Vleminckx, K., Vakaet, L.,Jr, Mareel, M., Fiers, W., & van Roy, F. (1991). Genetic manipulation of E-cadherin expression by epithelial tumor cells reveals an invasion suppressor role. *Cell, 66*(1), 107-119.

Wang, H., Chen, Y., Ge, Y., Ma, P., Ma, Q., Ma, J., Wang, H., Xue, S., & Han, D. (2005). Immunoexpression of tyro 3 family receptors--tyro 3, axl, and mer--and their ligand GAS6 in postnatal developing mouse testis. *The Journal of Histochemistry and Cytochemistry : Official Journal of the Histochemistry Society*, *53*(11), 1355-1364.

Wang, Y., Li, R., Du, D., Zhang, C., Yuan, H., Zeng, R., & Chen, Z. (2006). Proteomic analysis reveals novel molecules involved in insulin signaling pathway. *Journal of Proteome Research, 5*(4), 846-855.

Wong, C. C., & Lee, W. M. (2002). The proximal cis-acting elements Sp1, Sp3 and E2F regulate mouse mer gene transcription in Sertoli cells. *European Journal of Biochemistry / FEBS, 269*(15), 3789-3800.

Wu, H., Tang, H., Chen, Y., Wang, H., & Han, D. (2008). High incidence of distal vaginal atresia in mice lacking Tyro3 RTK subfamily. *Molecular Reproduction and Development, 75*(12), 1775-1782.

Xiong, W., Chen, Y., Wang, H., Wang, H., Wu, H., Lu, Q., & Han, D. (2008). GAS6 and the tyro 3 receptor tyrosine kinase subfamily regulate the phagocytic function of Sertoli cells. *Reproduction, 135*(1), 77-87.

Yarden, Y., & Ullrich, A. (1988). Growth factor receptor tyrosine kinases. *Annual Review of Biochemistry, 57*, 443-478.

Zhang, F. P., Poutanen, M., Wilbertz, J., & Huhtaniemi, I. (2001). Normal prenatal but arrested postnatal sexual development of luteinizing hormone receptor knockout (LuRKO) mice. *Molecular Endocrinology, 15*(1), 172-183.

Zhang, Q. K., Boast, S., de los Santos, K., Begemann, M., & Goff, S. P. (1996). Transforming activity of retroviral genomes encoding gag-axl fusion proteins. *Journal of Virology, 70*(11), 8089-8097.

Zhang, Y. X., Knyazev, P. G., Cheburkin, Y. V., Sharma, K., Knyazev, Y. P., Orfi, L., Szabadkai, I., Daub, H., Keri, G., & Ullrich, A. (2008). AXL is a potential target for therapeutic intervention in breast cancer progression. *Cancer Research, 68*(6), 1905-1915.

Zwingman, T., Erickson, R. P., Boyer, T., & Ao, A. (1993). Transcription of the sex-determining region genes sry and zfy in the mouse preimplantation embryo. *Proceedings of the National Academy of Sciences of the United States of America, 90*(3), 814-817.